UNCLASSIFIED

AD 275 949

Reproduced
by the

ARMED SERVICES TECHNICAL INFORMATION AGENCY
ARLINGTON HALL STATION
ARLINGTON 12, VIRGINIA

UNCLASSIFIED

NOTICE: When government or other drawings, specifications or other data are used for any purpose other than in connection with a definitely related government procurement operation, the U. S. Government thereby incurs no responsibility, nor any obligation whatsoever; and the fact that the Government may have formulated, furnished, or in any way supplied the said drawings, specifications, or other data is not to be regarded by implication or otherwise as in any manner licensing the holder or any other person or corporation, or conveying any rights or permission to manufacture, use or sell any patented invention that may in any way be related thereto.

275 949

STEVENS INSTITUTE
OF TECHNOLOGY

CASTLE POINT STATION
HOBOKEN, NEW JERSEY

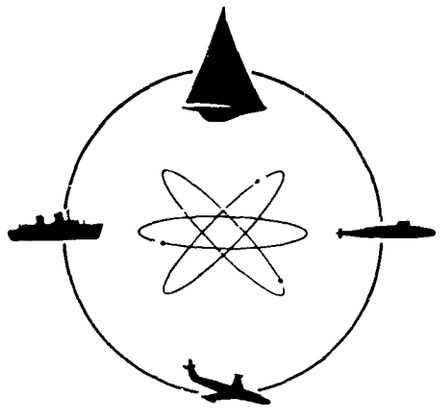

DAVIDSON LABORATORY

MAY 18 1962

WAVE FORCES ON SUBMERGED BODIES

by Charles J. Henry, Milton Martin, and Paul Kaplan

Nonr 263(15)
RESEARCH WAS CARRIED OUT UNDER
THE BUREAU OF SHIPS
FUNDAMENTAL HYDROMECHANICS RESEARCH PROGRAM
S-R001 01 01

ADMINISTERED BY
DAVID TAYLOR MODEL BASIN

R-808 June 1961

WAVE FORCES ON SUBMERGED BODIES

by Charles J. Henry, Milton Martin, and Paul Kaplan

Report 808
Project HY 1862
June 1961

CONTRACT Nonr 263(15)
RESEARCH WAS CARRIED OUT UNDER THE
BUREAU OF SHIPS
FUNDAMENTAL HYDROMECHANICS RESEARCH PROGRAM
SR001-01-01
ADMINISTERED BY
DAVID TAYLOR MODEL BASIN

DAVIDSON LABORATORY
Stevens Institute of Technology
Castle Point Station
Hoboken, New Jersey

TABLE OF CONTENTS

		page
Nomenclature		ix
Abstract		xiii
I.	Introduction	1
II.	Experimental Setup	3
	A. Apparatus	3
	B. Calibration	4
	C. Test Procedure	6
	D. Data Reduction	7
III.	Discussion of Results	9
	A. Vertical Plane	9
	B. Horizontal Plane	9
IV.	Comparison with Theory	13
V.	Conclusions	17
VI.	References	19
Appendix A		A-1
Appendix B		B-1

LIST OF TABLES

Table		Page
I.	Model Characteristics	21
II.	Test Conditions and Frequency of Encounter (cycles per second)	23
III.	Wave Speeds	25

LIST OF ILLUSTRATIONS

Figure

1. Seakeeping Installation Tank No. 2
2. Experimental Apparatus
3. Block Diagram of Instrumentation
4. Oscillating Beam
5. Phase Diagram
6. Heave Force per Unit Wave Amplitude versus Wave Length/Body Length at 0° Heading Angle
7. Heave Force per Unit Wave Amplitude versus Wave Length/Body Length at 30° Heading Angle
8. Heave Force per Unit Wave Amplitude versus Wave Length/Body Length at 60° Heading Angle
9. Heave Force per Unit Wave Amplitude versus Wave Length/Body Length at 90° Heading Angle
10. Pitching Moment per Unit Wave Amplitude versus Wave Length/Body Length at 0° Heading Angle
11. Pitching Moment per Unit Wave Amplitude versus Wave Length/Body Length at 30° Heading Angle
12. Pitching Moment per Unit Wave Amplitude versus Wave Length/Body Length at 60° Heading Angle
13. Pitching Moment per Unit Wave Amplitude versus Wave Length/Body Length at 90° Heading Angle
14. Side Force per Unit Wave Amplitude versus Wave Length/Body Length at 30° Heading Angle (without Conning Tower)
15. Side Force per Unit Wave Amplitude versus Wave Length/Body Length at 60° Heading Angle (without Conning Tower)
16. Side Force per Unit Wave Amplitude versus Wave Length/Body Length at 90° Heading Angle (without Conning Tower)
17. Yawing Moment per Unit Wave Amplitude versus Wave Length/Body Length at 30° Heading Angle (without Conning Tower)
18. Yawing Moment per Unit Wave Amplitude versus Wave Length/Body Length at 60° Heading Angle (without Conning Tower)

Figure

19. Yawing Moment per Unit Wave Amplitude versus Wave Length/ Body Length at 90° Heading Angle (without Conning Tower)

20. Side Force per Unit Wave Amplitude versus Wave Length/ Body Length at 30° Heading Angle (with Conning Tower)

21. Side Force per Unit Wave Amplitude versus Wave Length/ Body Length at 60° Heading Angle (with Conning Tower)

22. Side Force per Unit Wave Amplitude versus Wave Length/ Body Length at 90° Heading Angle (with Conning Tower)

23. Yawing Moment per Unit Wave Amplitude versus Wave Length/ Body Length at 30° Heading Angle (with Conning Tower)

24. Yawing Moment per Unit Wave Amplitude versus Wave Length/ Body Length at 60° Heading Angle (with Conning Tower)

25. Yawing Moment per Unit Wave Amplitude versus Wave Length/ Body Length at 90° Heading Angle (with Conning Tower)

26. Roll Moment per Unit Wave Amplitude versus Wave Length/ Body Length at 30° Heading Angle (with Conning Tower)

27. Roll Moment per Unit Wave Amplitude versus Wave Length/ Body Length at 60° Heading Angle (with Conning Tower)

28. Roll Moment per Unit Wave Amplitude versus Wave Length/ Body Length at 90° Heading Angle (with Conning Tower)

29. Phase Lag of Heave Force versus Wave Length/Body Length at 0° Heading Angle

30. Phase Lag of Heave Force versus Wave Length/Body Length at 30° Heading Angle

31. Phase Lag of Heave Force versus Wave Length/Body Length at 60° Heading Angle

32. Phase Lag of Heave Force versus Wave Length/Body Length at 90° Heading Angle

33. Phase Lag of Pitching Moment versus Wave Length/Body Length at 0° Heading Angle

34. Phase Lag of Pitching Moment versus Wave Length/Body Length at 30° Heading Angle

35. Phase Lag of Pitching Moment versus Wave Length/Body Length at 60° Heading Angle

Figure

36. Phase Lag of Pitching Moment versus Wave Length/Body Length at 90° Heading Angle

37. Phase Lag of Side Force versus Wave Length/Body Length at 30° Heading Angle (without Conning Tower)

38. Phase Lag of Side Force versus Wave Length/Body Length at 60° Heading Angle (without Conning Tower)

39. Phase Lag of Side Force versus Wave Length/Body Length at 90° Heading Angle (without Conning Tower)

40. Phase Lag of Yawing Moment versus Wave Length/Body Length at 30° Heading Angle (without Conning Tower)

41. Phase Lag of Yawing Moment versus Wave Length/Body Length at 60° Heading Angle (without Conning Tower)

42. Phase Lag of Yawing Moment versus Wave Length/Body Length at 90° Heading Angle (without Conning Tower)

43. Phase Lag of Side Force versus Wave Length/Body Length at 30° Heading Angle (with Conning Tower)

44. Phase Lag of Side Force versus Wave Length/Body Length at 60° Heading Angle (with Conning Tower)

45. Phase Lag of Side Force versus Wave Length/Body Length at 90° Heading Angle (with Conning Tower)

46. Phase Lag of Yawing Moment versus Wave Length/Body Length at 30° Heading Angle (with Conning Tower)

47. Phase Lag of Yawing Moment versus Wave Length/Body Length at 60° Heading Angle (with Conning Tower)

48. Phase Lag of Yawing Moment versus Wave Length/Body Length at 90° Heading Angle (with Conning Tower)

49. Phase Lag of Roll Moment versus Wave Length/Body Length at 30° Heading Angle (with Conning Tower)

50. Phase Lag of Roll Moment versus Wave Length/Body Length at 60° Heading Angle (with Conning Tower)

51. Phase Lag of Roll Moment versus Wave Length/Body Length at 90° Heading Angle (with Conning Tower)

52. Variation of Velocity Corrections with Depth

53. System of Coordinates

NOMENCLATURE

A_{22}, A_{33}, A_{42}	Virtual inertias
a	Wave amplitude
a_1, a_2	Amplitude of motion of model and strut, respectively
b	Distance from centerline to tip of fin (Appendix A) and strut semi chord (Appendix B)
$C(\kappa)$	Theodorsen function
c	Wave speed
D	Maximum diameter of model
d	Distance from wave wire to CB of model
d_c	Correction factor for depth of submergence
d_o	Correction factor for roll moment due to conning tower
g	Gravitational constant
h	Depth of submergence to coordinate axis
h_m	Depth to midspan of conning tower in model diameters
h_o	Depth to model centerline in model diameters
h_1	Depth of submergence to model centerline for each test in model diameters
h_2	Common depth of submergence = 2.5D
I_{zz}	Mass polar moment of inertia of model about the z axis
i	$\sqrt{-1}$
$J_n(\kappa)$	n^{th} order Bessel function of the first kind
K	Roll moment

k	Wave number, $k = 2\pi/\lambda = g/c^2$
k_β	Stiffness of balance in yaw
k_δ	Stiffness of balance in side sway
k_1, k_2	Stiffness of balance and bridge in side sway
L	Model length and lift force on strut (Appendix B)
L_o	Amplitude of lift on strut
L_o'	Amplitude of lift on strut per unit span
L_{2D}	Total two dimensional lift on strut
$L_h(\kappa, AR)$	Unsteady lift coefficient corrected for aspect ratio
ℓ	Distance from center of balance to CB, positive if CB is forward
M	Pitch moment about CB
m	Stripwise mass of the displaced fluid $\pi\rho R^2$ (Appendix A) and mass of model (Appendix B)
m_1, m_2	Mass of model and strut, respectively
N	Yaw moment about CB
N_o	Amplitude of yaw moment
$N_{\dot{v}}, N_{\dot{y}}, N_{\ddot{\beta}}, N_{\dot{\beta}}, N_\beta$	Hydrodynamic yaw moment derivatives relative to CB of model
R	Radius of circular cross section of model
t	Time
T_w	Wave period
V	Model or ship speed
v, w	Lateral and vertical orbital velocities, respectively
v_o, w_o	Values of v,w taken at center of cross section
x, y, z	Orthogonal cartesian coordinates fixed in the model

x_b	Distance from origin to bow
x_s	Distance from origin to stern
x_1, x_2	Displacement of masses m_1 and m_2
Y	Side force
Y_o	Amplitude of side force
$Y_y, Y_{\dot{y}}, Y_\beta, Y_{\dot{\beta}}$	Hydrodynamic side force derivatives relative to CB of model
$\dot{y}_o$	Amplitude of model oscillation in y direction
Z	Heave force
α	Phase lag correction for offset between CB and wave wire
β	Phase lag obtained from records and distortion of balance in yaw (Appendix B)
β_o	Amplitude of distortion of balance in yaw
γ	Phase lag correction due to electrical filters
δ	Distortion of balance in y direction
δ_o	Amplitude of δ
ϵ	Phase lag relative to wave height at CB of model
ϵ_1, ϵ_2	Phase lag of x_1 and x_2, respectively
η	Wave height at CB
η_c	Frequency of wave encounter
θ	Heading angle
κ	Argument of Theodorsen function, $= 2\pi b/\lambda$
ϕ	Velocity potential and phase lag of lift force on strut
μ	Argument of Bessel functions, $= 2\pi b \cos \theta/\lambda$
ξ	Distance from center of gravity to center of bouyancy, positive if CB is forward

ρ	Mass density of water
ω	Circular frequency of wave encounter
ω_1^2, ω_2^2	Uncoupled natural frequencies, $\omega_1^2 = k_1/m_1$, $\omega_2^2 = k_2/m_2$

ABSTRACT

A series of experiments, in which the forces and moments acting on a slender, submerged body-of-revolution moving under regular waves were measured, provided data to verify theoretical predictions of these forces and moments. The measured and predicted results over a range of speeds, heading angles, and wave lengths agreed. The measured and predicted roll moments, acting on the same model but with a conning tower, did not agree; however, the measured and predicted heave and side forces and the pitch and yaw moments did agree.

I. INTRODUCTION

In the development of optimum underwater vehicles, increasing importance has been given to the prediction of motions due to wave forces. In the past, these predictions were attempted theoretically, and expressions for the forces and moments acting on a spheroid moving obliquely under regular waves were developed (reference 1). As a result of choosing this simple model, the expressions for the forces and moments were in closed form. However, the range of shapes to which the results applied was limited. An extension to more general shapes, using strip theory, provided more practical results for the case of slender bodies in head seas. An empirical correction factor applied to the theoretical results provided agreement between theory and experiment. This correction accounted for wave-body interactions. An extension of Lagally's Theorem to unsteady flows provided means for predicting the forces and moments acting on a slender body-of-revolution moving obliquely under waves (reference 2). Again using strip theory but including the wave-body interactions, a method was found by which the forces due to added masses of fins could be included with the prediction of forces and moments on a slender body (reference 3). The results of reference 3 agree with those of reference 2.

Previous experimental investigations were for head seas only. These results did not provide information for the oblique seas case. Therefore, a series of experiments was conducted with a slender body-of-revolution at various heading angles and several forward speeds and wave lengths. Measurements of the magnitude and phase of the heave and side force and the yaw and pitch moment which acted on the model showed good agreement with the values predicted by the theory

in reference 3. In another series of tests, a conning tower was attached to the model. The measured roll moment showed poor agreement with the theory; however, the other measured forces and moments showed good agreement with theory.

II. EXPERIMENTAL SETUP

A. APPARATUS

The experiments were performed in the Seakeeping Facility (Figure 1) described in reference 4.

1. Model

A series-58 Hull was used in all tests. This family of bodies-of-revolution is described in reference 5. The model dimensions are given in Table I. The afterportion of the model was altered by cutting off the last three inches to accomodate the sting. The effect of this change was neglected; the model length used in all calculations was 4.5 feet. For the calculation of the inertial properties of the model, the water contained in the free-flooding cavities within the model was assumed to move rigidly with the model. The conning tower was an airfoil-shaped fin with a chord length of 0.45 foot and a span of 0.293 foot with the leading edge 1.27 feet aft of the bow.

2. Sting, Carriage, and Bridge

A sting, connected to a faired vertical strut, supported the model. The strut was supported from a carriage running on a rail beneath the truss-type bridge that spanned the tank. The angle of the bridge relative to the wave crests was adjustable. An internal balance between the sting and model measured the desired forces and moments (Figure 2).

3. Preliminary Tests

Preliminary tests of this apparatus indicated two difficulties. The vibrations caused by the rolling carriage wheels and other extraneous sources completely obscured the desired outputs from the balance. In addition, the flexibility

of the supporting structure permitted appreciable vertical and horizontal motions of the model. The resulting dynamic and hydrodynamic effects could not be neglected.

Supports extending to the walls and ceiling trusses of the building decreased the vertical oscillations of the bridge considerably, but the horizontal motion remained. Much of this motion was due to flexibility in the bridge-rail-carriage system and could not be reduced easily.

4. Instrumentation

The transducers used as sensing elements in the balance were Schaevitz linear differential transformers.

To provide the necessary information to correct for dynamic effects, accelerometers installed at the center-of-gravity of the model measured the horizontal and vertical accelerations. Low-pass filters reduced the noise in the outputs of the Schaevitz gages and the accelerometers.

A resistance wave-wire supported from the carriage at a known distance ahead of the model measured the wave height.

The five filtered outputs from the balance, the two filtered outputs from the accelerometers, and the unfiltered wave-wire output were recorded (Figure 3).

B. CALIBRATION

1. Filters

A sinusoidal signal was fed into the primary terminals of eight transformers. The outputs from the secondaries of seven of these transformers were fed into the recorder, each through its own filter. The output of the eighth transformer was put directly into channel eight of the recorder. In this way, eight signals from a single source

were recorded simultaneously, with and without the effect of the filters, under the same electrical conditions as used in the experiments (Figure 4). The attenuation and phase shift of each channel, relative to the unfiltered one (channel eight), obtained at several input frequencies covering the range anticipated gave the information necessary to correct for the electrical attenuation and phase shift due to the filters. The filters effectively suppressed high-frequency noise and passed the desired signal, which was in the range 0.6 to 2.5 cycles per second. Spot checks with differing amplitudes of the common input signal gave no difference in the results.

2. Accelerometers

The accelerometers were mounted on beam as shown in Figure 4. The beam was oscillated at a known amplitude and at several frequencies and the accelerometer outputs were passed through filters and into the recorder. The amplitude and frequency of the recorded signal were plotted against the amplitude of the acceleration at the accelerometer. Correcting for the filter attenuation at each frequency gave a linear calibration curve.

3. Wave-Wire

The unfiltered output from the resistance wave-wire was recorded on channel eight of the recorder. After recording a zero position, the wave-wire was moved known distances to either side of the zero position to obtain the calibration curve.

4. Balance

An initial check of the balance characteristics while they were mounted in the model but in air showed that the cross coupling among the force and moment components was negligible and that each component was linear. An extensive calibration was then done in air.

C. TEST PROCEDURE

Tests were made over a range of speeds, wave lengths, and heading angles (Table II). In addition, Table II shows the frequencies of encounter (η_c) for each condition as given by the relation

$$\eta_c = \frac{V \cos \theta + c}{\lambda} \tag{1}$$

where V = speed of advance of the model
θ = heading angle relative to wave direction
c = wave speed
λ = wave length.

Each day's testing began and ended with a calibration of the balance and wave wire. The bridge was moved to give the desired heading angle and then was braced as described previously. To get the desired wave length, the period of the wave-maker was set at the desired value (T_w) given by

$$T_w = \sqrt{\frac{2\pi\lambda}{g}} \tag{2}$$

where g is the gravitational constant. The corresponding wave speeds were found from

$$c = \sqrt{\frac{g\lambda}{2\pi}} \tag{3}$$

For wave-length/body-length ratios of 1.0 and 1.5, the wave amplitude was set at 1/20 of the wave length. At the longer wave lengths, smaller amplitudes were used so as not to stress the wavemaking equipment.

A constant-speed electric motor drove the carriage through a gear and pulley system. The gear ratio and pulley radius were adjustable to give a range of speeds in discrete steps of varying size.

Starting the model as soon as the regular wave train was established over the course of the test minimized the

interference of the wave system reflected from the beach. The zero speed tests were made with the model near the middle of the tank; the beam sea tests were made across the middle of the tank. Thus, the tests were usually completed before the reflected wave reached the model.

After each run, the model was returned to the starting position and the next speed was set. This procedure was repeated with the conning tower attached.

D. DATA REDUCTION

Analysis of the experimental data gave the magnitude and phase angle of the forces and moments acting on the model.

Five or six cycles from each run were chosen and the data reported were the values averaged over this segment. The frequency of encounter determined from the recorded wave height agreed with the values given in Table II. The wave height was obtained from this record using the calibration curve described previously. Similarly, the magnitudes of the forces and moments were computed from the corresponding records and calibration rates. In addition, the force and moment magnitudes were corrected for the filter attenuation at the frequency of encounter according to the following relation:

$$\text{tape magnitude} \times \frac{\text{calibration rate}}{\text{filter attenuation}} = \text{force magnitude} \qquad (4)$$

These results divided by the wave amplitude gave force per unit wave amplitude. The factor d_c corrected for minor variations in depth of submergence and was given by

$$d_c = \frac{\exp\left(-\frac{2\pi D}{\lambda} h_2\right)}{\exp\left(-\frac{2\pi D}{\lambda} h_1\right)} \qquad (5)$$

where D = maximum model diameter,
h_1 = depth of submergence for each test, and
h_2 = common depth of submergence = 2.5D.

The predicted values of force and moment per unit wave amplitude were computed for a depth of 2.5 model diameters by taking the product of the results of equations 4 and 5 divided by the corresponding wave amplitudes.

The phase angle (β) between the maximum recorded force and the recorded wave-crest was taken from the record for each component. This value was corrected for the phase shift due to the filter (γ) at the frequency of encounter and for the phase difference between the wave-height at the wave-wire and the wave-height above the center-of-buoyancy (CB) of the model (α). The latter correction may be found from the relation:

$$\alpha = \frac{d}{\lambda} (360°) \cos \theta \qquad (6)$$

where d is the distance from the wave-wire to the CB. The desired phase angle (ϵ) between the force maximum at CB and the time at which a wave-crest is over the CB was then found from

$$\epsilon = \beta - (\alpha + \gamma) \qquad (7)$$

A vector diagram in Figure 5 shows the phase relations which, in general, were found throughout the investigation. Also shown in Figure 5 is a phase correction (δ) due to dynamic effects.

III. DISCUSSION OF RESULTS

A. VERTICAL PLANE

The measured heave force and pitching moment magnitudes were corrected to 2.5 diameters submergence (Figures 6 through 13). The corresponding phase angles are shown in Figures 29 through 36. The scatter and inconsistencies in these results are indicative of the inadequacies of the experimental setup. Most of the scatter in the vertical plane results is due to poor measurement of the wave-height. Otherwise, these measurements are considered dependable.

No differences were found in the measurements with and without the conning tower.

B. HORIZONTAL PLANE

1. Dynamic Effects

In the theoretical analysis, the model was constrained to move in a straight line at constant speed. The flexibility of the supporting structure in the experiments caused the model to oscillate slightly in response to periodic wave forces. An investigation was made of the effect of this motion on the measured forces and moments.

The natural frequencies of the apparatus for all rotations of the model and for vertical translation of the model were sufficiently high; therefore, corrections for dynamic effects were neglected. The natural frequency in vertical translation was about 10 cps, and the natural frequency in roll was about 20 cps. The largest frequency of

encounter was 2.38 cps which was less than 1/4 of the lowest of these natural frequencies and resulted in a magnification factor in the measured force of less than 2 percent.

However, the horizontal motion of the model-strut-carriage mass with the elastic support of the rail and bridge acting as a spring had a natural frequency of about 2.4 cps. At short wave lengths and high speeds, the magnification of lateral effects due to resonance was, therefore, not negligible. The derivation of the corrections for this dynamic response is discussed in Appendix B. Several corrected values are plotted in Figure 16 (the flagged points) for the side force and Figure 19 for the yaw moment, as examples of these results. This correction was less than 10 percent of the measured values for the side force magnitude and 5 degrees for the phase lag for 90 percent of the data. The moment corrections are less than those for the side force. These corrections are based on crude guesses of the worst possible conditions.

2. Without Conning Tower

A sinusoidal curve was visually faired through the data at the wave encounter frequency from which the measurements of the magnitude and phase angle of the side force and yaw moment were obtained. The resulting loss in accuracy caused the increased scatter, particularly in the phase angles when compared with the data for the vertical plane.

3. With Conning Tower

The contribution of the force on the conning tower to the force on the body in the horizontal plane was not large; therefore, significant changes in the side force and yaw moment were not observed.

The roll moment, however, was entirely due to the force on the conning tower. The roll moment magnitudes are shown in Figures 26 through 28 and the phase lags in Figures 49 through 51.

The analysis of the roll moment data was hampered by the same dynamic effects as the side force and yaw moment. However, for the roll, the dynamic magnification due to resonance was negligible since the natural frequency of oscillation in roll of the model was about 20 cps. There still remains the effect of the transverse oscillatory motion of the model at the frequency of wave encounter and at the natural frequency of transverse oscillations. Due to the smaller magnitude of the roll moments, the relative error introduced by the transverse oscillations caused greater scatter and more inaccuracy in this component. Again, a sinusoidal curve was faired through the record at the frequency of wave encounter resulting in the same loss in accuracy mentioned previously.

IV. COMPARISON WITH THEORY

Considering the loss in accuracy due to the poor wave-height measurement and due to dynamic effects, the agreement between theoretical and experimental results is good. The discrepancies may be due to poor experimental conditions as well as to inaccuracies in the theory.

The measured heave force and pitch moment magnitudes and phase lag show good agreement with theory at the large wave-lengths. At short wave-lengths a discrepancy in the phase angle is evident. This discrepancy may be due to the assumptions involved in slender-body theory, which would not be appropriate at small wave lengths. The theoretical and experimental magnitudes are in good agreement at short wave-lengths.

The side force and yaw moment magnitudes and phases indicate that the same conclusions apply. Agreement between theory and experiment is good for magnitudes and phase lag at the long wave-lengths but at short wave-lengths, slender-body-theory apparently does not give an accurate prediction of the phase angle. The experimental and theoretical magnitudes are in good agreement at short wave-lengths.

The discrepancy between the measured roll moment magnitudes and the corresponding predicted values, is largely due to the transverse oscillations of the model. However, a cursory investigation showed that better agreement was obtained using the following corrections to the theory. First, the wave orbital velocity at the midspan of the conning tower was used to calculate the roll moment. The theory presented in reference 3 uses the velocity at the centerline of the model. The variation of the wave orbital velocity with depth

is shown in Figure 52. The corrected roll moment magnitudes are shown as dashed lines in Figures 26 through 28. At each heading better agreement between the corrected theory and experiment is achieved at higher speeds, whereas, at zero speed, the original good agreement is now poor. Secondly, the theoretical roll moment at zero speed is calculated on the basis of two-dimensional theory. At zero speed, the roll moment is given by:

$$L = z_o \, m \, \frac{\partial v}{\partial t}$$

where, z_o = distance from x-axis to midspan of conning tower,

m = added mass of conning tower,

$\frac{\partial v}{\partial t}$ = normal component of orbital acceleration near the conning tower.

A better approximation for m than that used in the theory of reference 3 might be

$$m = \frac{6.3 \, \rho a^2 b}{\sqrt{a^2 + b^2}} \cdot 2b \qquad (8)$$

from reference 6. In this equation

ρ = density of fluid

a = semi-chord length

b = semi span

The factor of 2 in equation 8 was included to account for the presence of the body. The zero speed roll moment magnitude calculated with this value of added mass is shown in Figures 26 through 28 as a dash-dot line. The original good agreement between theory and experiment is again realized with this correction. The magnitude of this correction decreases as speed increases since the contribution to the total force on the conning tower of added mass effects decreases.

These corrections are discussed here to indicate possible approaches to a more exact theory. It is not intended that these corrections should be included with future theoretical computations based on the theory in reference 3. If more exact theoretical results are desired a more exact theory is needed.

V. CONCLUSIONS

The flexibility of the model supports caused considerable hash and some dynamic effects, which accounts for much of the scatter in the plotted data, especially in the horizontal plane. Nevertheless, the theory developed in reference 3 predicts with reasonable accuracy the forces and moments acting on a slender body moving obliquely under regular waves.

Two consistent discrepancies were found. The measured phase lags for all forces and moments at the 90-degree heading angle exceeded the computed values at all speeds. This discrepancy diminished as the wave length increased and at the highest wave length the phase lags agreed with theory in all cases tested. Secondly, the measured roll moment magnitudes do not agree with the theory at the higher speeds. Both of these discrepancies are indicative of the inadequacies of slender-body-theory.

VI. REFERENCES

1. Havelock, T. H., "The Forces on a Submerged Body Moving Under Waves," Trans. Institute of Naval Architects, Vol. 96, 1954.

2. Cummins, W. E., "Hydrodynamic Forces and Moments Acting on a Slender Body of Revolution Moving Under a Regular Train of Waves," DTMB Report No. 910, December 1954.

3. Kaplan, P. and Hu, P., "Virtual Mass and Slender-Body Theory for Bodies in Waves," DL Note 543, June 1959.

4. Numata, E., Spens, P., and Muley, A., "New Facilities at Stevens for Research in Seakeeping Qualities of Ships," DL Report No. 677, October 1957.

5. Landweber, L. and Gertler, M., "Mathematical Formulation of Bodies of Revolution," DTMB Report 719, September 1950.

6. Yu Yeetak, "Virtual Mass of Rectangular Plates and Parallelpipeds in Water," Journal of Applied Physics, November 1945.

TABLE I: MODEL CHARACTERISTICS

Length-diameter ratio	7.34
Length	4.5 feet
Maximum diameter	0.613 feet
Maximum cross sectional area	0.295 $feet^2$
Wetted surface	6.366 $feet^2$
Projected area	1.999 $feet^2$
Volume	0.797 $feet^3$
Prismatic coefficient	0.600
Weight in air	21.0 pounds
Buoyant force minus weight in water	28.7 pounds
LCB aft of bow	2.005 feet
LCG aft of bow	2.047 feet
Center-of-balance aft of bow	2.671 feet

TABLE II: TEST CONDITIONS AND FREQUENCY OF ENCOUNTER (CYCLES PER SECOND)

		HEADING ANGLE θ (degrees)			
λ/L	V (ft/sec)	0	30	60	90
1.0	0	1.055	1.055	1.055	1.055
	2.02	1.504	1.444	1.280	1.055
	3.96	1.936	1.818	1.496	1.055
	5.95	2.378	2.201	1.717	1.055
1.5	0	.895	.895	.895	.895
	2.02	1.219	1.176	1.058	.895
	3.96	1.530	1.445	1.213	.895
	5.95	1.848	1.720	1.372	.895
2.0	0	.746	.746	.746	.746
	2.02	0.970	0.940	0.858	.746
	3.96	1.186	1.127	0.966	.746
	5.95	1.407	1.318	1.076	.746
2.5	0	.668	.668	.668	.668
	2.02	0.848	0.824	0.758	.668
	3.96	1.020	0.973	0.844	.668
	5.95	1.197	1.126	0.933	.668

TABLE III: WAVE SPEEDS

λ/L	λ (feet)	c (ft/sec)
1.0	4.5	4.75
1.5	6.75	5.60
2.0	9.0	6.71
2.5	11.25	7.52

FIG. 1

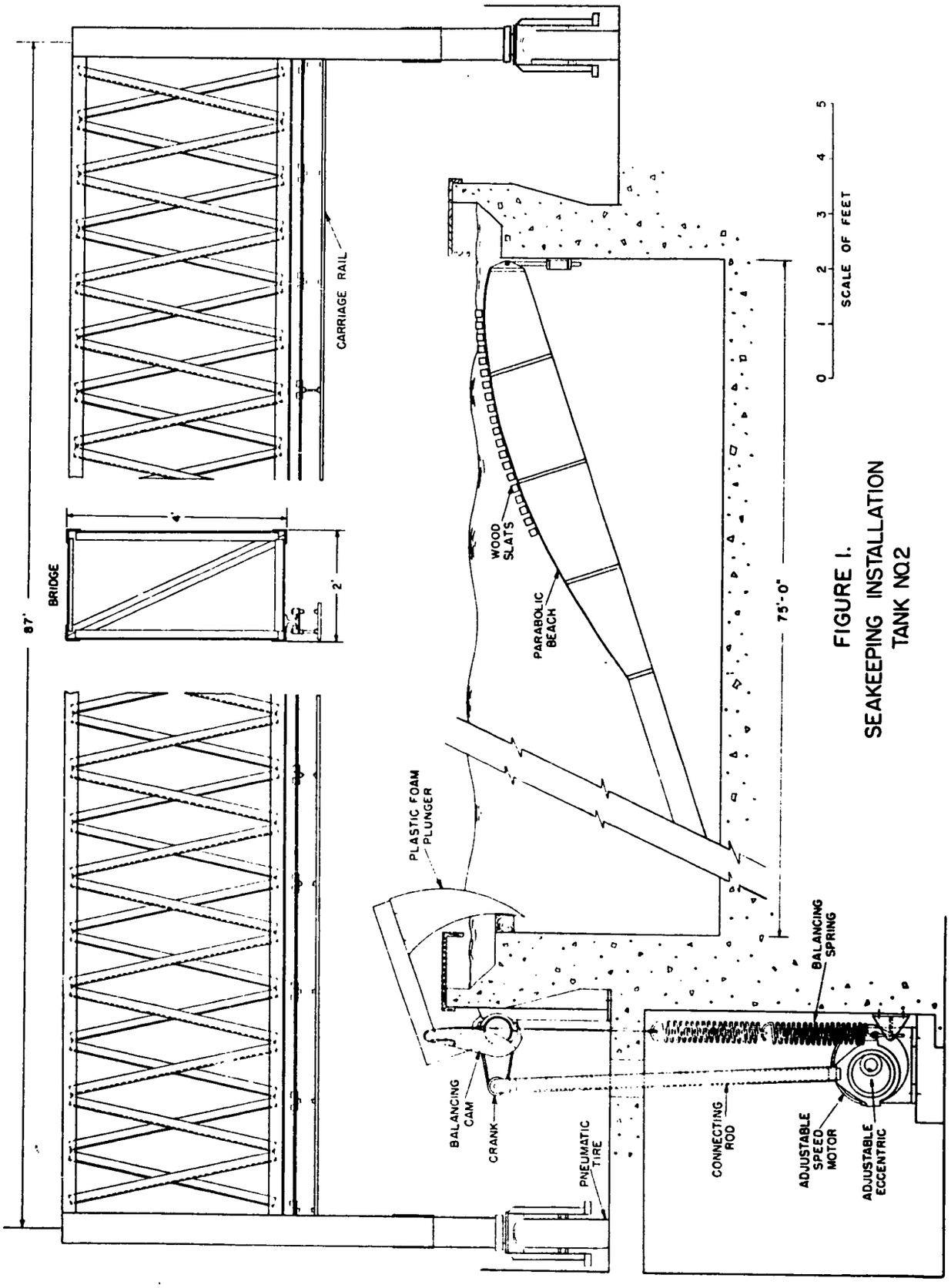

FIGURE 1.
SEAKEEPING INSTALLATION
TANK NO2

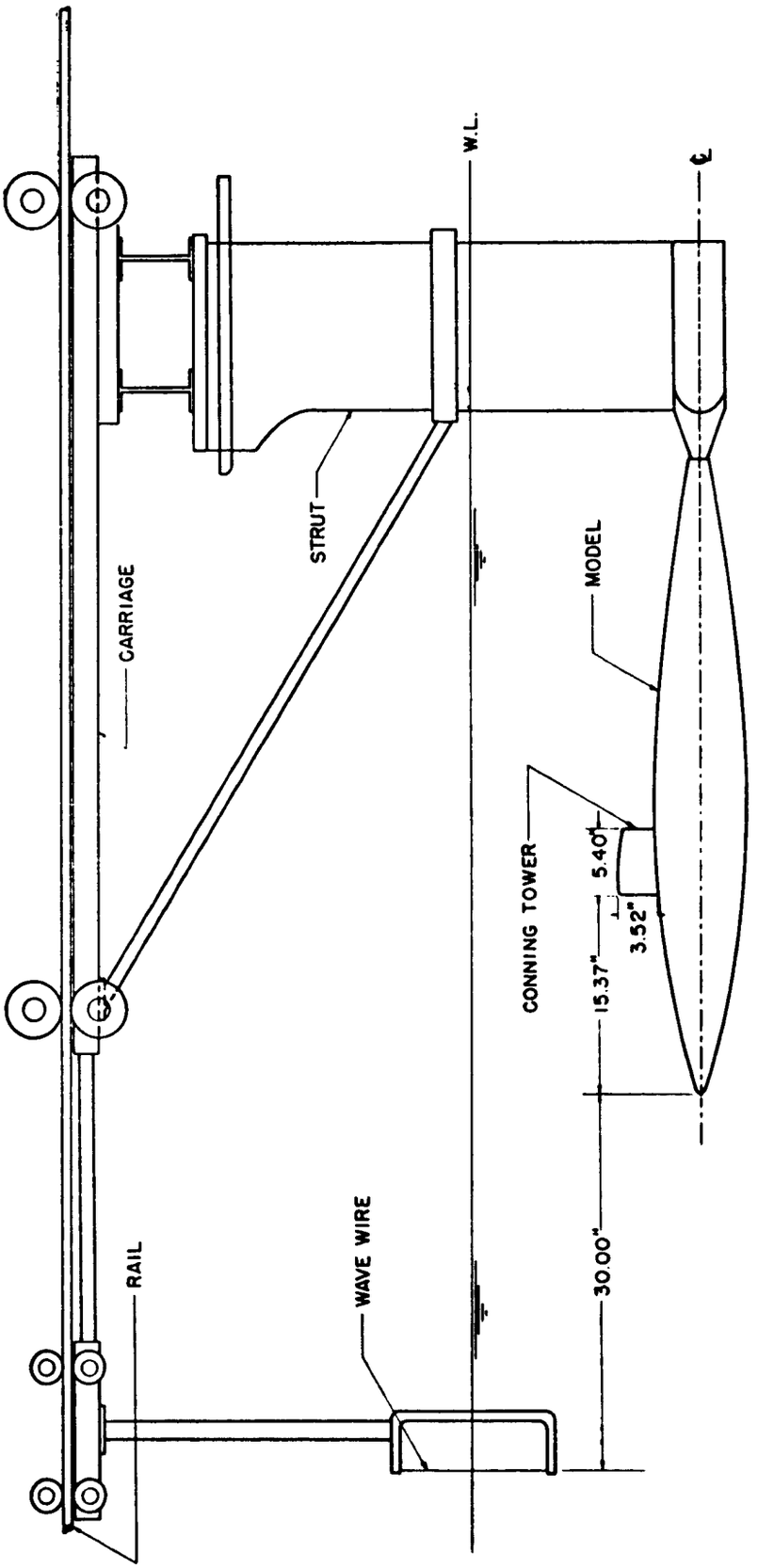

FIGURE 2. EXPERIMENTAL APPARATUS

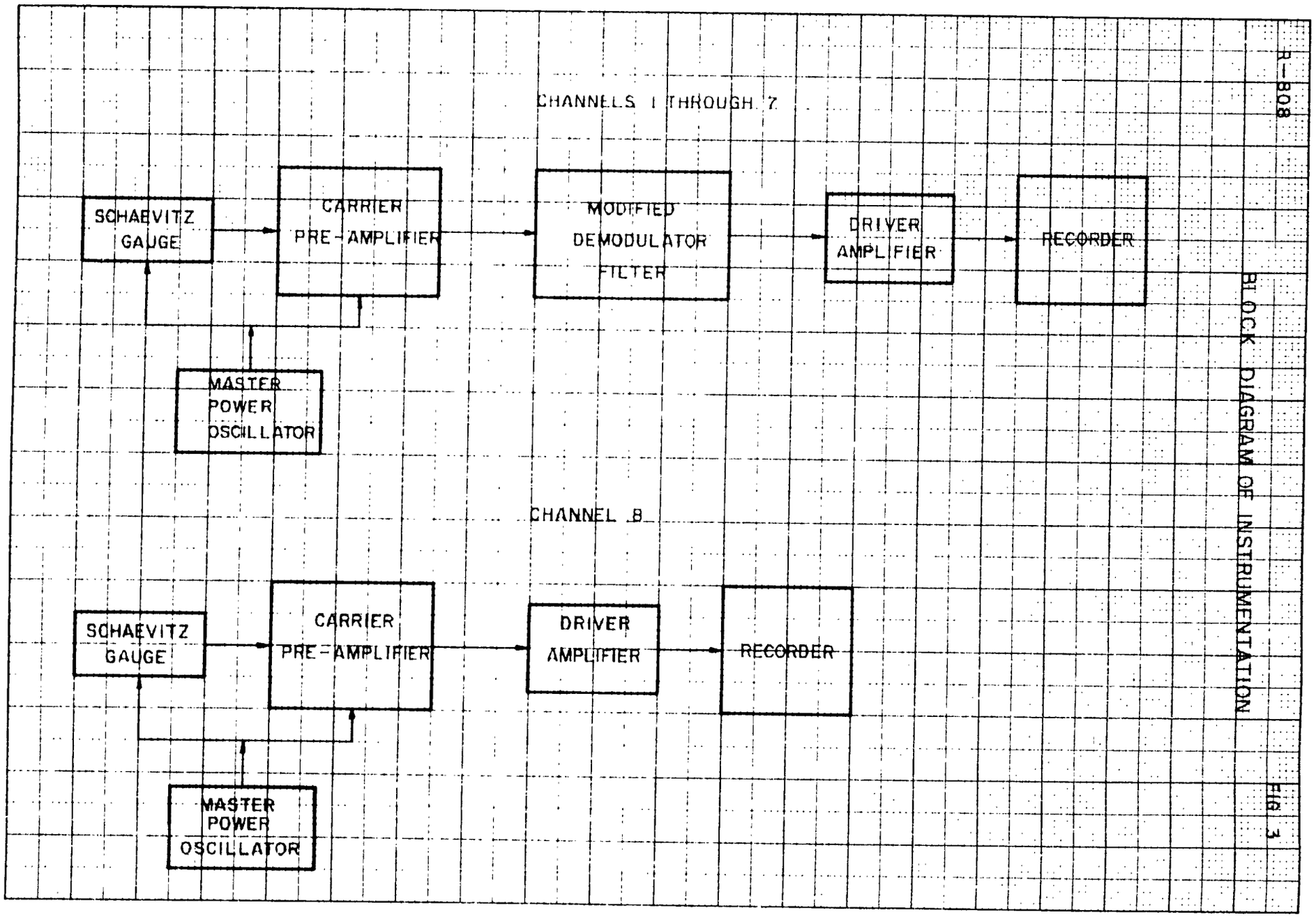

R-808

BLOCK DIAGRAM OF INSTRUMENTATION

FIG 3

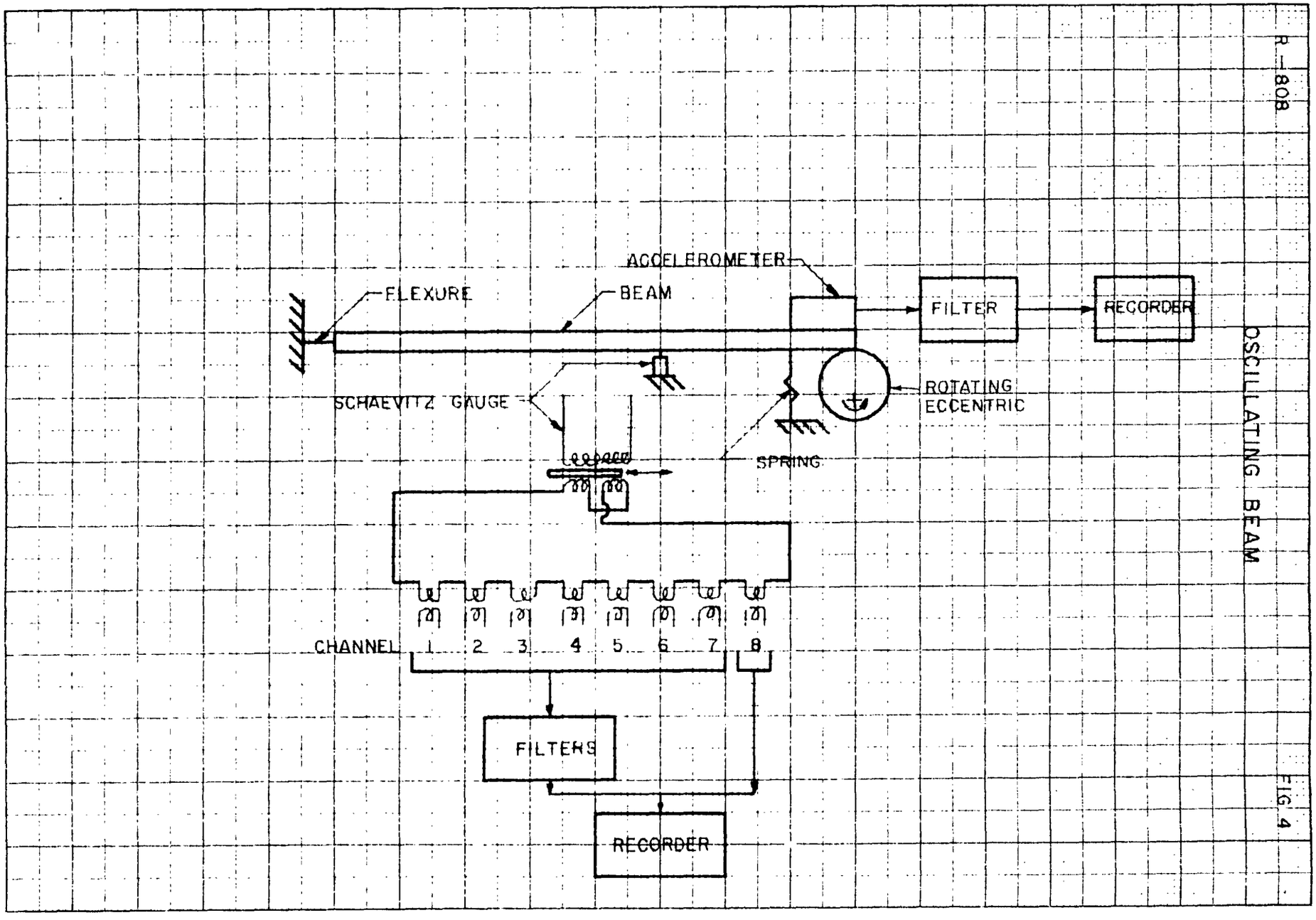
R-808
OSCILLATING BEAM
ACCELEROMETER
FLEXURE
BEAM
FILTER
RECORDER
ROTATING
ECCENTRIC
SCHAEVITZ GAUGE
SPRING
CHANNEL 1 2 3 4 5 6 7 8
FILTERS
RECORDER
FIG 4

FIG. 5

PHASE DIAGRAM

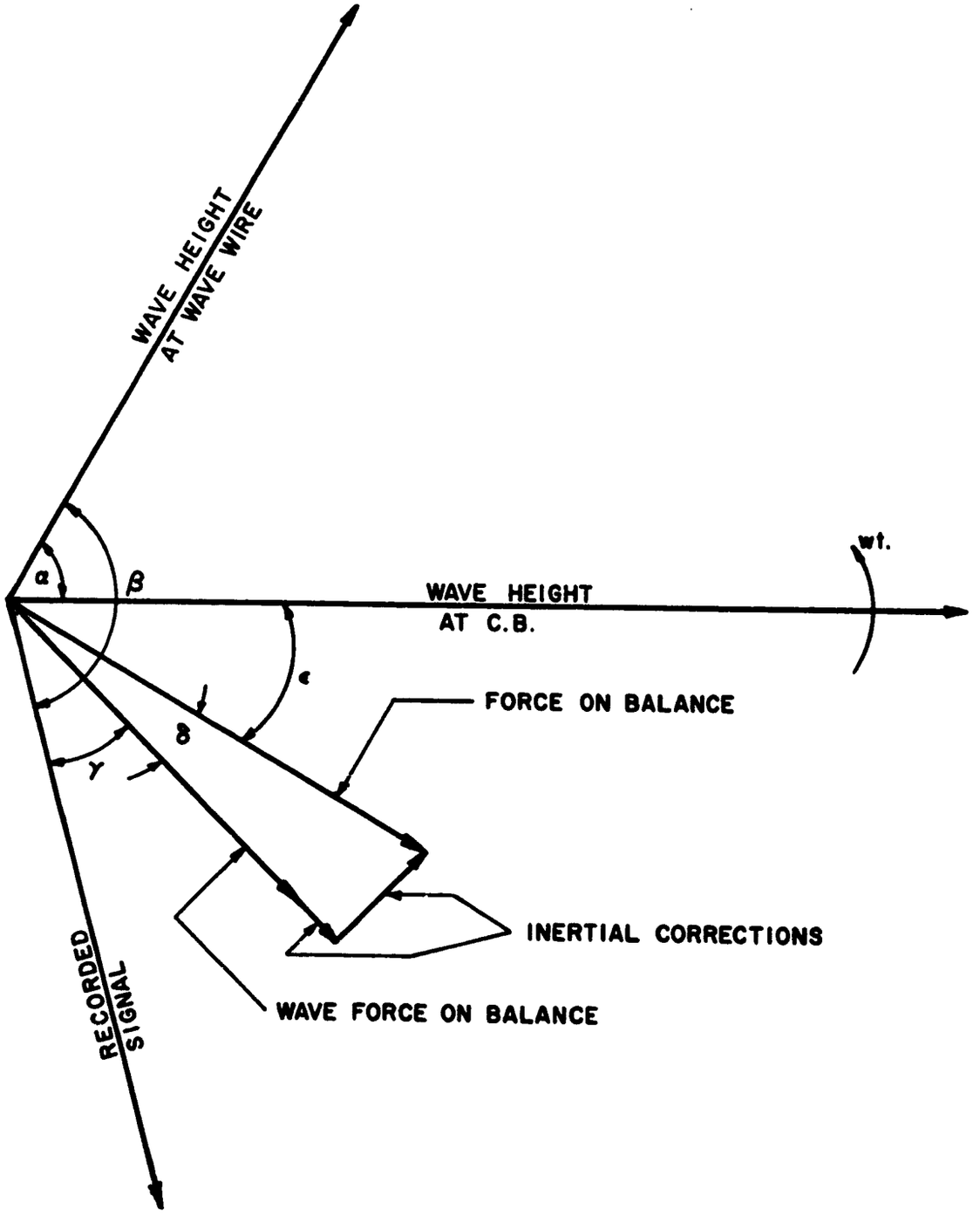

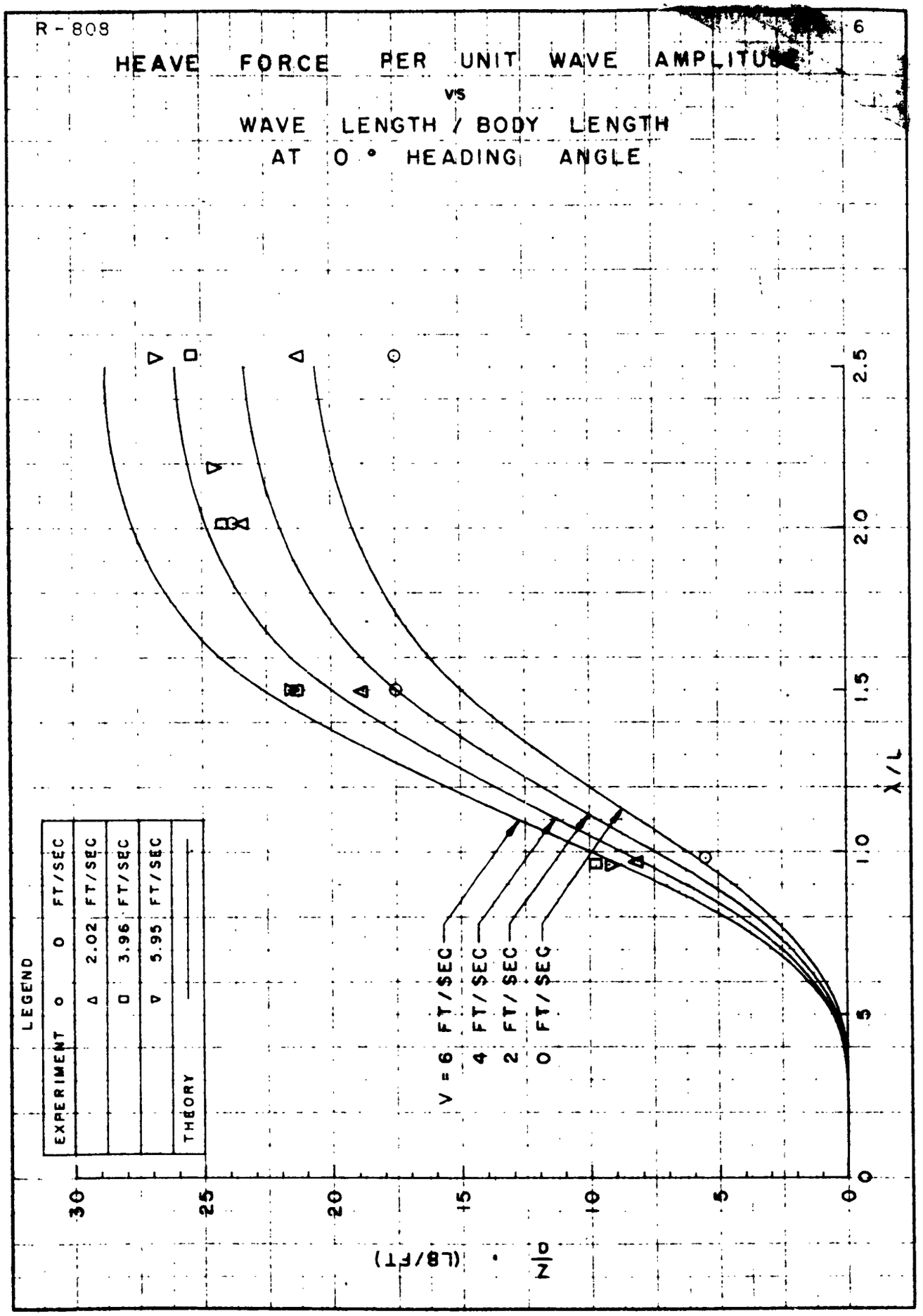
R - 808
6
HEAVE FORCE PER UNIT WAVE AMPLITUDE
VS
WAVE LENGTH / BODY LENGTH
AT 0 ° HEADING ANGLE
LEGEND
EXPERIMENT
0 FT/SEC
2.02 FT/SEC
3.96 FT/SEC
5.95 FT/SEC
THEORY
V = 6 FT/SEC
4 FT/SEC
2 FT/SEC
0 FT/SEC
λ/L
0
.5
1.0
1.5
2.0
2.5
0
5
10
15
20
25
30
(LB/FT)

R-808

FIG. 7

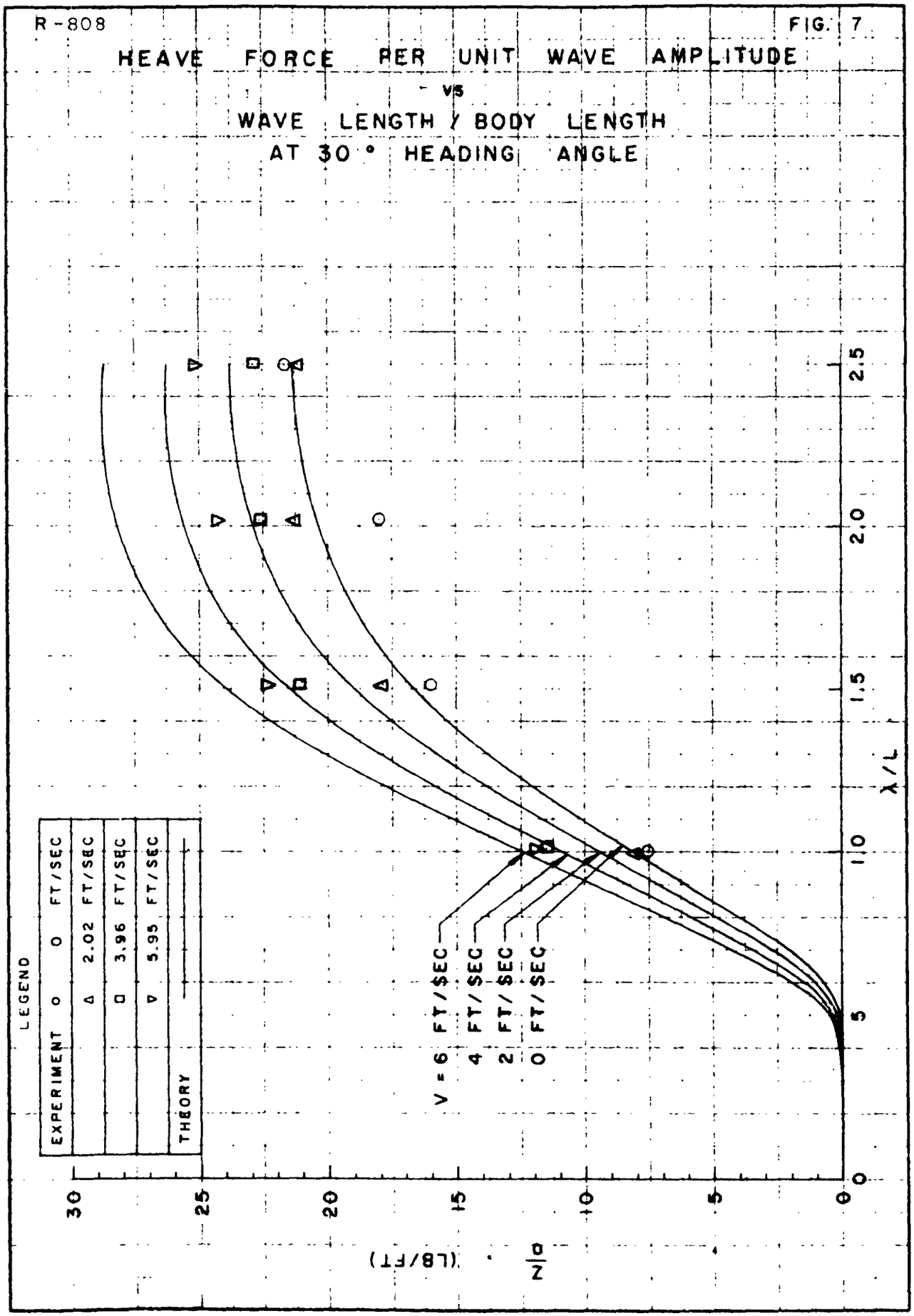
HEAVE FORCE PER UNIT WAVE AMPLITUDE
VS
WAVE LENGTH / BODY LENGTH
AT 30° HEADING ANGLE
LEGEND
EXPERIMENT
○ 0 FT/SEC
△ 2.02 FT/SEC
□ 3.96 FT/SEC
▽ 5.95 FT/SEC
THEORY
V = 6 FT/SEC
4 FT/SEC
2 FT/SEC
0 FT/SEC
λ/L
0
.5
1.0
1.5
2.0
2.5
30
25
20
15
10
5
0
N/a (LB/FT)

R-808

FIG. 8

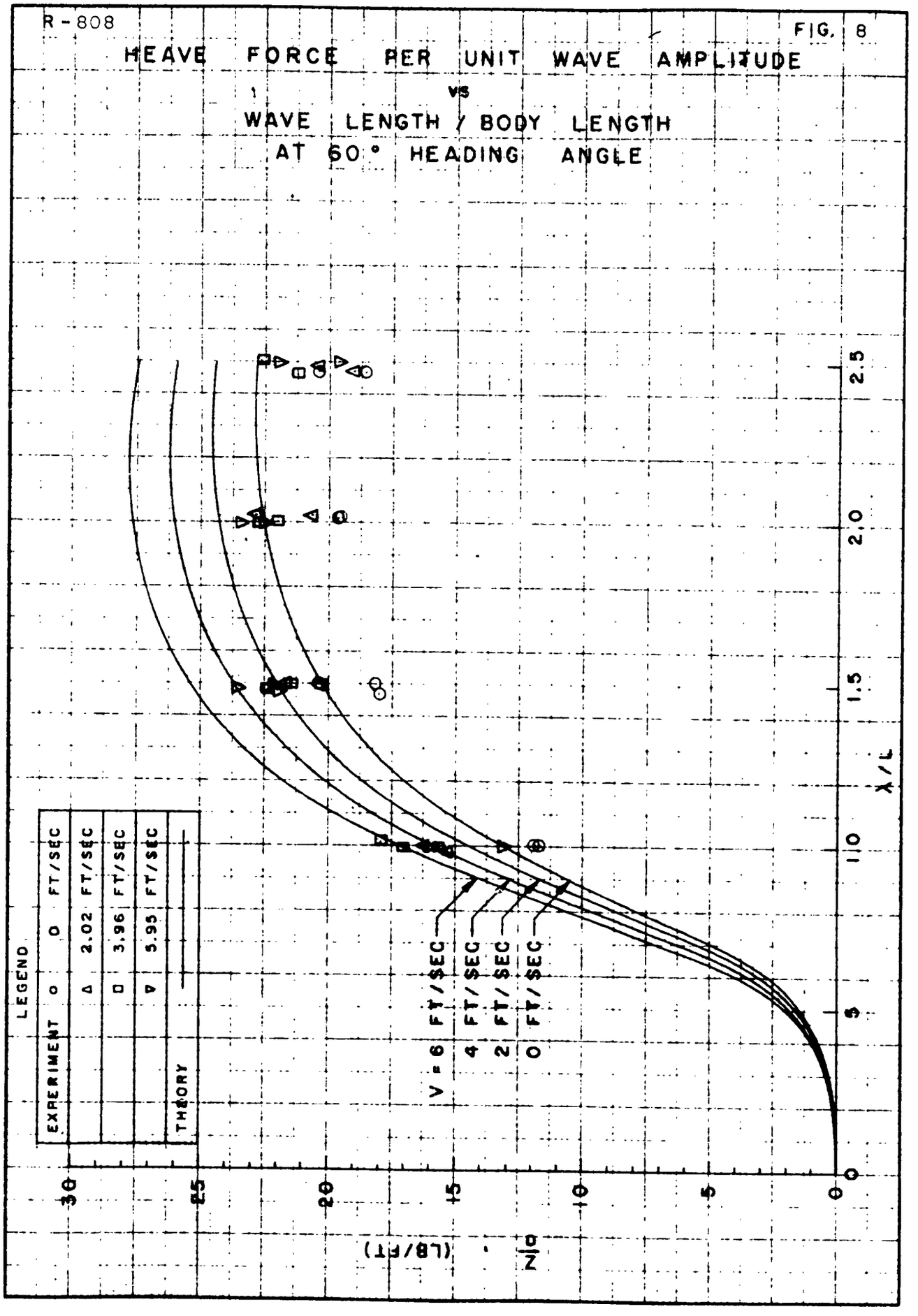
HEAVE FORCE PER UNIT WAVE AMPLITUDE
VS
WAVE LENGTH / BODY LENGTH
AT 60° HEADING ANGLE
LEGEND
EXPERIMENT
○ 0 FT/SEC
△ 2.02 FT/SEC
□ 3.96 FT/SEC
▽ 5.95 FT/SEC
THEORY
V = 6 FT/SEC
4 FT/SEC
2 FT/SEC
0 FT/SEC
λ/L
0
.5
1.0
1.5
2.0
2.5
0
5
10
15
20
25
30
(LB/FT) · Z/a

FIG. 9

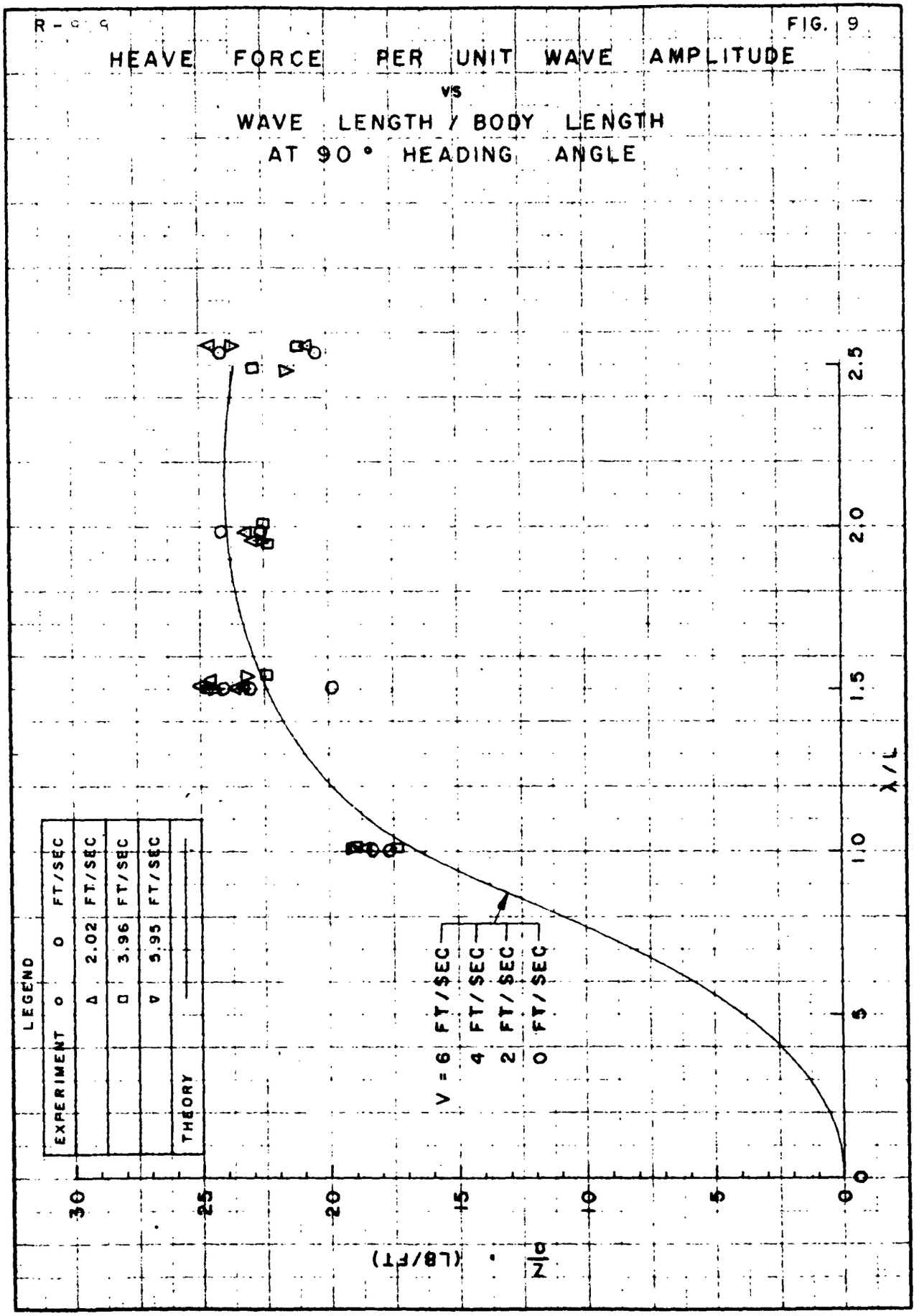
HEAVE FORCE PER UNIT WAVE AMPLITUDE
VS
WAVE LENGTH / BODY LENGTH
AT 90° HEADING ANGLE
LEGEND
EXPERIMENT
○ 0 FT/SEC
△ 2.02 FT/SEC
□ 3.96 FT/SEC
▽ 5.95 FT/SEC
THEORY
V = 6 FT/SEC
4 FT/SEC
2 FT/SEC
0 FT/SEC
λ/L
0
.5
1.0
1.5
2.0
2.5
0
5
10
15
20
25
30
(LB/FT) / a

R-808

FIG. 10

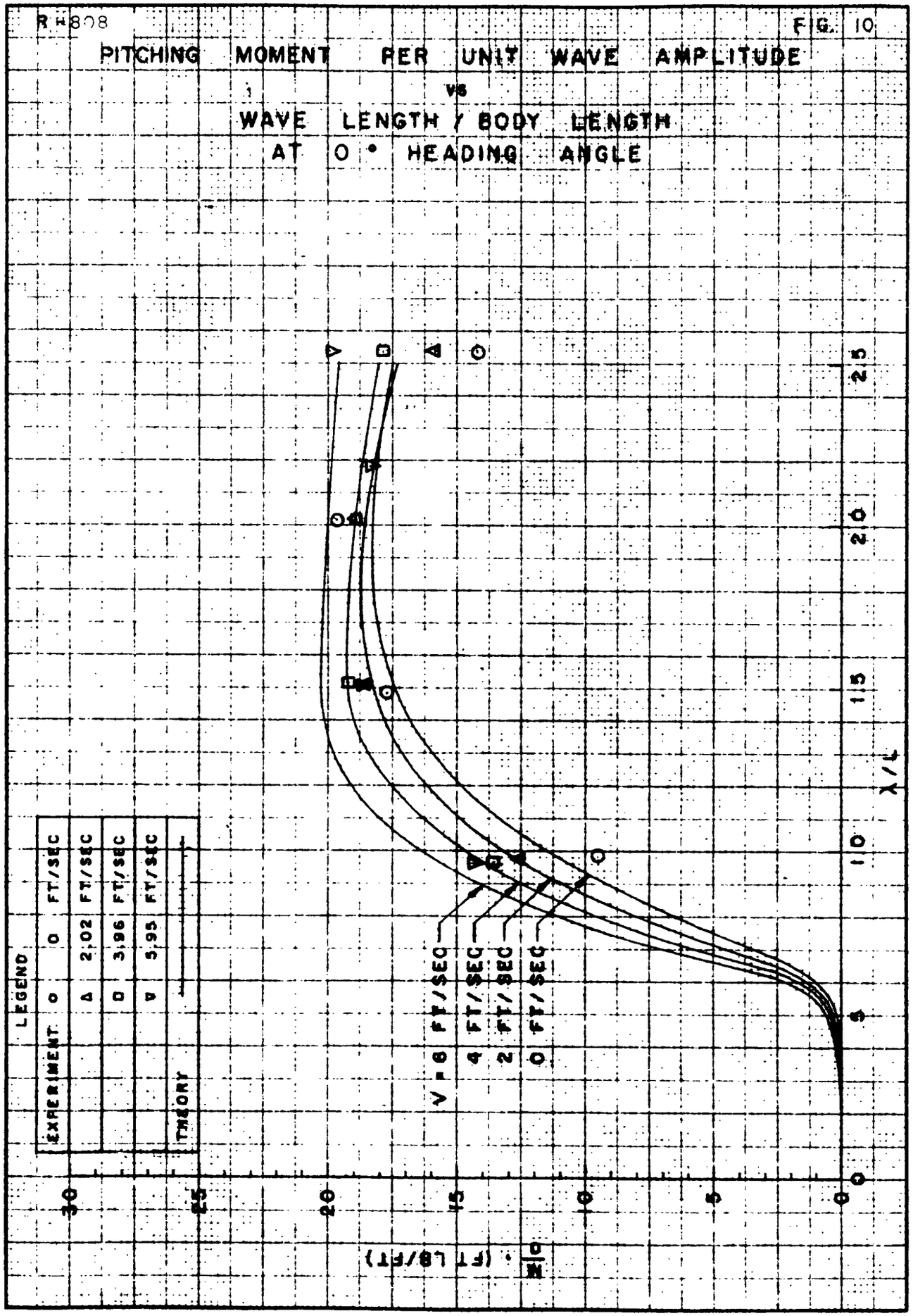
PITCHING MOMENT PER UNIT WAVE AMPLITUDE
VS
WAVE LENGTH / BODY LENGTH
AT 0 ° HEADING ANGLE
LEGEND
EXPERIMENT
○ 0 FT/SEC
△ 2.02 FT/SEC
□ 3.96 FT/SEC
▽ 5.95 FT/SEC
THEORY
V = 6 FT/SEC
4 FT/SEC
2 FT/SEC
0 FT/SEC
M/a (FT LB/FT)
λ/L

R-808

FIG. 11

PITCHING MOMENT PER UNIT WAVE AMPLITUDE

VS

WAVE LENGTH / BODY LENGTH

AT 30° HEADING ANGLE

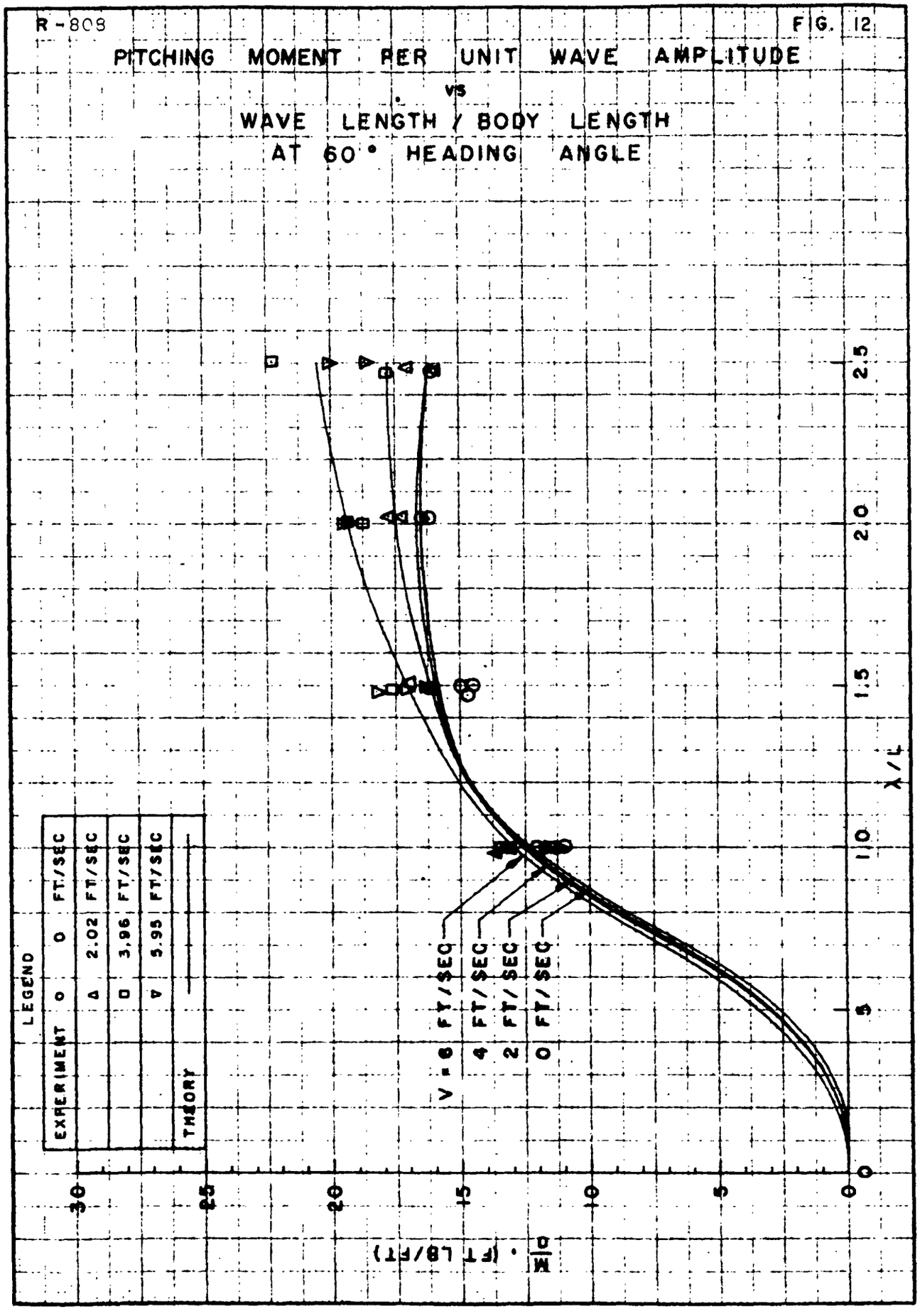
R-808
FIG. 12
PITCHING MOMENT PER UNIT WAVE AMPLITUDE
VS
WAVE LENGTH / BODY LENGTH
AT 60° HEADING ANGLE
LEGEND
EXPERIMENT
○ 0 FT/SEC
△ 2.02 FT/SEC
□ 3.96 FT/SEC
▽ 5.95 FT/SEC
THEORY
V = 6 FT/SEC
4 FT/SEC
2 FT/SEC
0 FT/SEC
M/a (FT LB/FT)
-30
-25
-20
-15
-10
-5
0
λ/L
0
.5
1.0
1.5
2.0
2.5

R - 808

FIG. 13

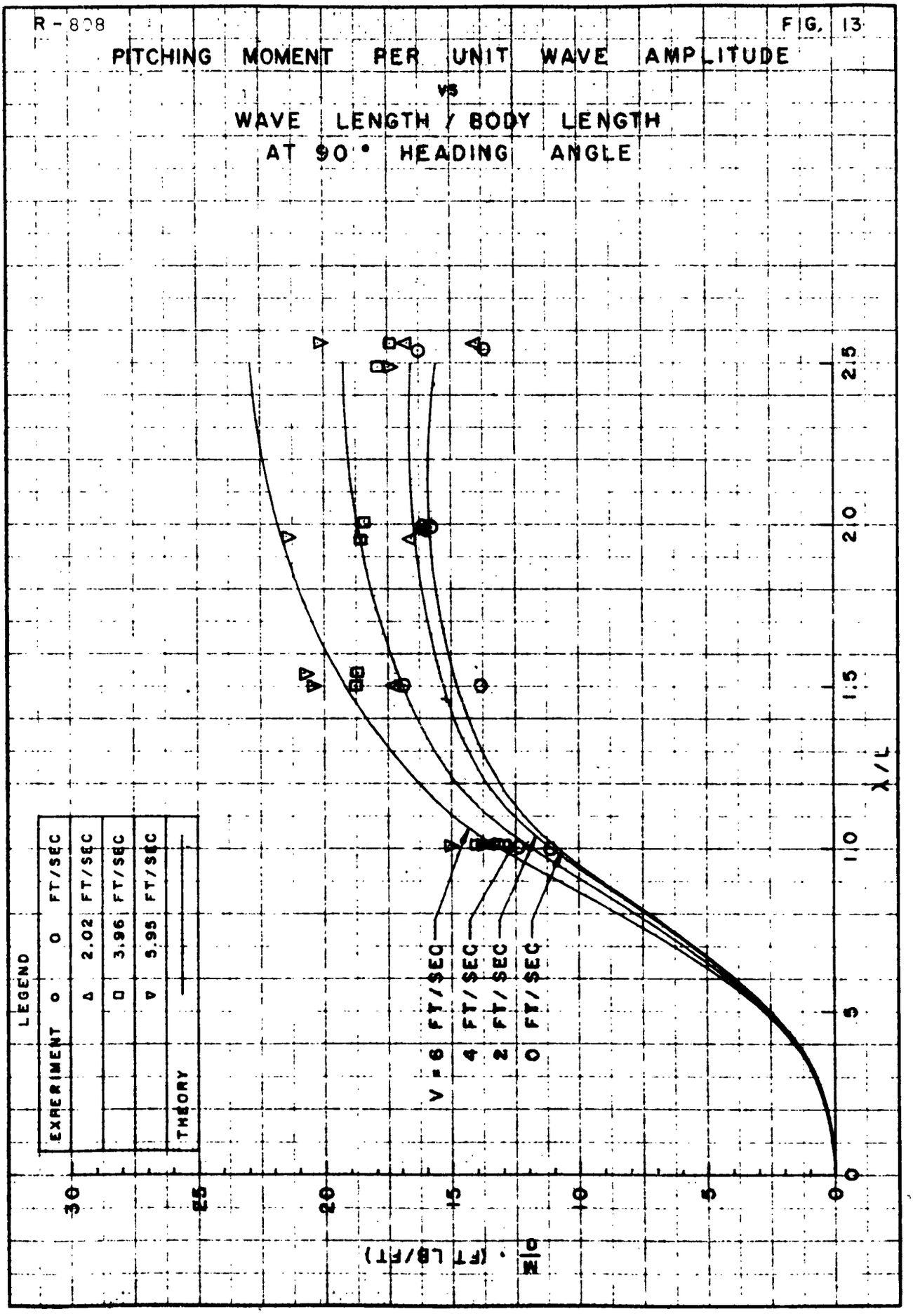
PITCHING MOMENT PER UNIT WAVE AMPLITUDE
VS
WAVE LENGTH / BODY LENGTH
AT 90° HEADING ANGLE
LEGEND
EXPERIMENT
0 FT/SEC
2.02 FT/SEC
3.96 FT/SEC
5.95 FT/SEC
THEORY
V = 6 FT/SEC
4 FT/SEC
2 FT/SEC
0 FT/SEC
λ/L
M/ρ (FT LB/FT)

R-809

FIG. 14

SIDE FORCE PER UNIT WAVE AMPLITUDE

VS

WAVE LENGTH / BODY LENGTH

AT 30° HEADING ANGLE

(WITHOUT CONNING TOWER)

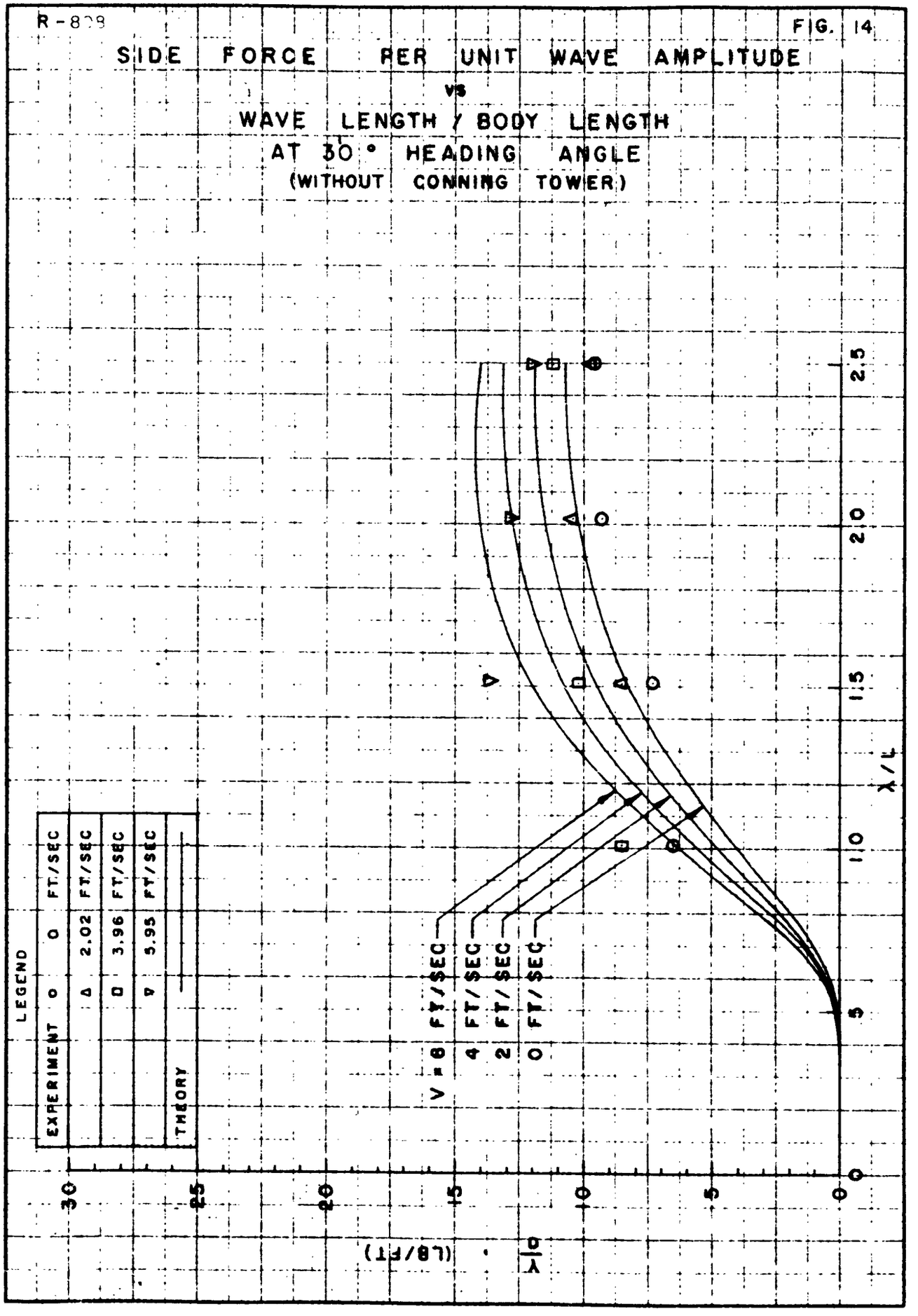

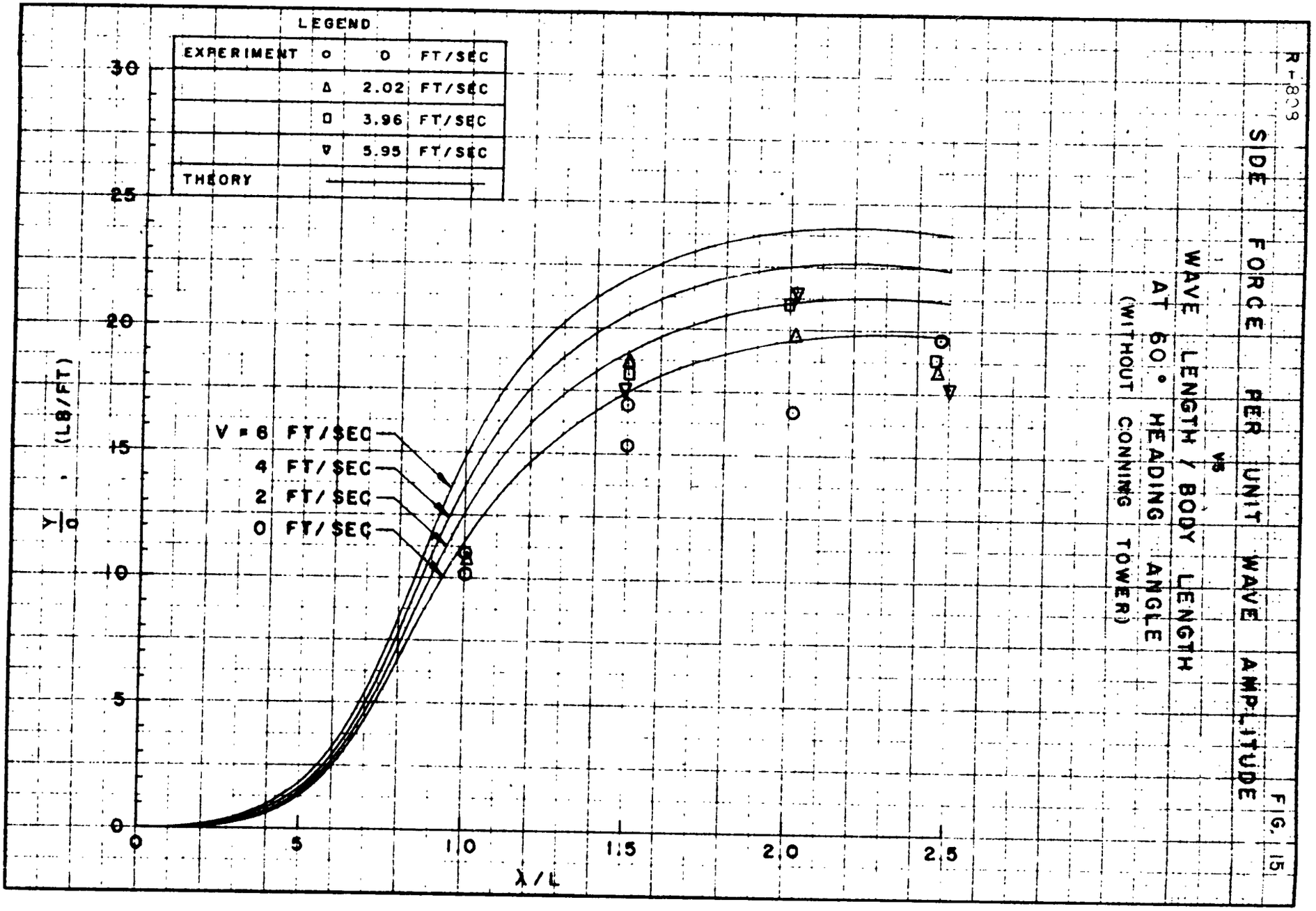
LEGEND
EXPERIMENT o 0 FT/SEC
Δ 2.02 FT/SEC
□ 3.96 FT/SEC
▽ 5.95 FT/SEC
THEORY
V = 6 FT/SEC
4 FT/SEC
2 FT/SEC
0 FT/SEC
Y/a (LB/FT)
λ/L
0
5
10
15
20
25
30
0
.5
1.0
1.5
2.0
2.5
SIDE FORCE PER UNIT WAVE AMPLITUDE
VS
WAVE LENGTH / BODY LENGTH
AT 60° HEADING ANGLE
(WITHOUT CONNING TOWER)
R-1809
FIG. 15

R-8 8

FIG. 16

SIDE FORCE PER UNIT WAVE AMPLITUDE

vs

WAVE LENGTH / BODY LENGTH

AT 90° HEADING ANGLE

(WITHOUT CONNING TOWER)

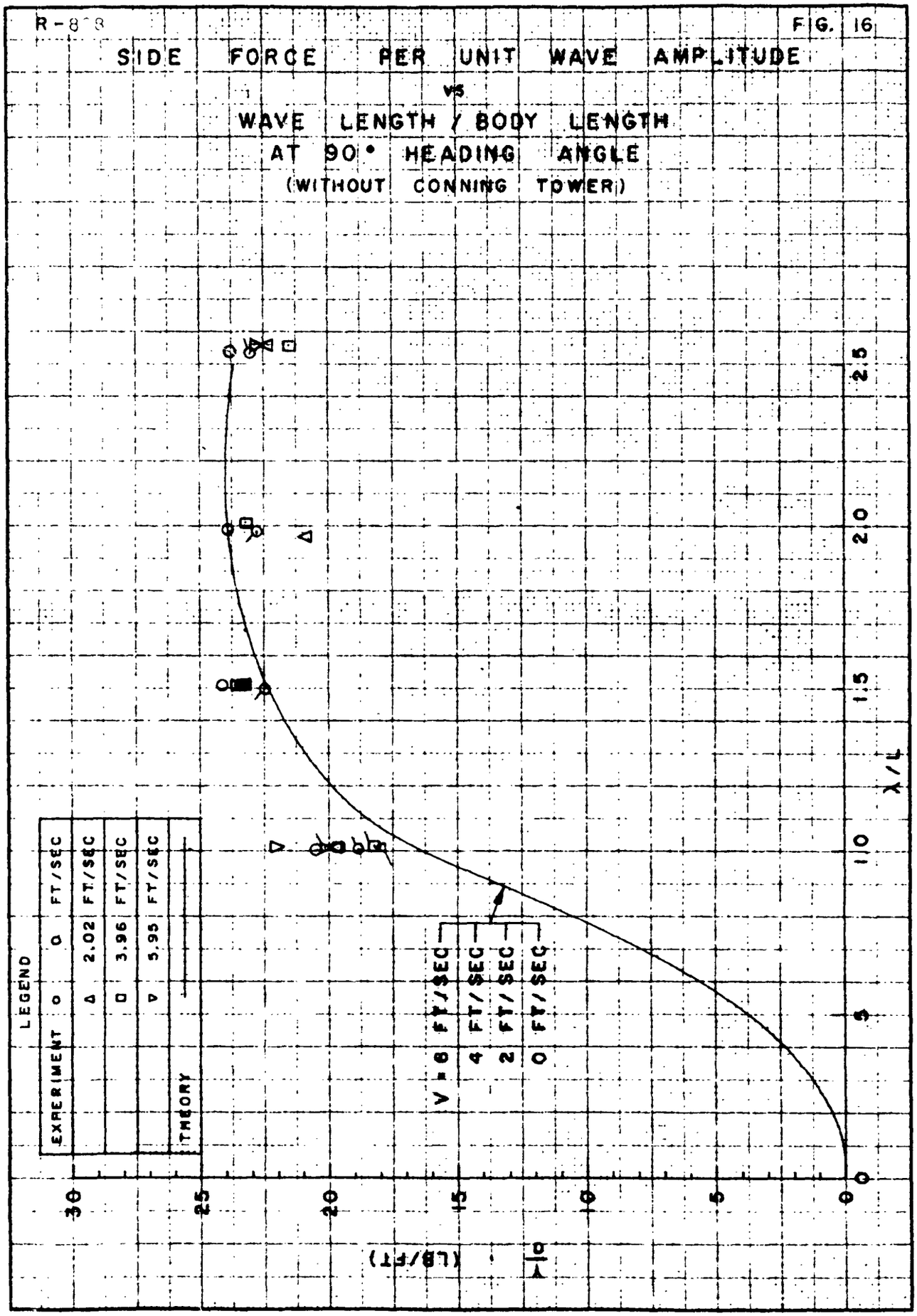

R-[illegible]

FIG. 17

YAWING MOMENT PER UNIT WAVE AMPLITUDE

VS

WAVE LENGTH / BODY LENGTH

AT 30° HEADING ANGLE

(WITHOUT CONNING TOWER)

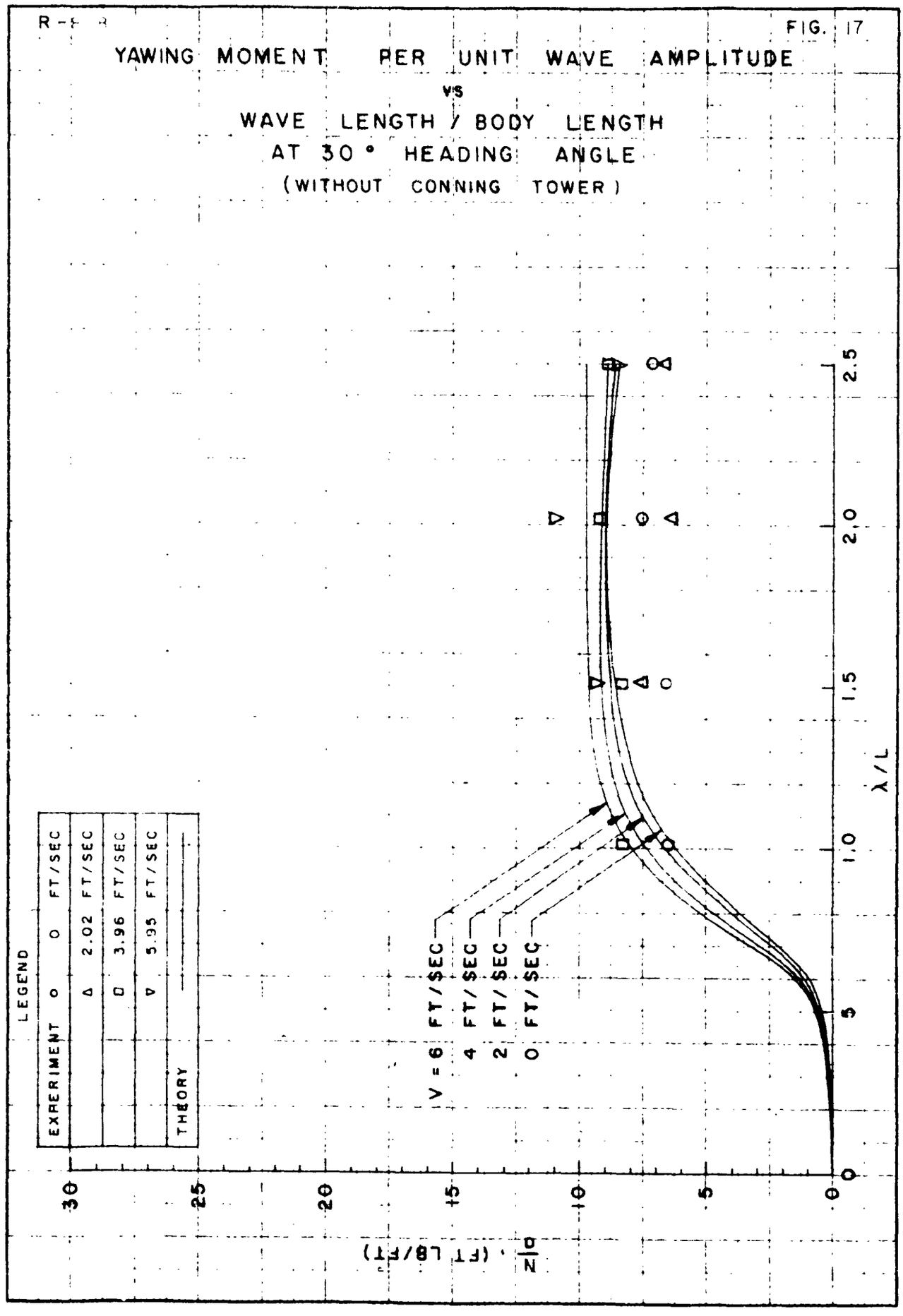

R-808

FIG. 18

YAWING MOMENT PER UNIT WAVE AMPLITUDE
VS
WAVE LENGTH / BODY LENGTH
AT 60° HEADING ANGLE
(WITHOUT CONNING TOWER)

R - 868

FIG. 19

YAWING MOMENT PER UNIT WAVE AMPLITUDE

VS.

WAVE LENGTH / BODY LENGTH

AT 90° HEADING ANGLE

(WITHOUT CONNING TOWER)

R-808

FIG. 20

SIDE FORCE PER UNIT WAVE AMPLITUDE

VS

WAVE LENGTH / BODY LENGTH

AT 30° HEADING ANGLE

(WITH CONNING TOWER)

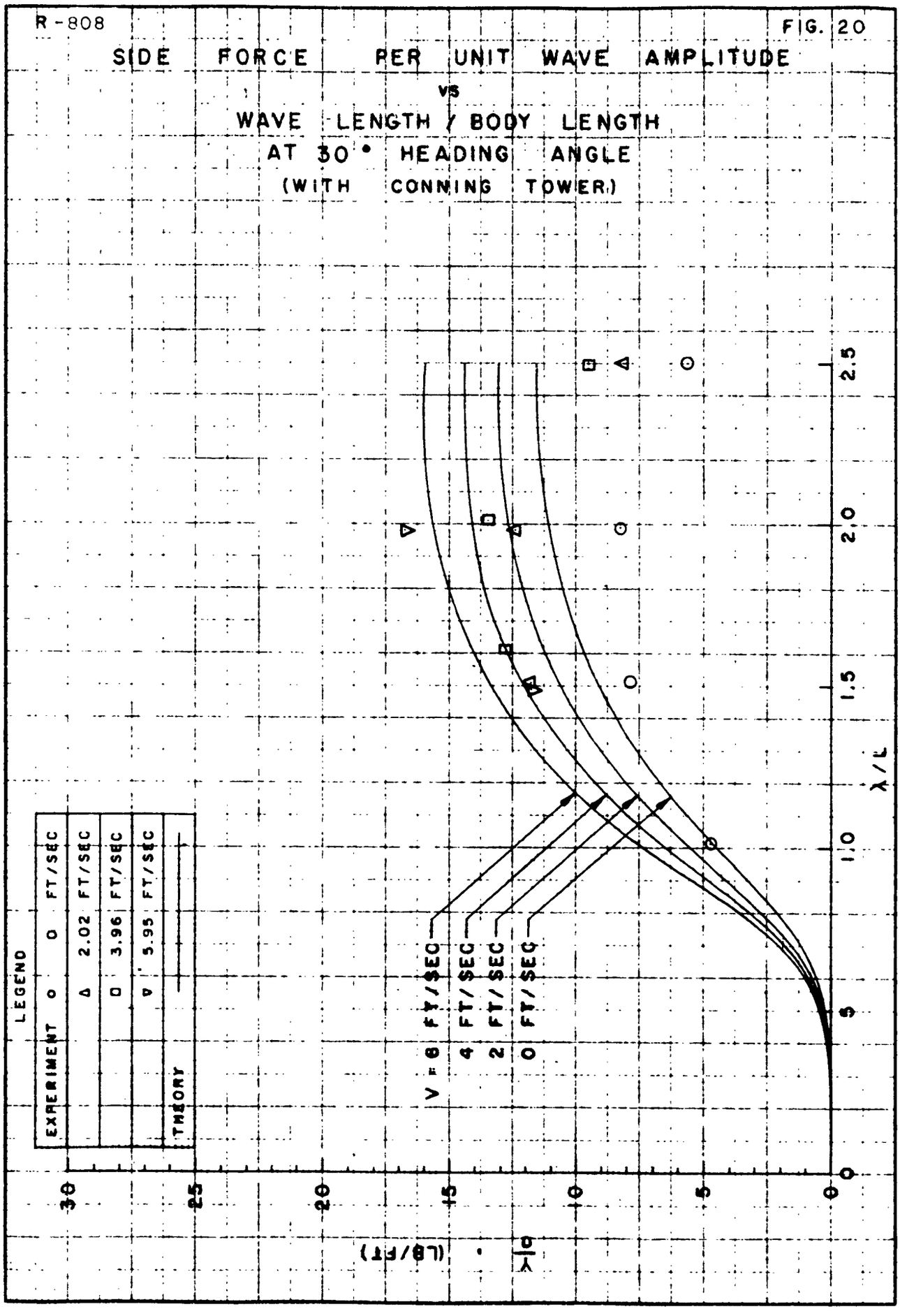

R-808

FIG. 21

SIDE FORCE PER UNIT WAVE AMPLITUDE

VS

WAVE LENGTH / BODY LENGTH

AT 60° HEADING ANGLE

(WITH CONNING TOWER)

R-808

FIG. 22

SIDE FORCE PER UNIT WAVE AMPLITUDE

VS

WAVE LENGTH / BODY LENGTH

AT 90° HEADING ANGLE

(WITH CONNING TOWER)

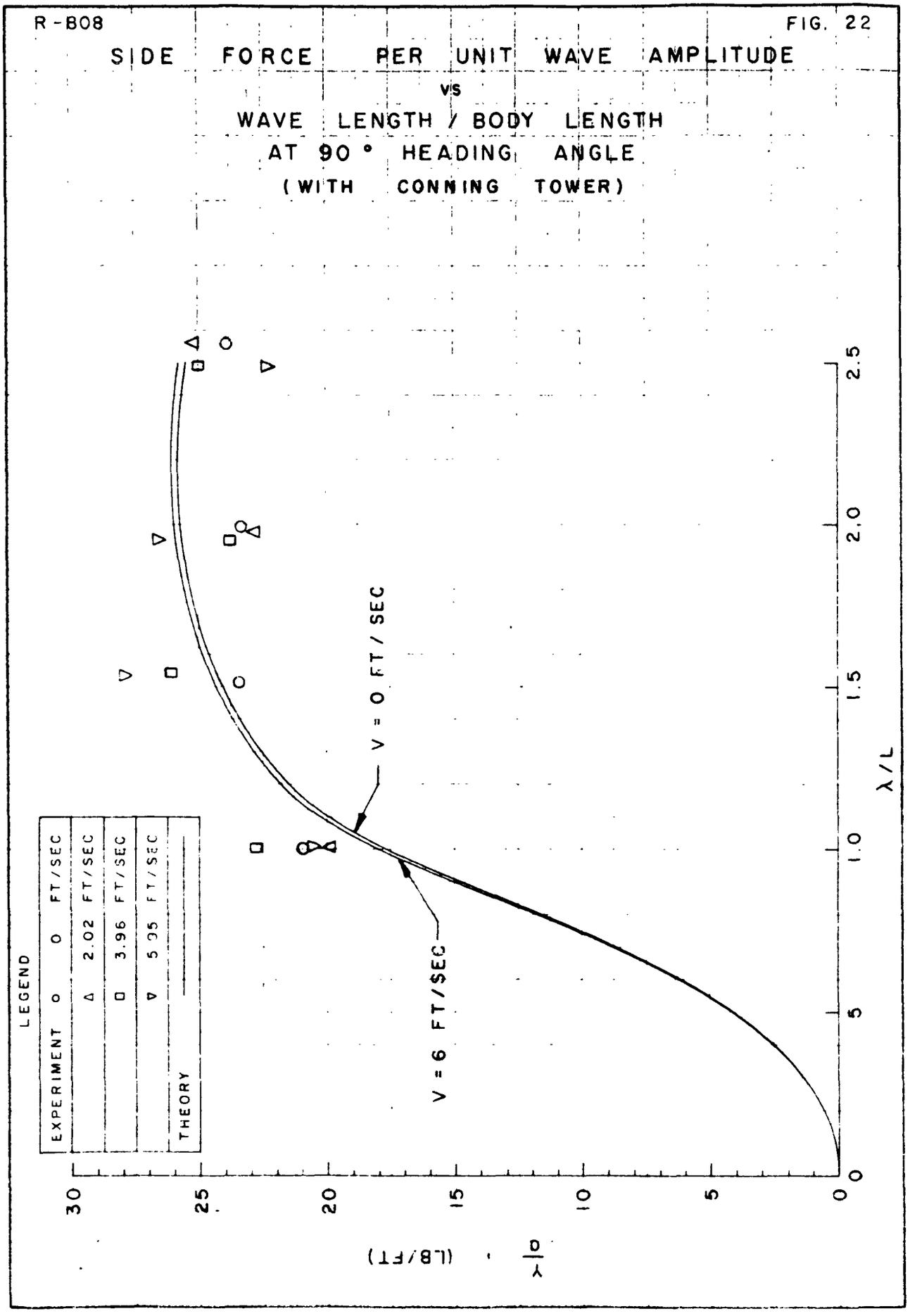

R-808

FIG. 23

YAWING MOMENT PER UNIT WAVE AMPLITUDE

vs

WAVE LENGTH / BODY LENGTH

AT 30° HEADING ANGLE

(WITH CONNING TOWER)

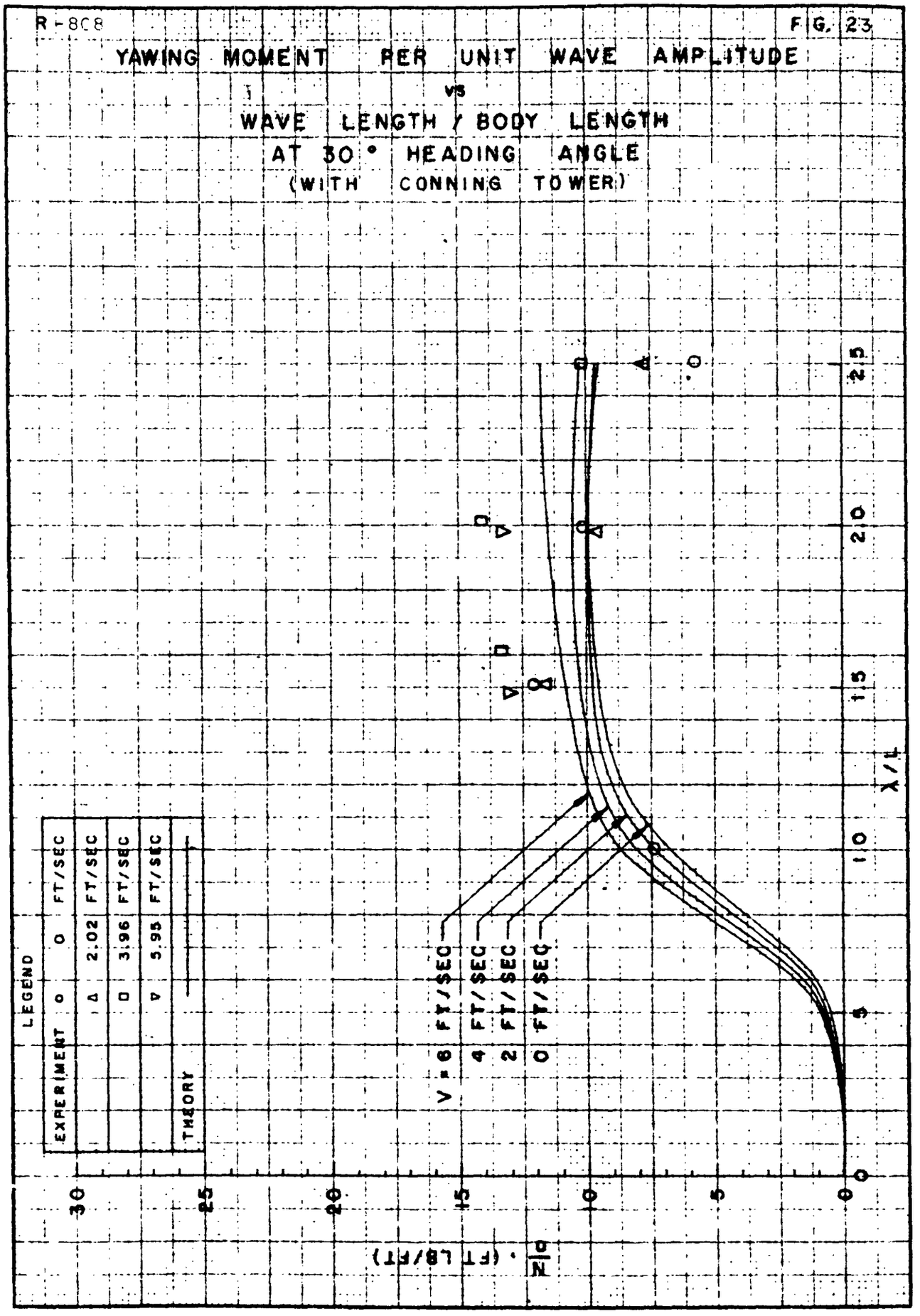

R-808

FIG. 24

YAWING MOMENT PER UNIT WAVE AMPLITUDE

vs

WAVE LENGTH / BODY LENGTH

AT 60° HEADING ANGLE

(WITH CONNING TOWER)

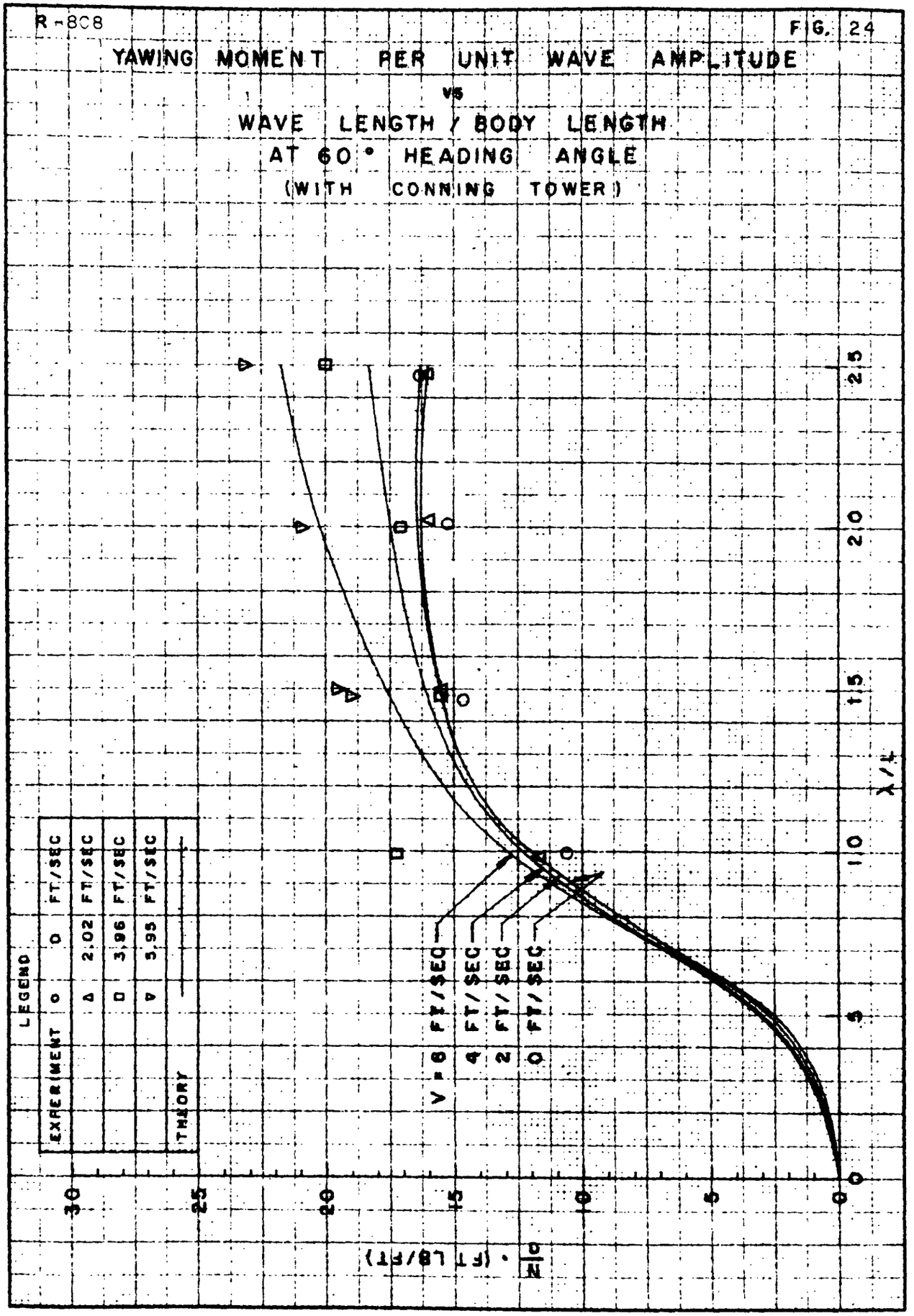

R-808

FIG. 25

YAWING MOMENT PER UNIT WAVE AMPLITUDE

VS

WAVE LENGTH / BODY LENGTH

AT 90° HEADING ANGLE

(WITH CONNING TOWER)

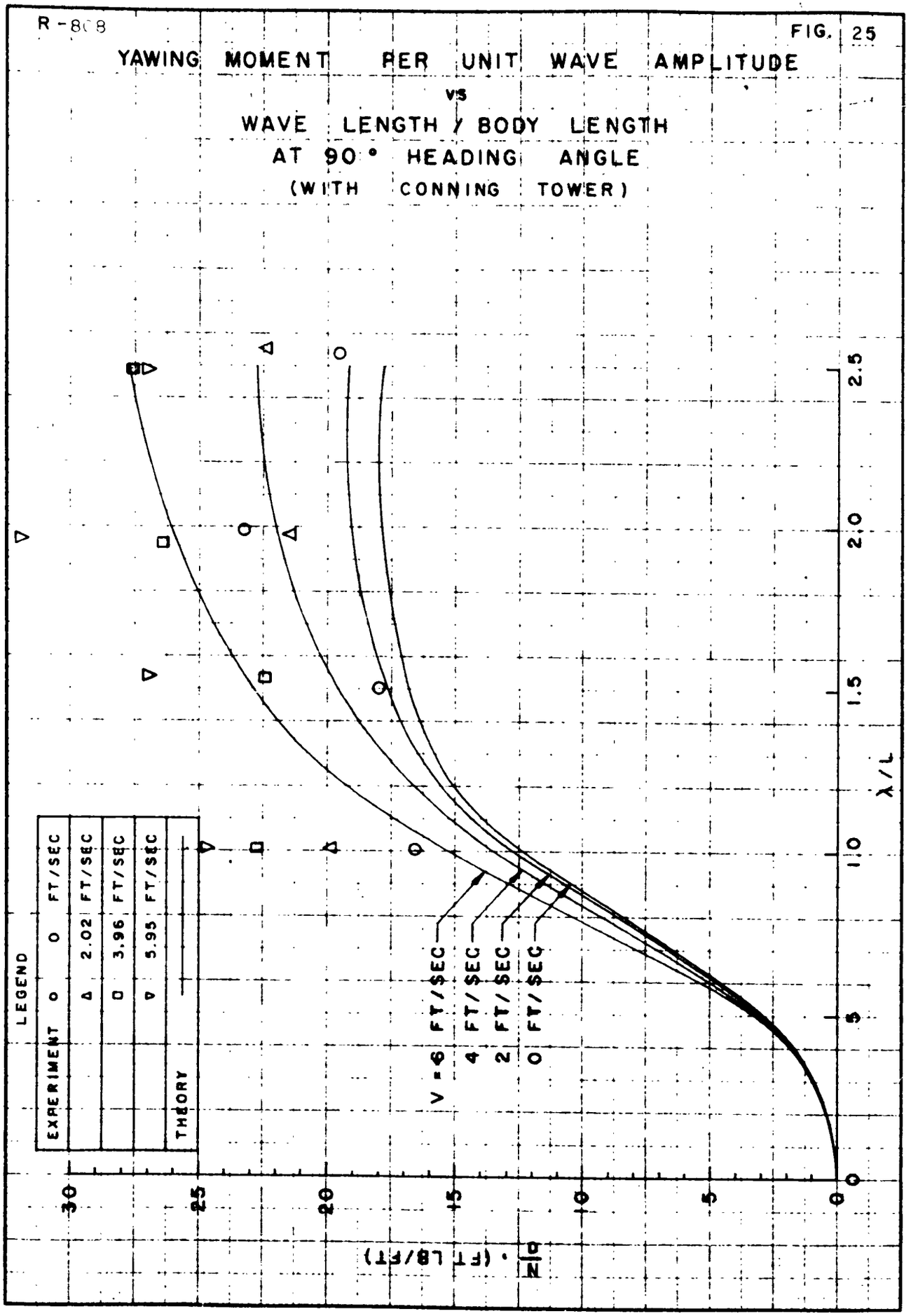

R-808

FIG. 26

ROLL MOMENT PER UNIT WAVE AMPLITUDE

vs

WAVE LENGTH / BODY LENGTH

AT 30° HEADING ANGLE

(WITH CONNING TOWER)

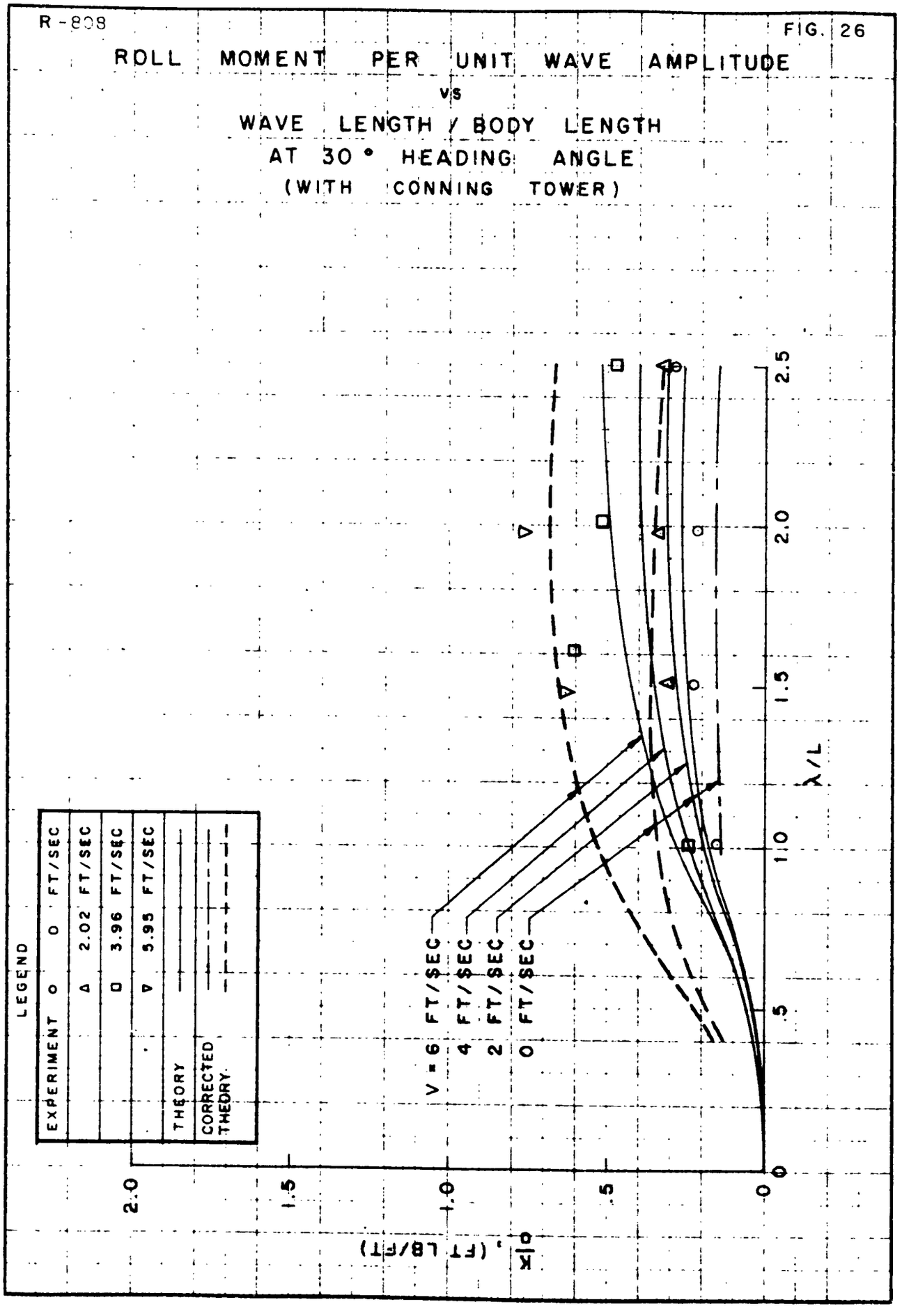

R-808

FIG. 27

ROLL MOMENT PER UNIT WAVE AMPLITUDE

vs

WAVE LENGTH / BODY LENGTH

AT 60° HEADING ANGLE

(WITH CONNING TOWER)

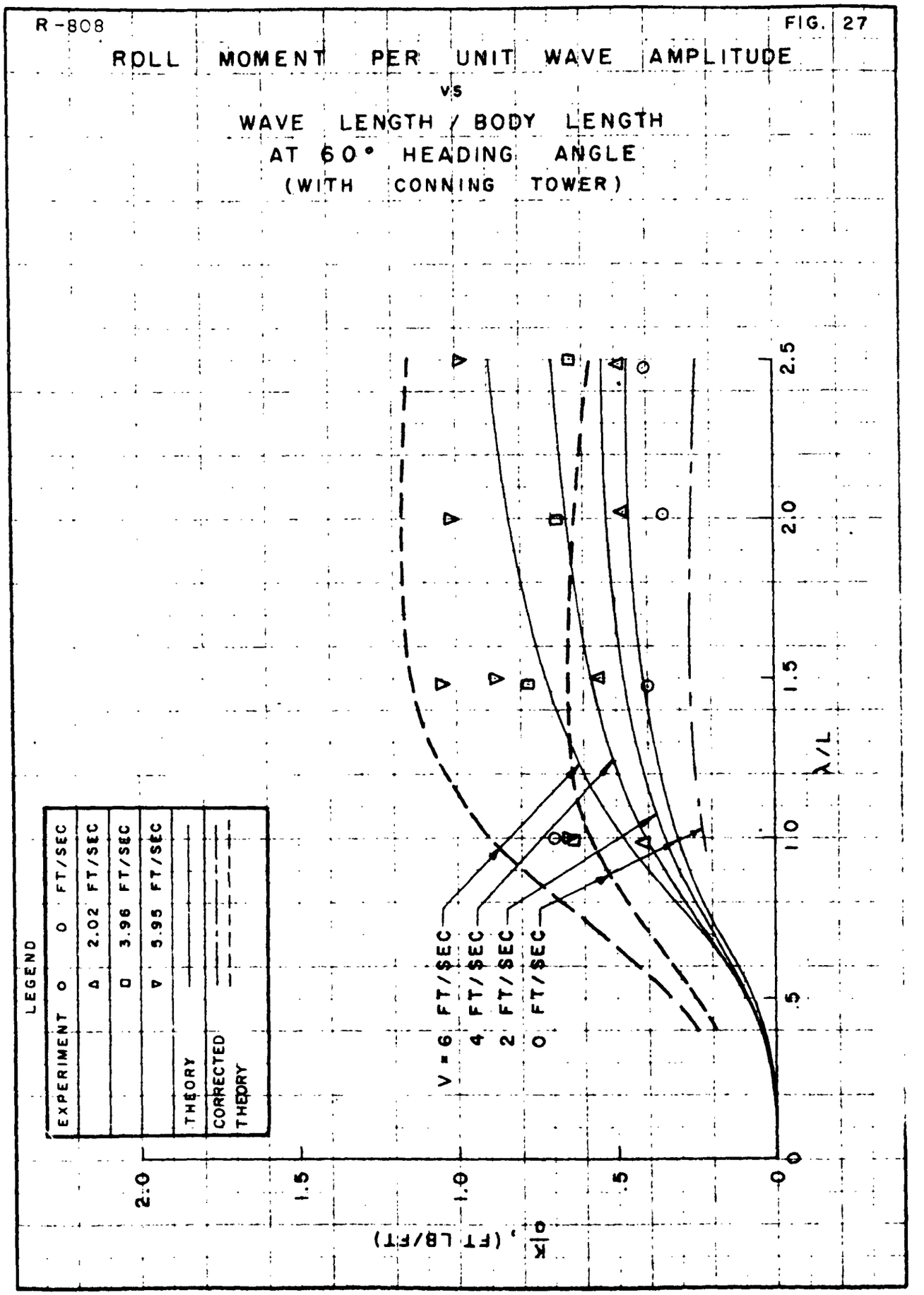

R-808

FIG. 28

ROLL MOMENT PER UNIT WAVE AMPLITUDE

vs

WAVE LENGTH / BODY LENGTH

AT 90° HEADING ANGLE

(WITH CONNING TOWER)

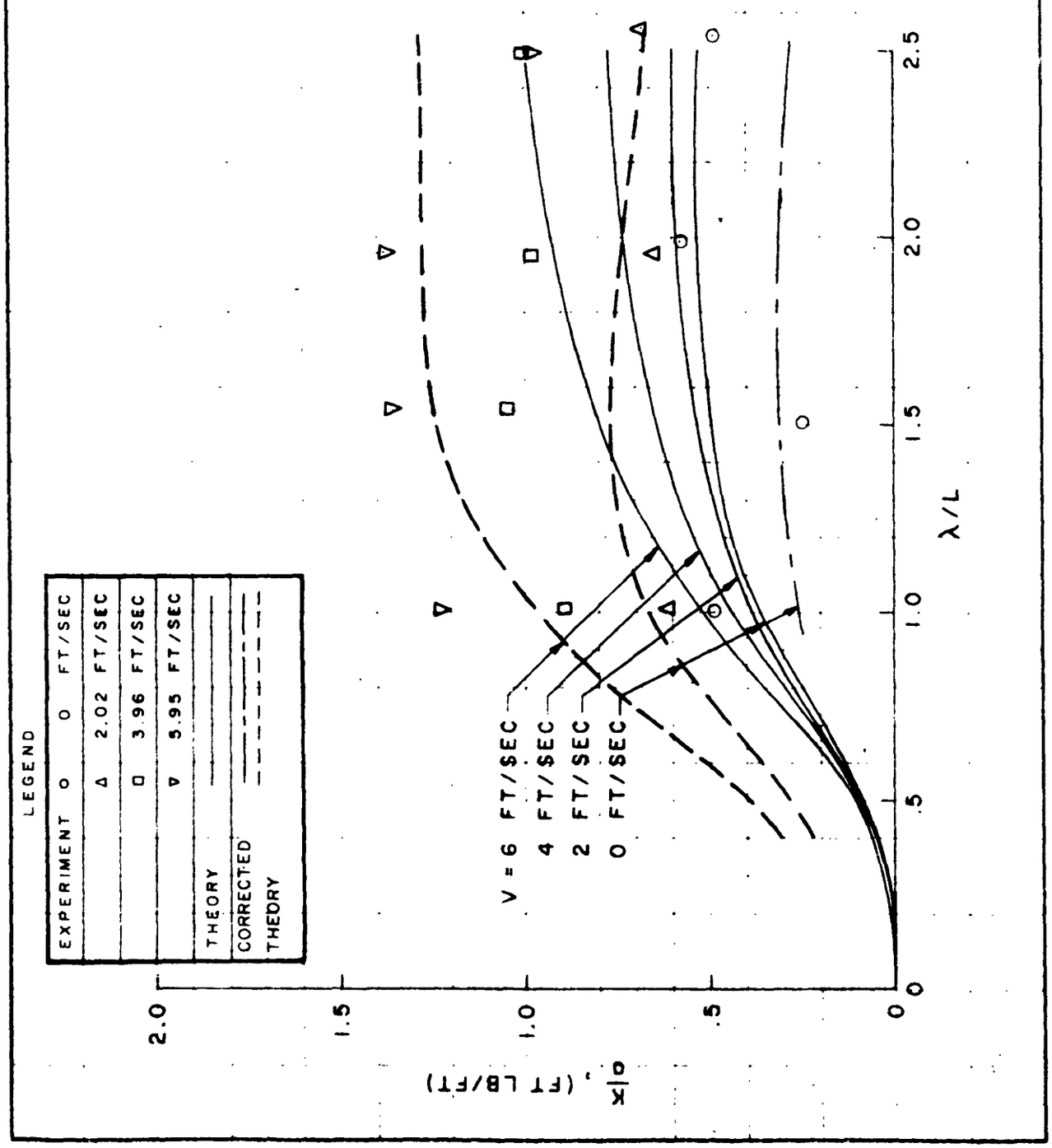

R - 808

FIG 29

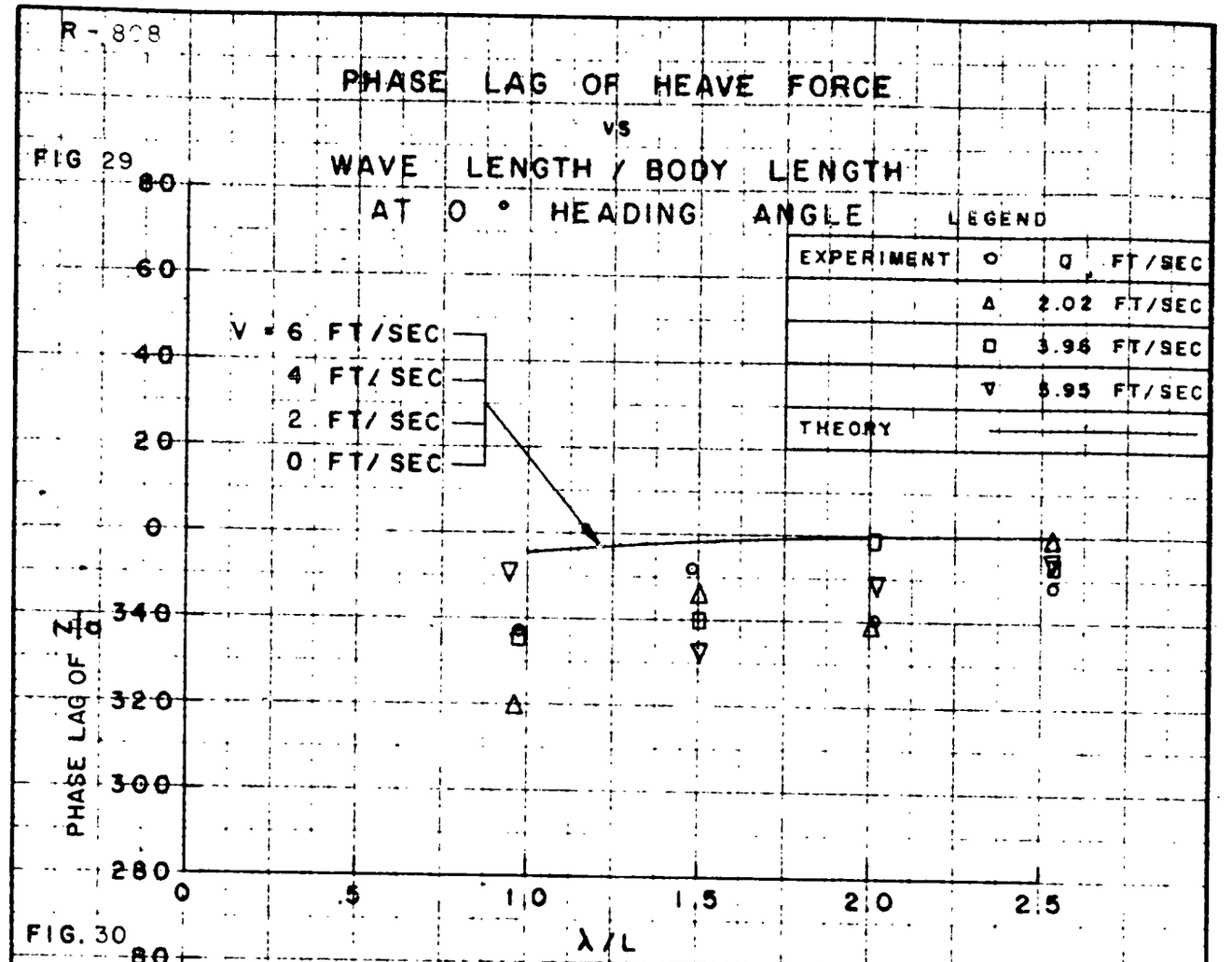

FIG. 30

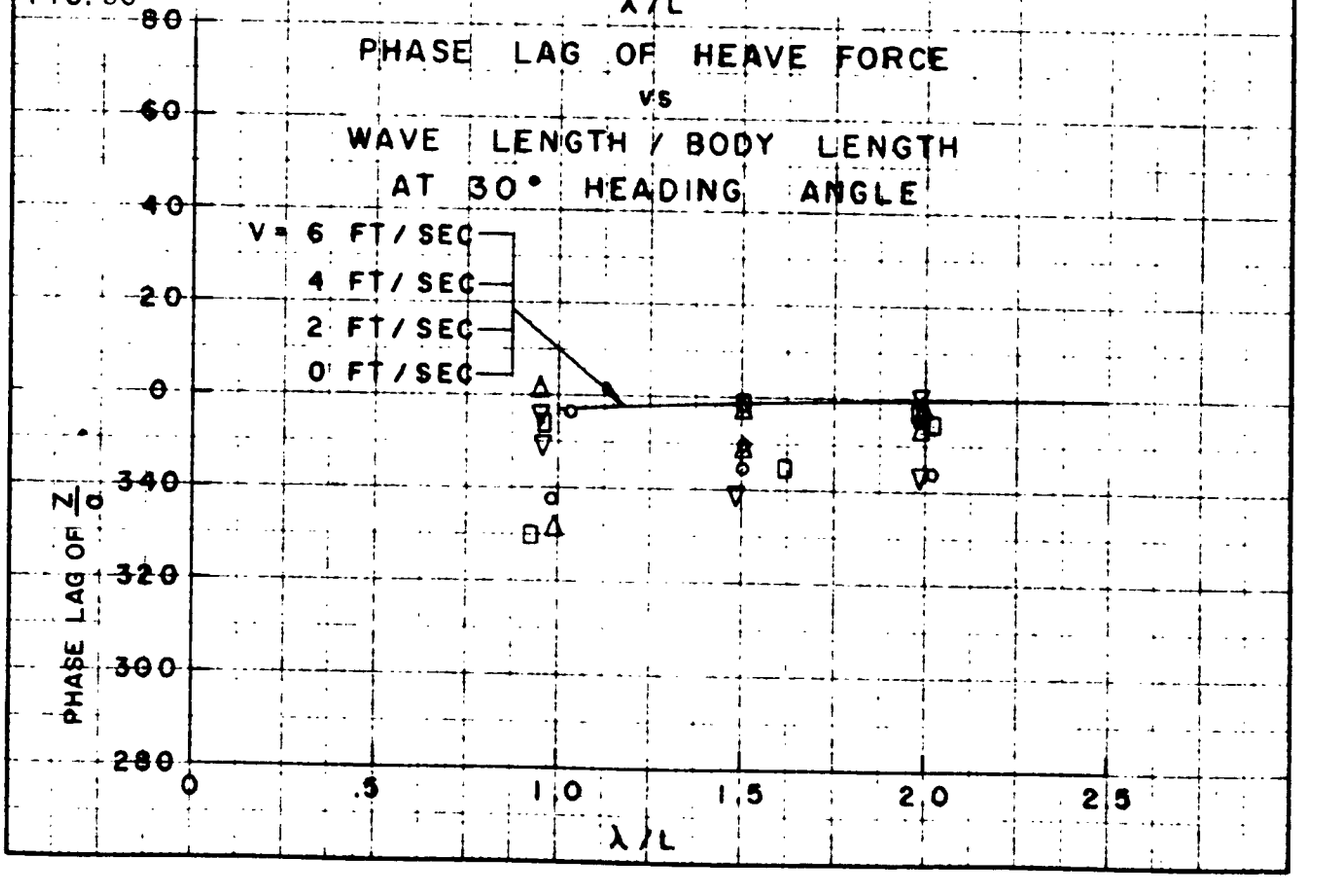

R-1808

FIG. 31

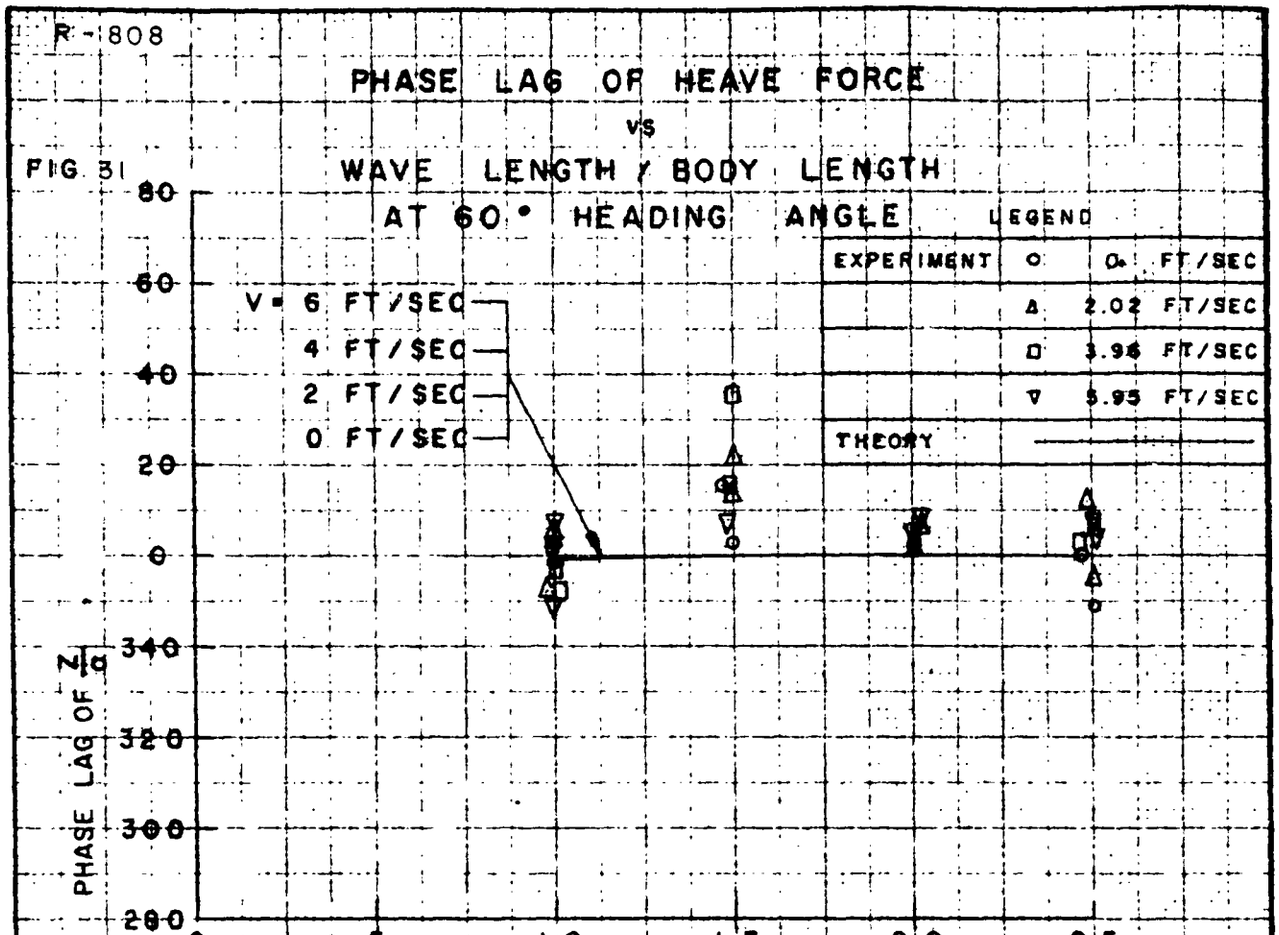

FIG. 32

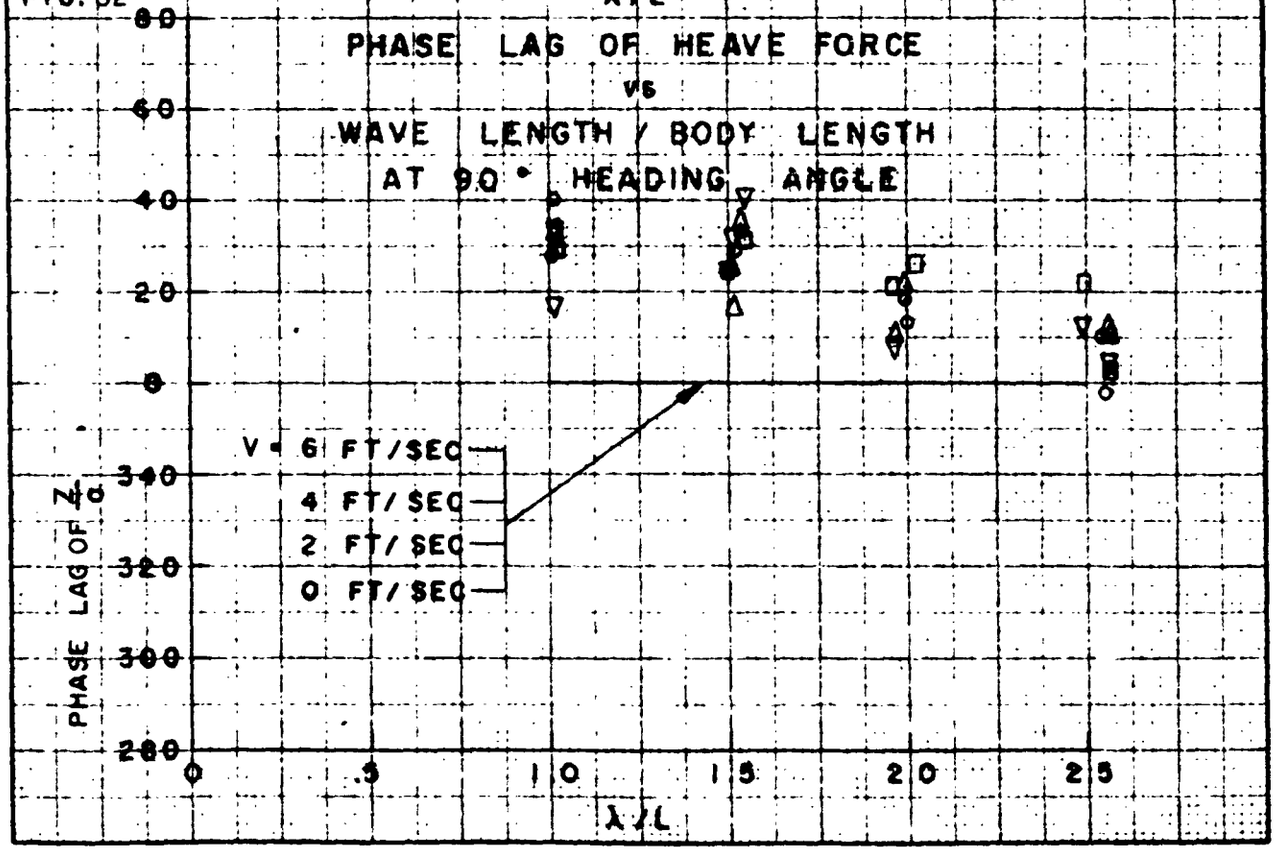

R-862

FIG 33

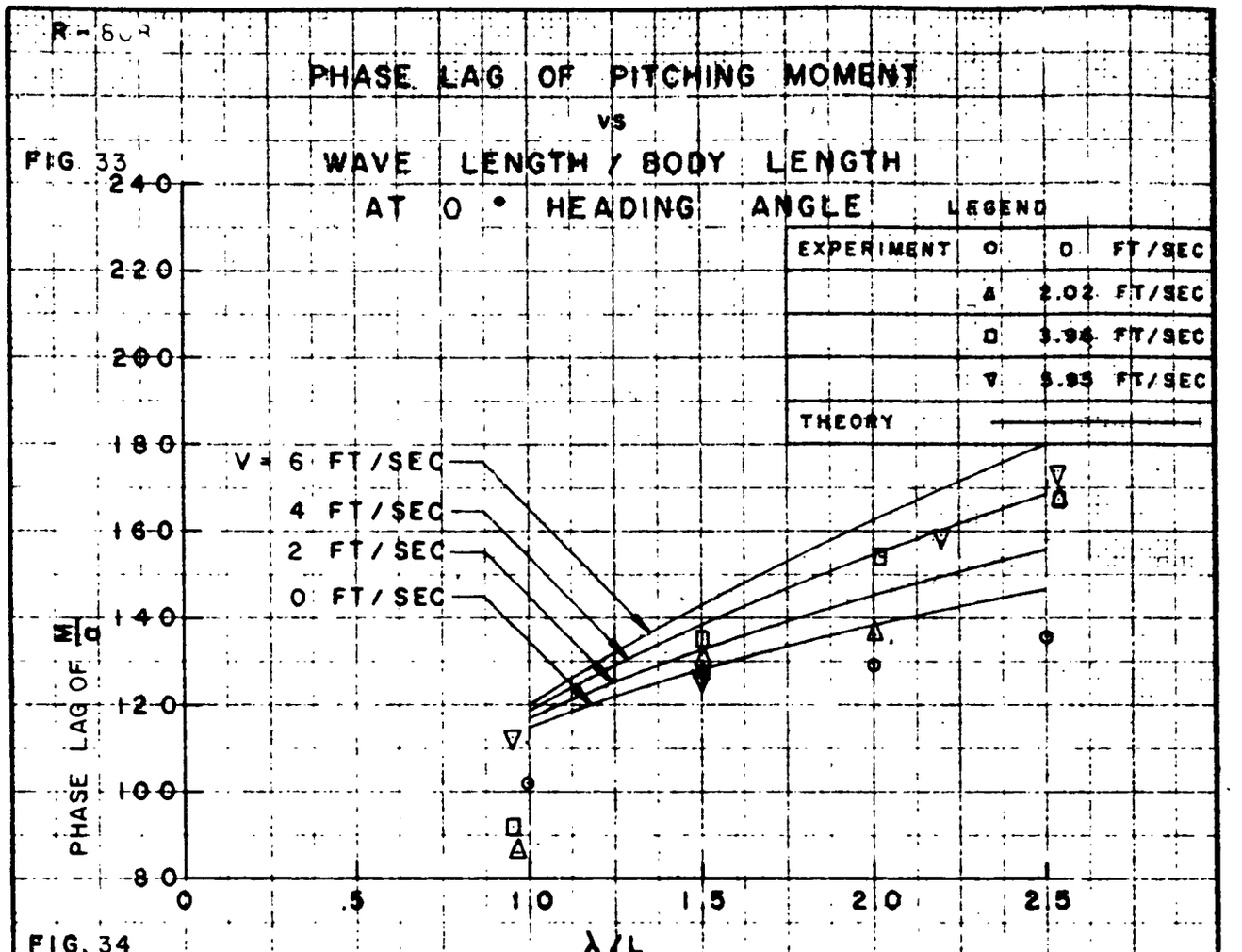

FIG. 34

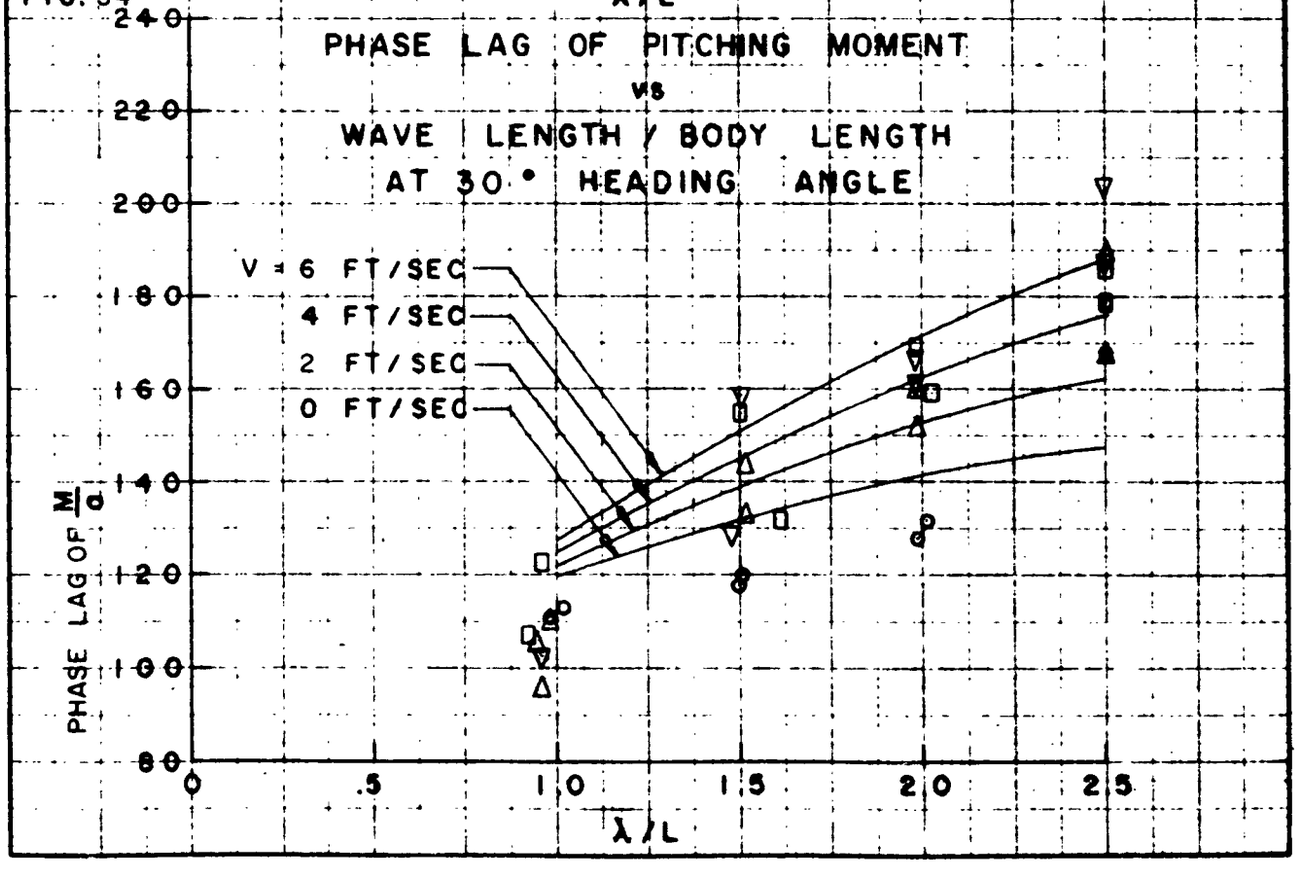

R - 808

FIG. 35

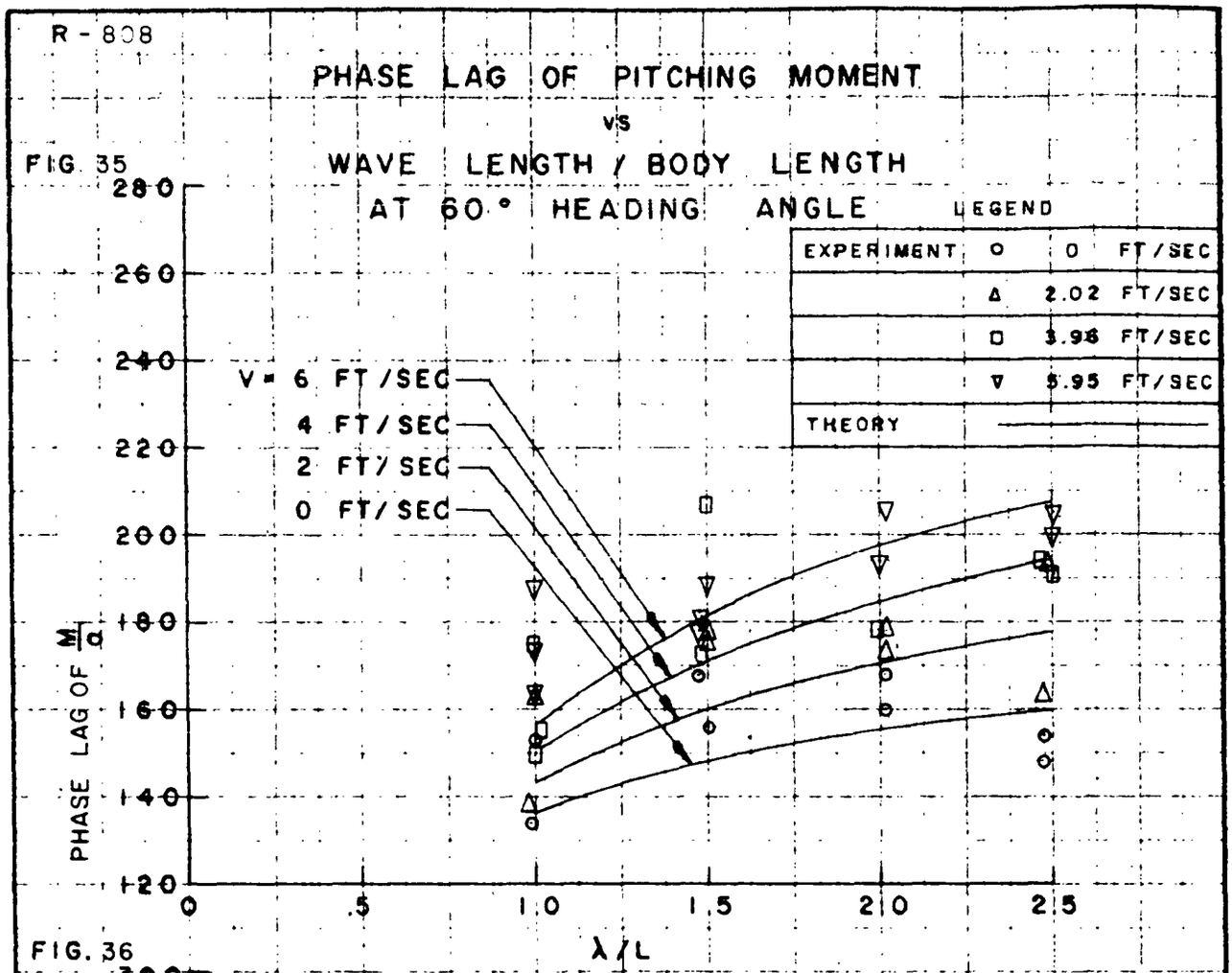

FIG. 36

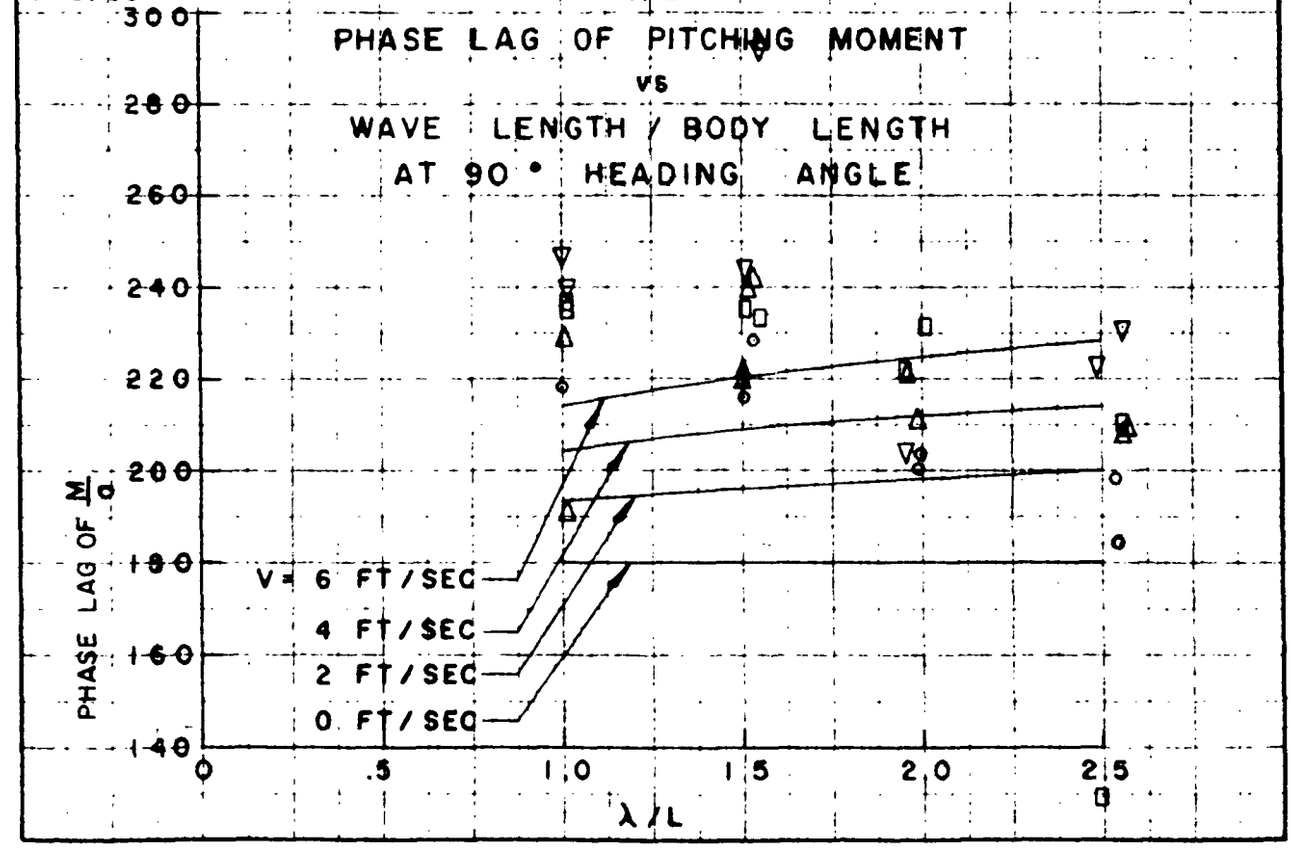

R - 808

FIG. 37

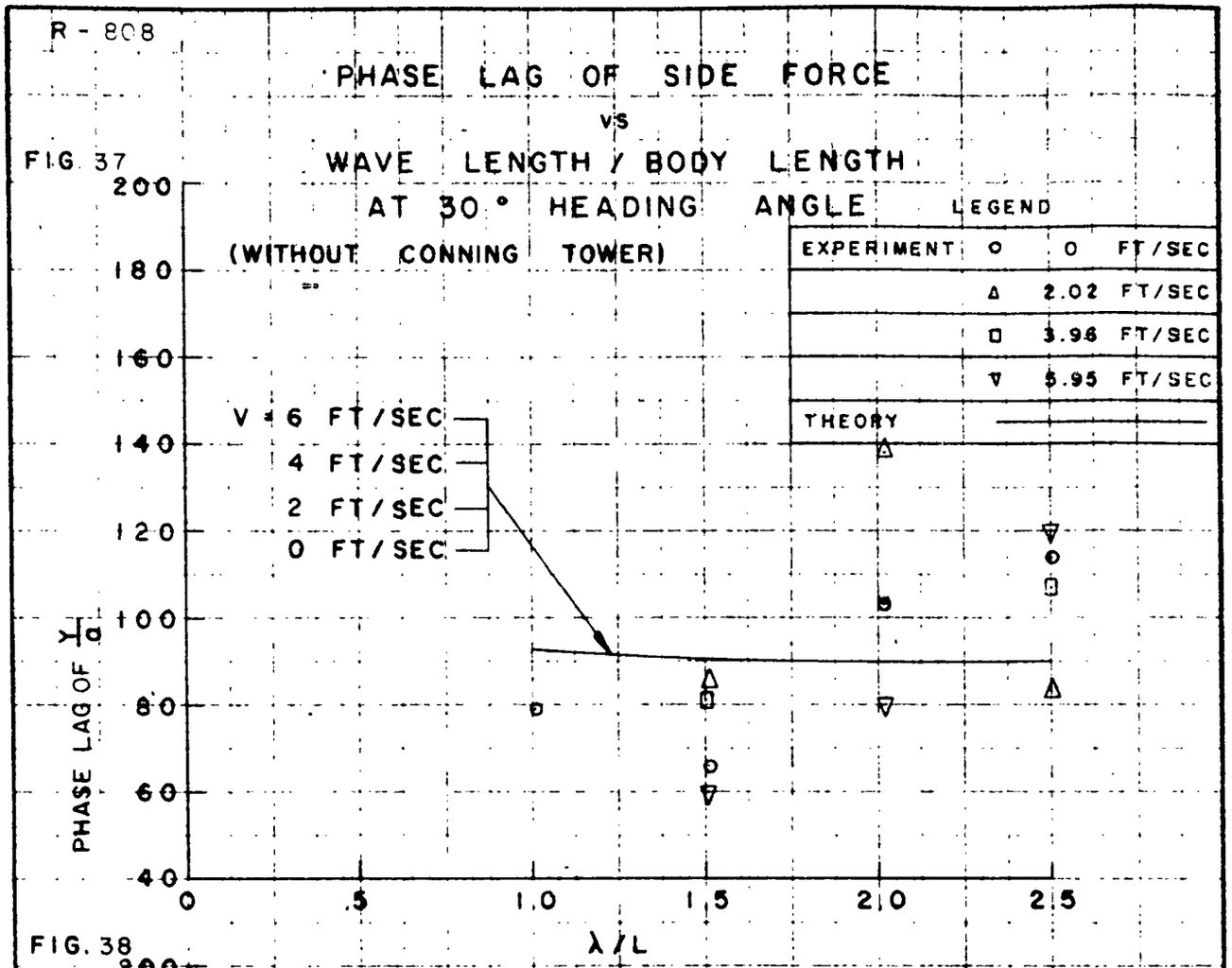

FIG. 38

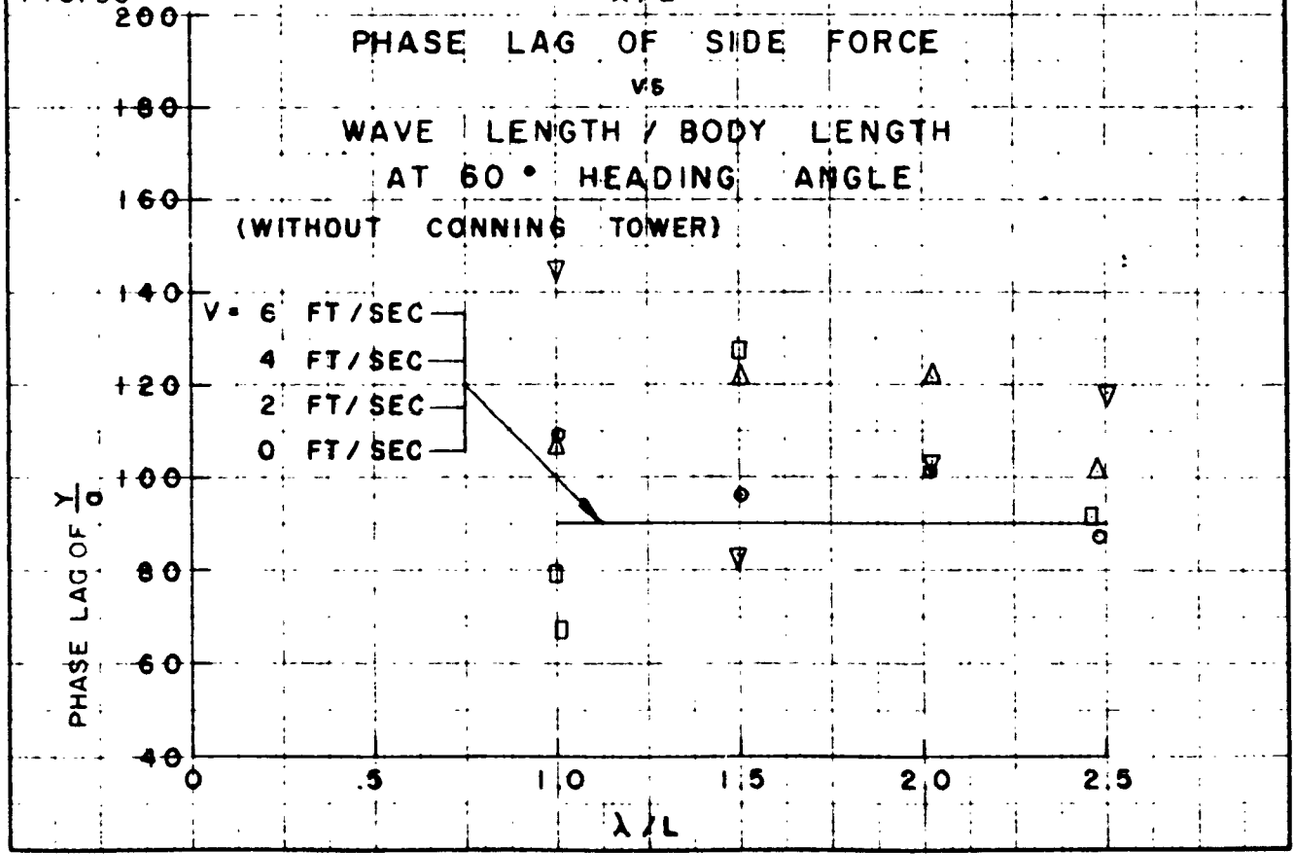

R - 808

FIG. 39

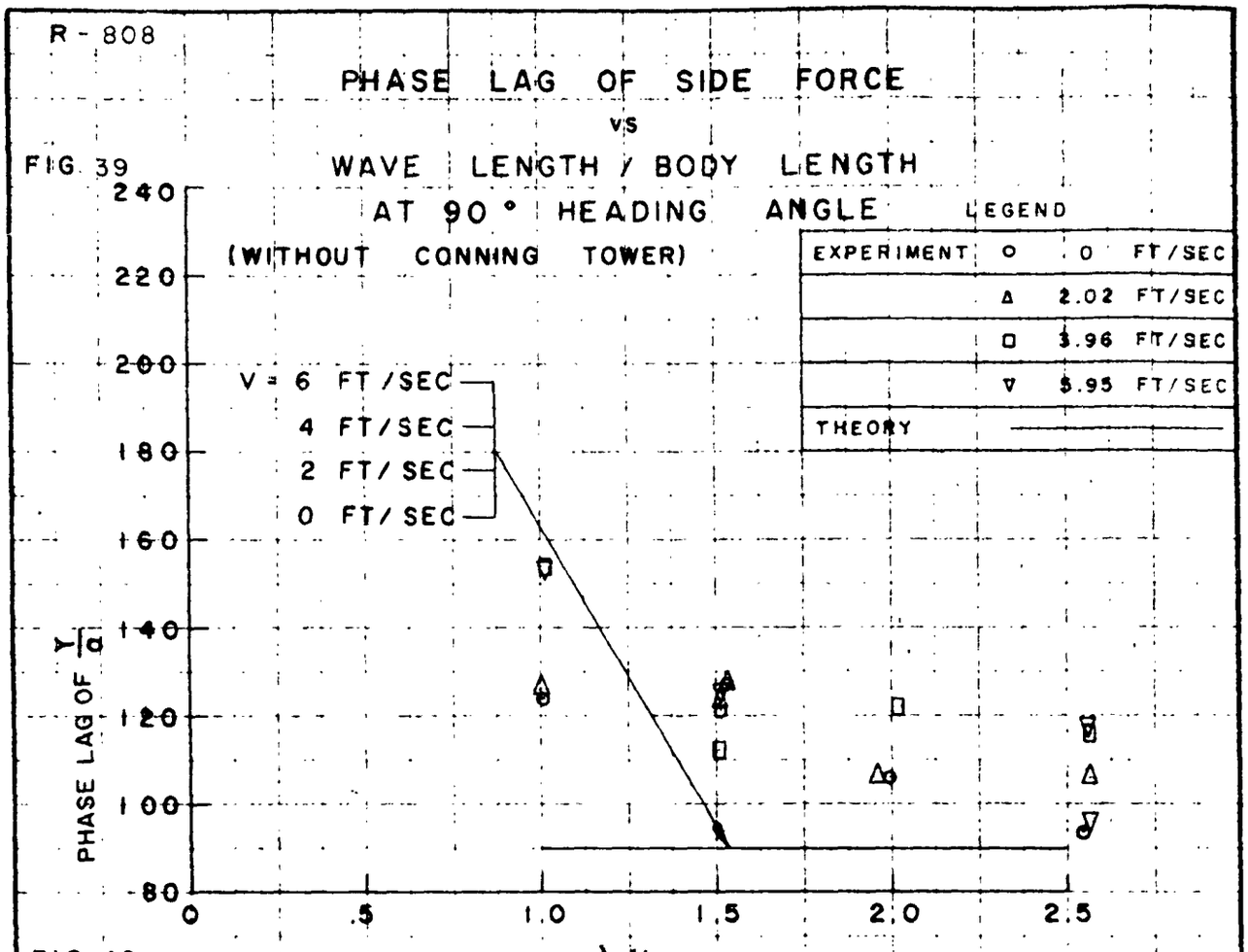

FIG. 40

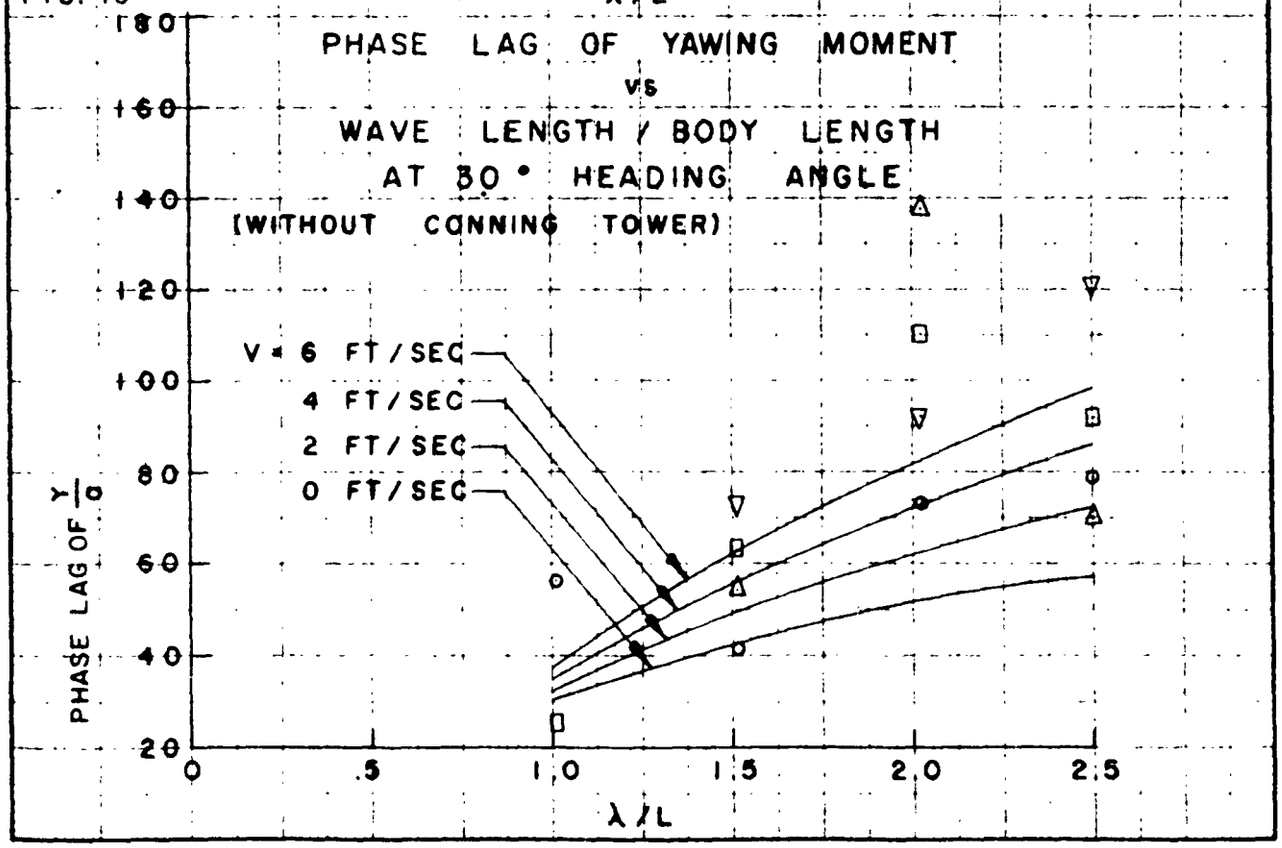

R - 808

FIG 41

PHASE LAG OF YAWING MOMENT
VS
WAVE LENGTH / BODY LENGTH
AT 60 ° HEADING ANGLE
(WITHOUT CONNING TOWER)

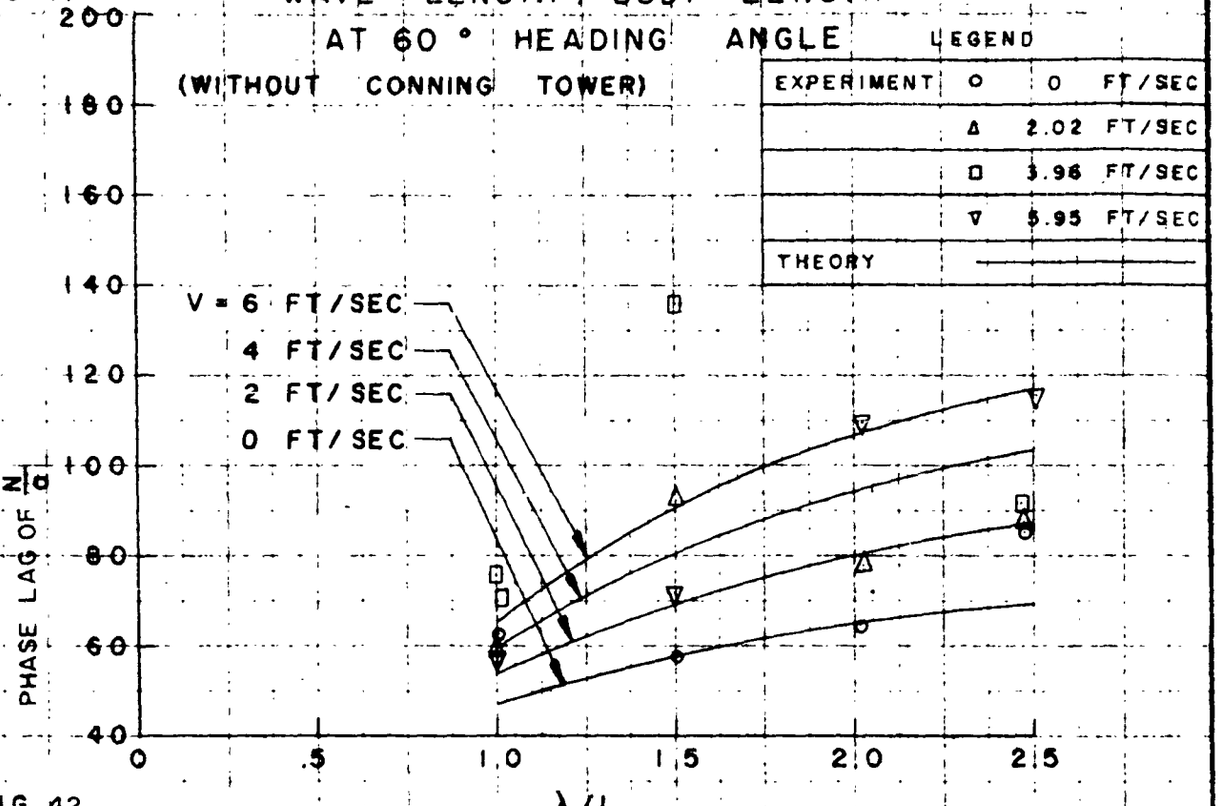

FIG. 42

PHASE LAG OF YAWING MOMENT
VS
WAVE LENGTH / BODY LENGTH
AT 90 ° HEADING ANGLE
(WITHOUT CONNING TOWER)

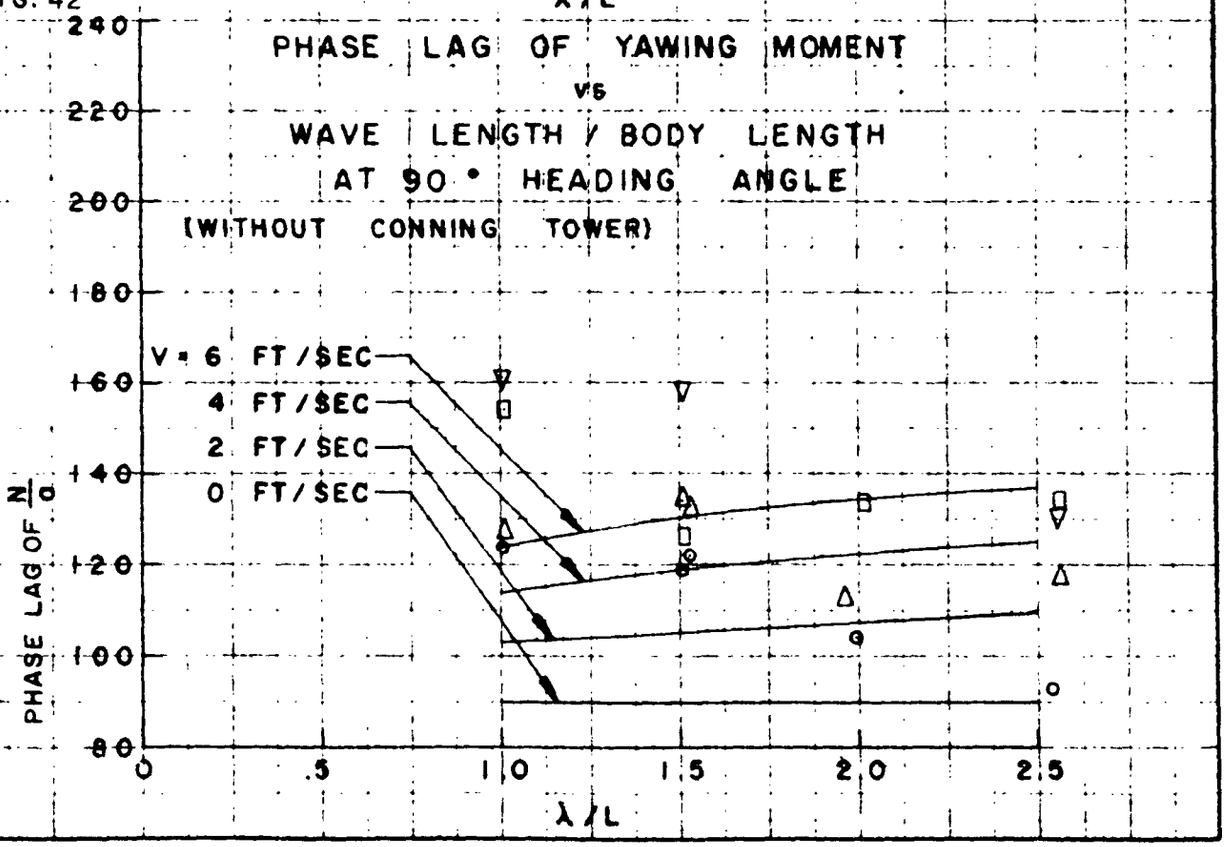

R - 808

FIG. 43

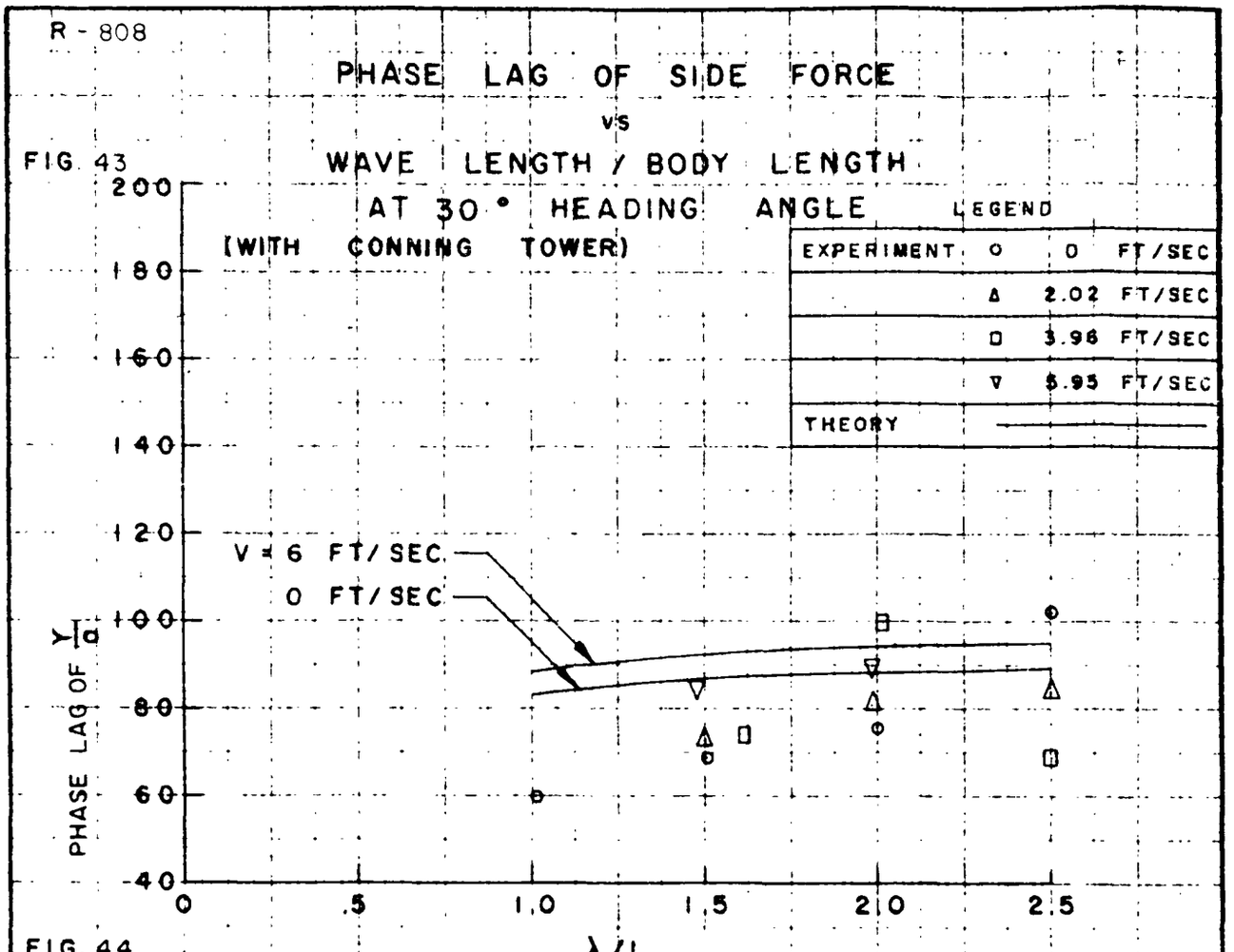

FIG. 44

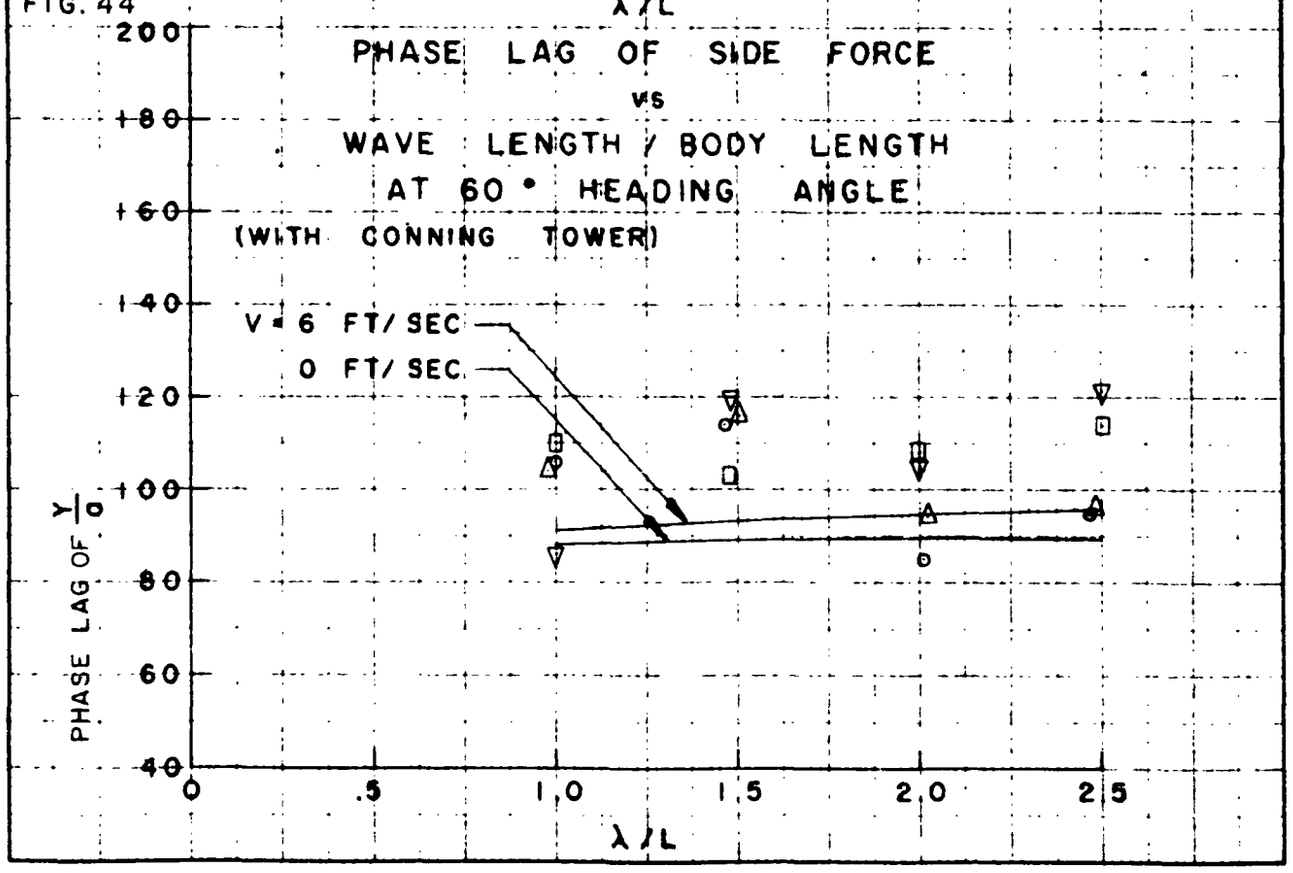

R-808

FIG 45

PHASE LAG OF SIDE FORCE

VS

WAVE LENGTH / BODY LENGTH

AT 90° HEADING ANGLE

(WITH CONNING TOWER)

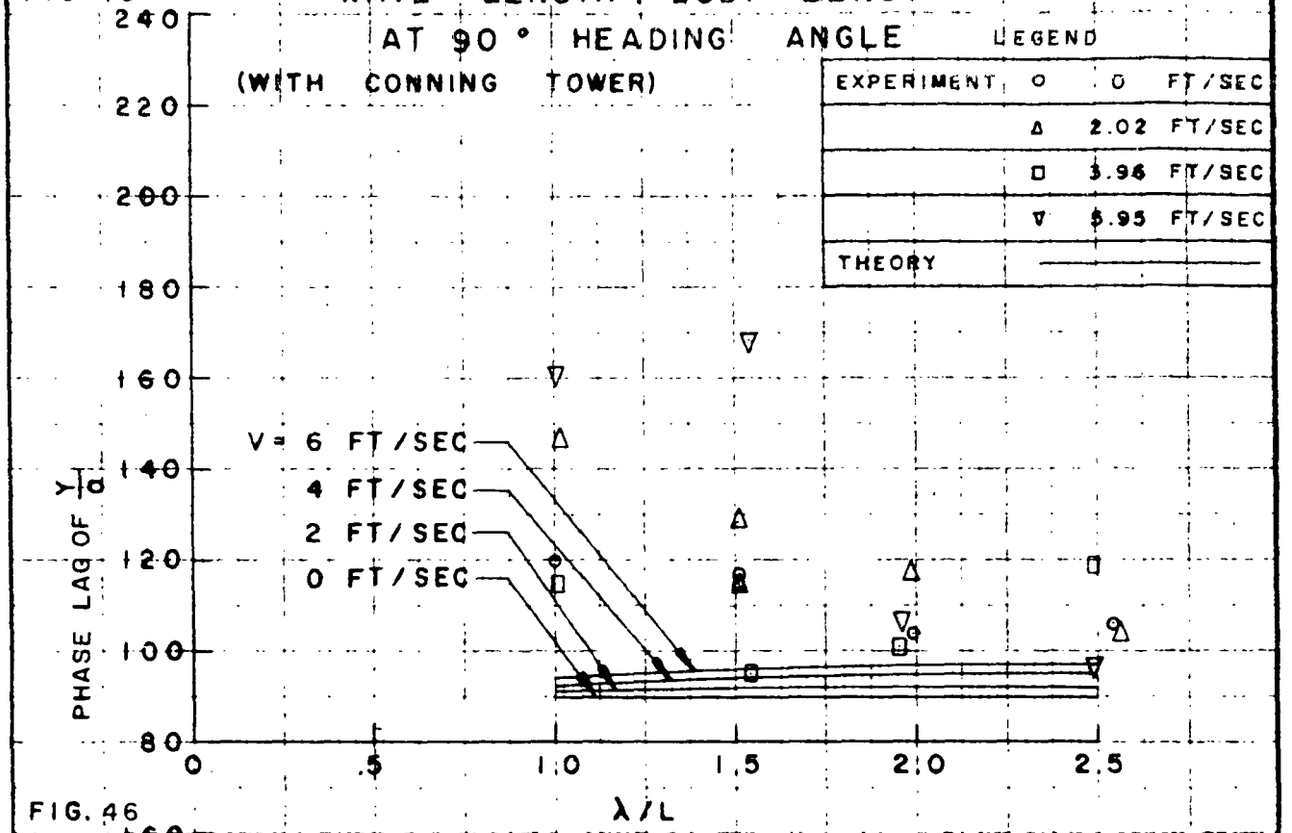

FIG. 46

PHASE LAG OF YAWING MOMENT

VS

WAVE LENGTH / BODY LENGTH

AT 30° HEADING ANGLE

(WITH CONNING TOWER)

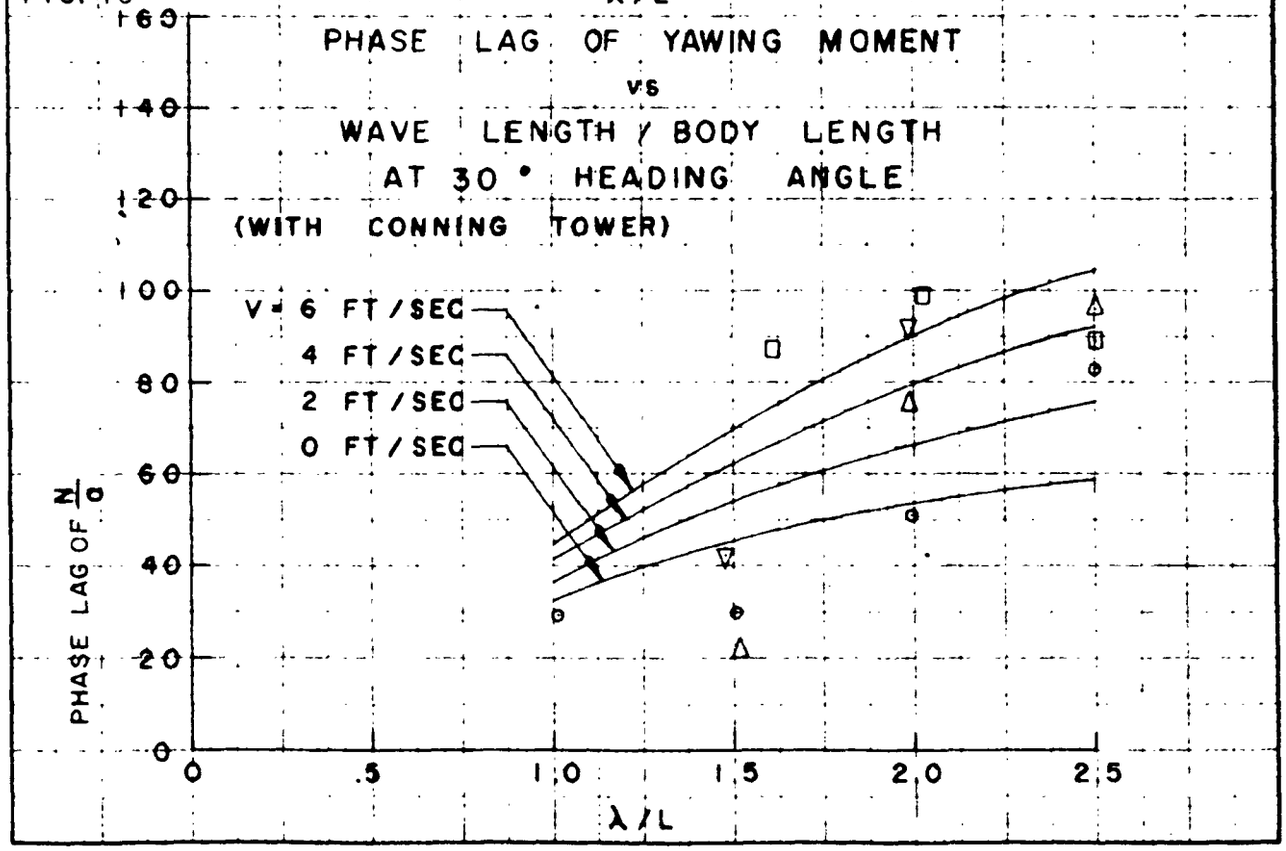

R - 808

FIG 47

PHASE LAG OF YAWING MOMENT

vs

WAVE LENGTH / BODY LENGTH

AT 60 ° HEADING ANGLE

(WITH CONNING TOWER)

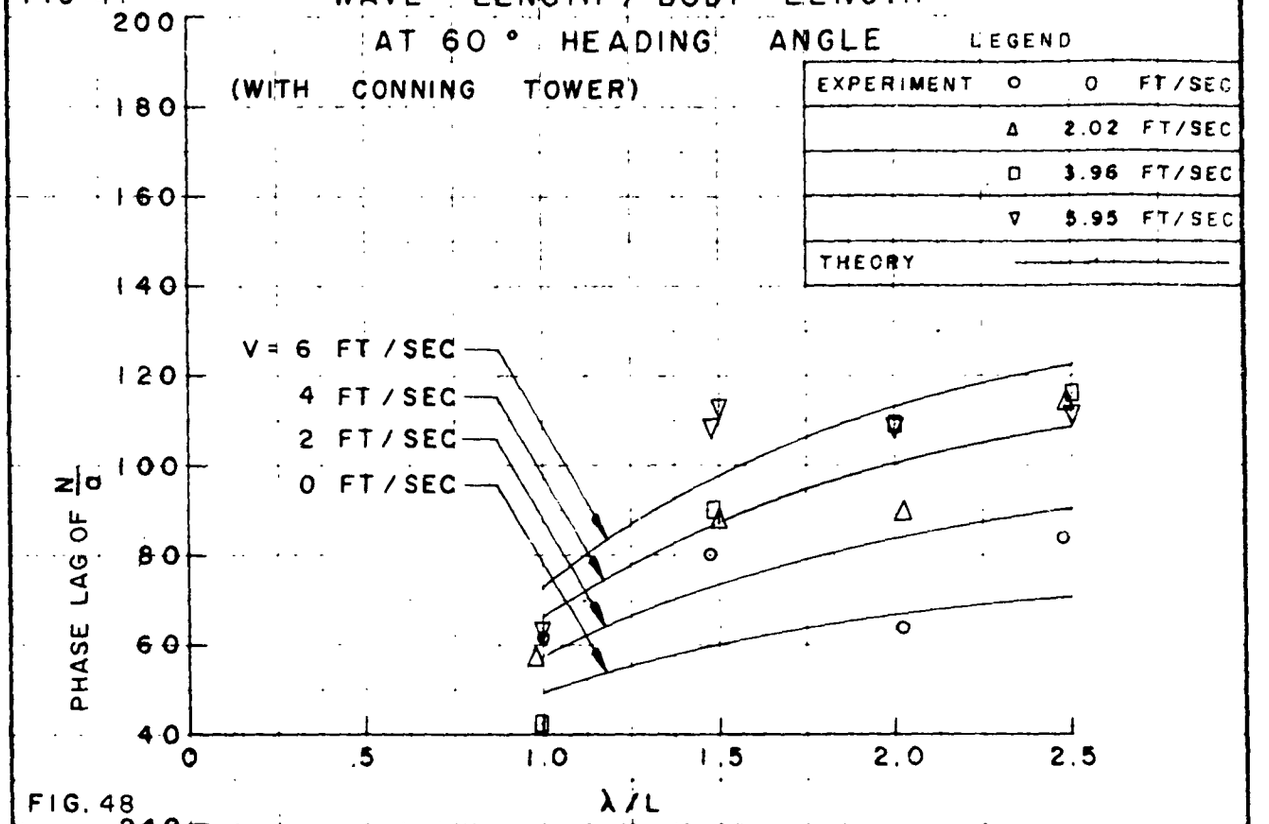

FIG. 48

PHASE LAG OF YAWING MOMENT

vs

WAVE LENGTH / BODY LENGTH

AT 90 ° HEADING ANGLE

(WITH CONNING TOWER)

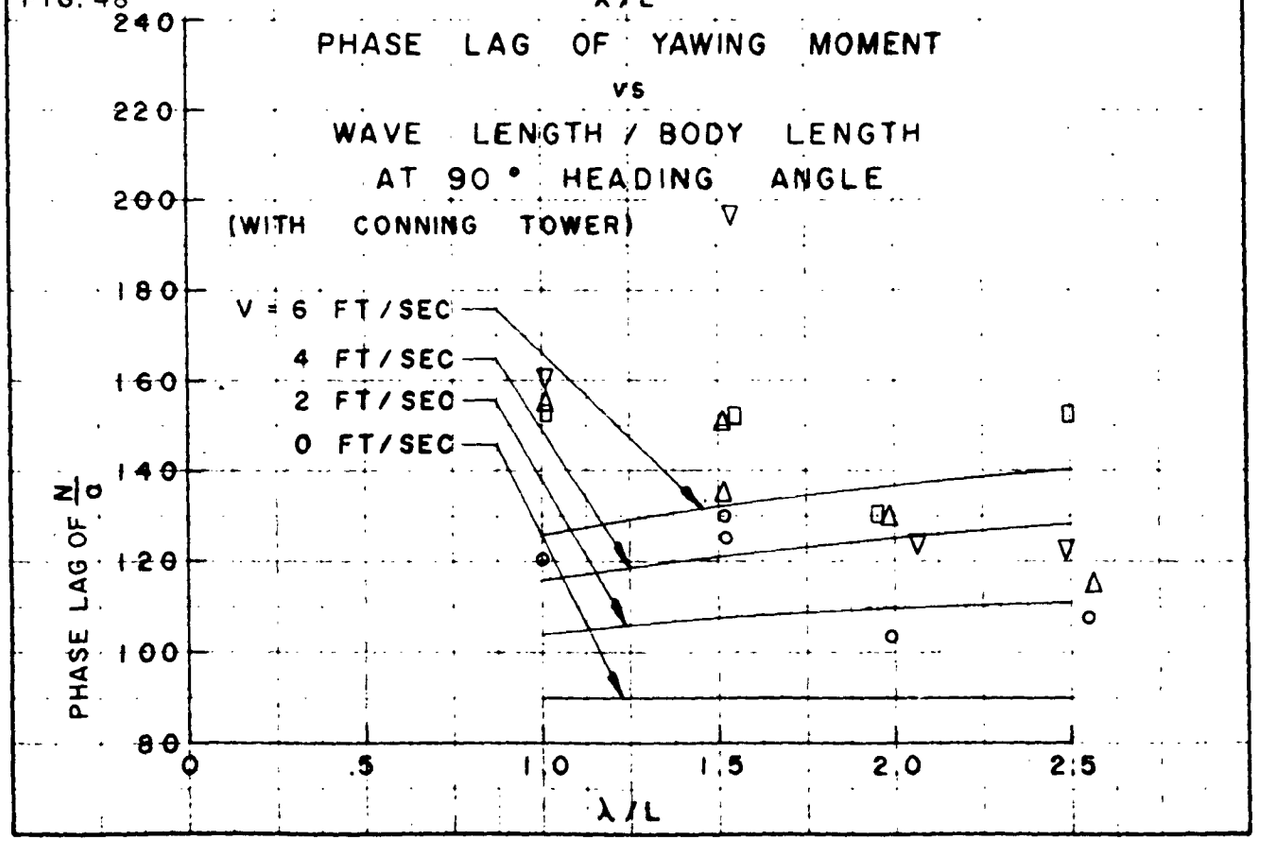

R - 808

FIG. 49

PHASE LAG OF ROLL MOMENT
VS
WAVE LENGTH / BODY LENGTH
AT 30° HEADING ANGLE
(WITH CONNING TOWER)

LEGEND		
EXPERIMENT	o	0 FT/SEC
	Δ	2.02 FT/SEC
	□	3.96 FT/SEC
	▽	5.95 FT/SEC
THEORY		

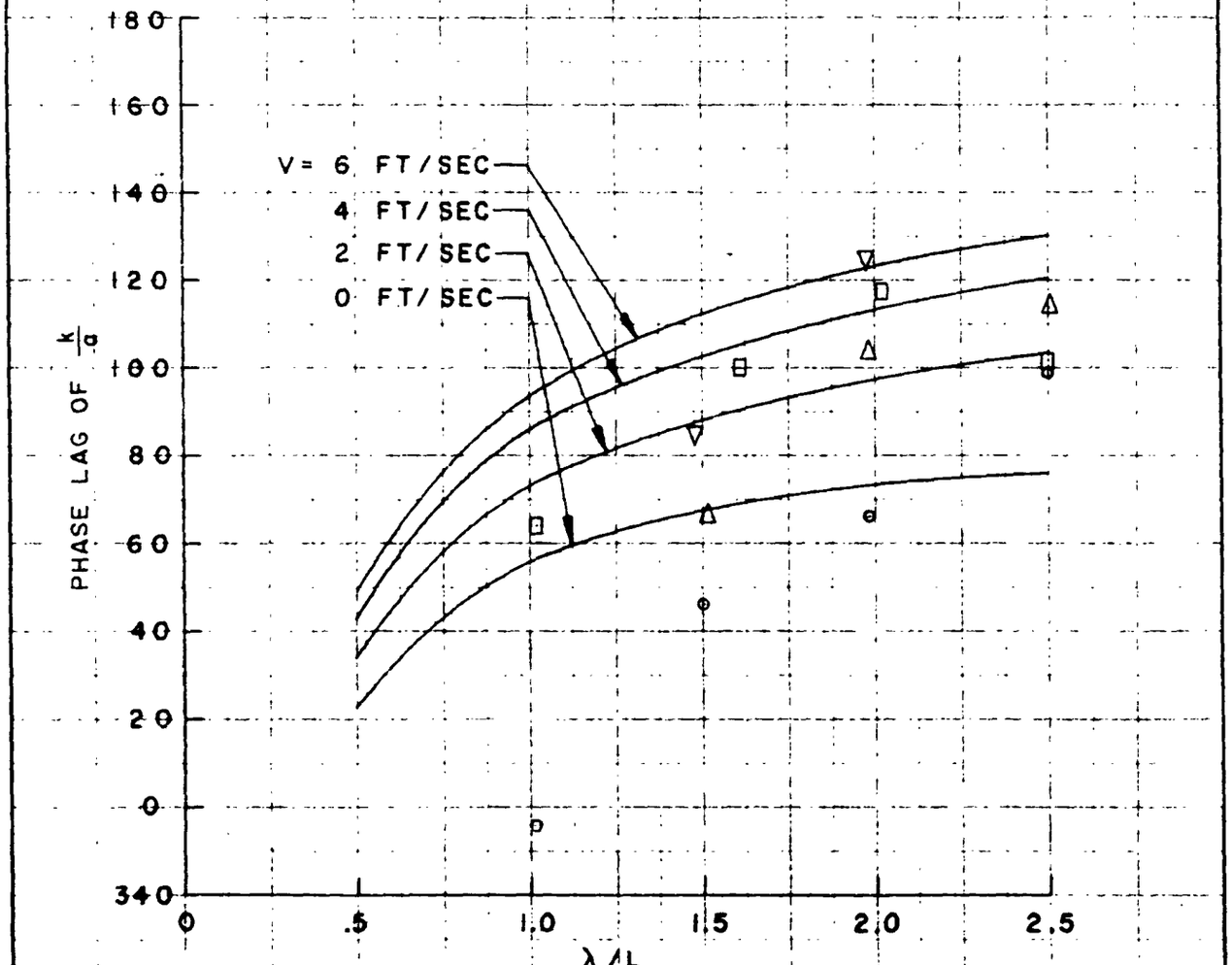

R - 808

FIG 50

PHASE LAG OF ROLL MOMENT

vs

WAVE LENGTH / BODY LENGTH

AT 60 ° HEADING ANGLE

(WITH CONNING TOWER)

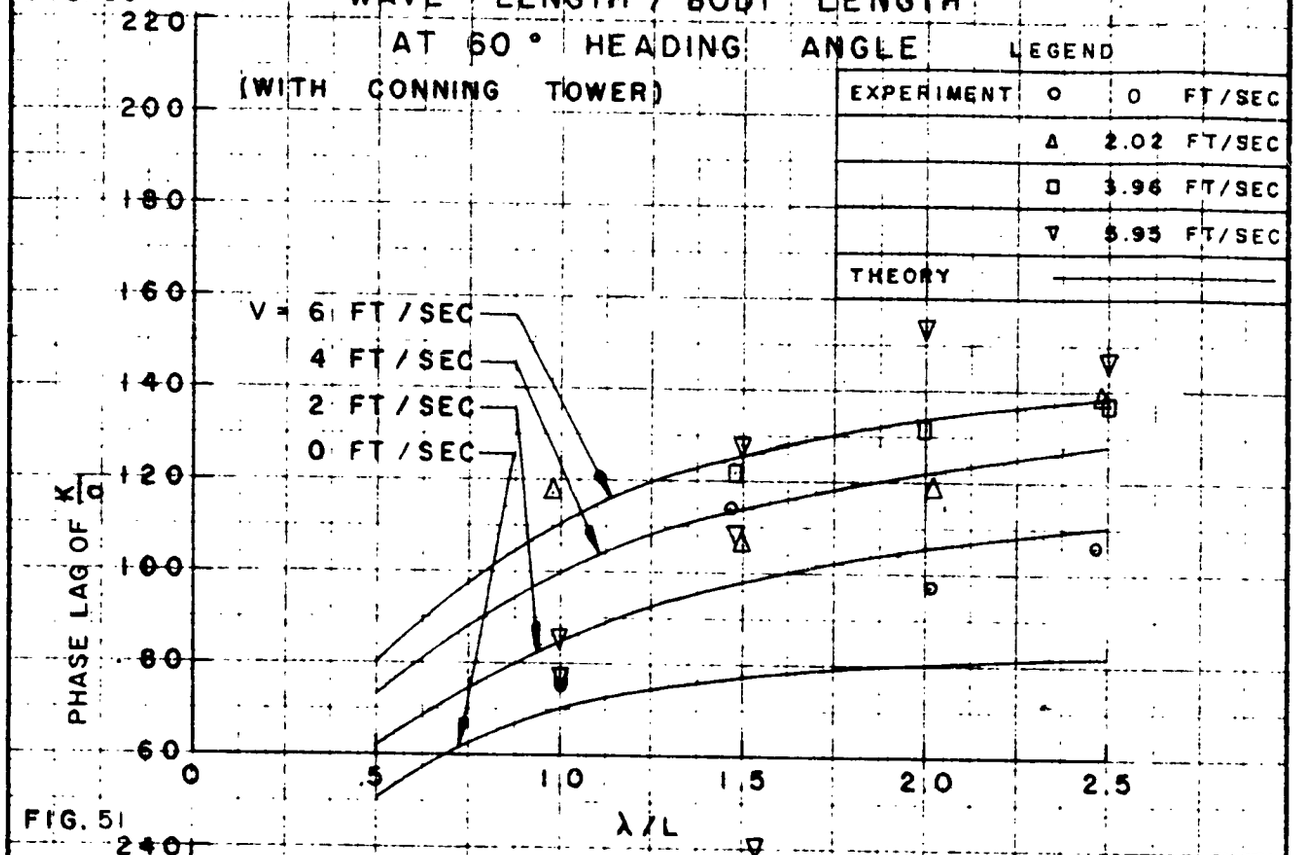

FIG. 51

PHASE LAG OF ROLL MOMENT

vs

WAVE LENGTH / BODY LENGTH

AT 90 ° HEADING ANGLE

(WITH CONNING TOWER)

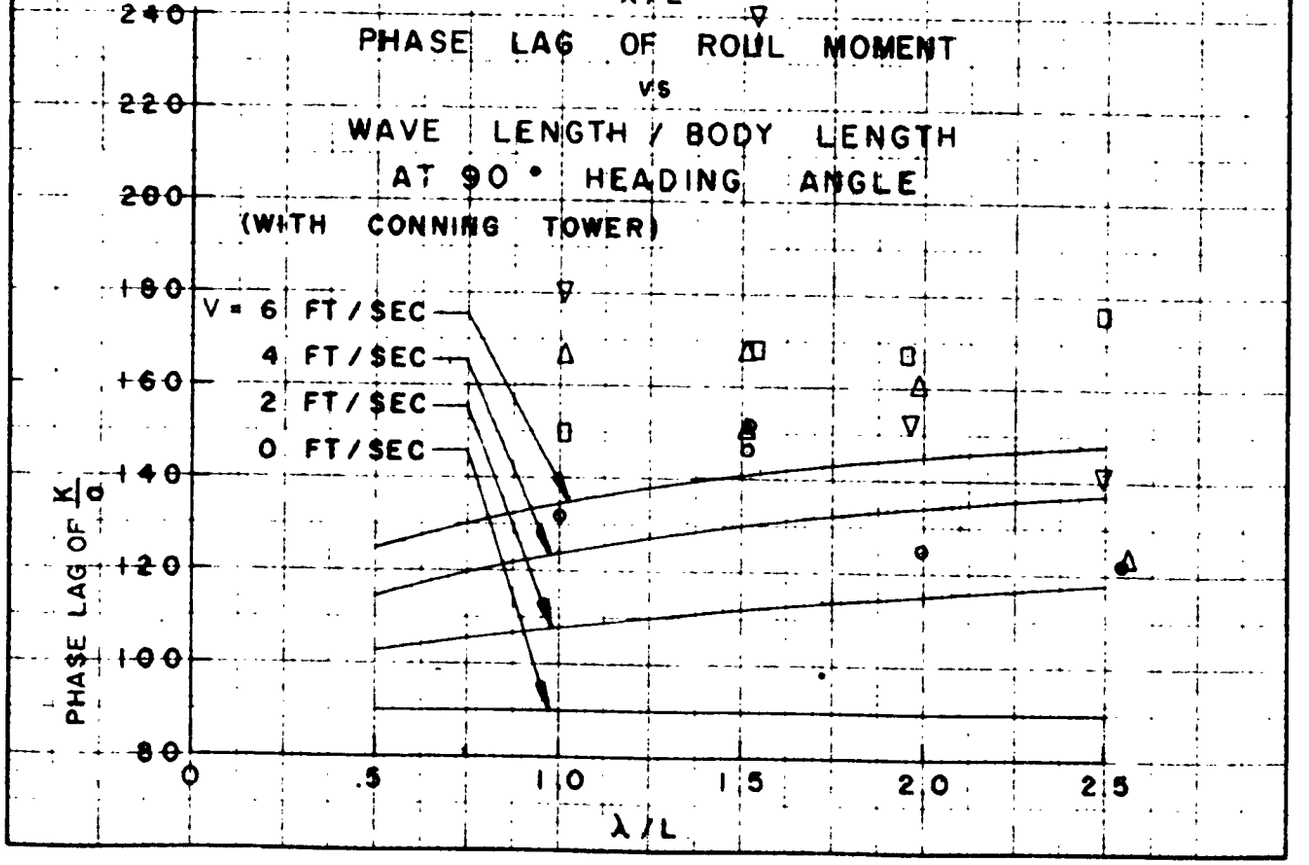

R-808

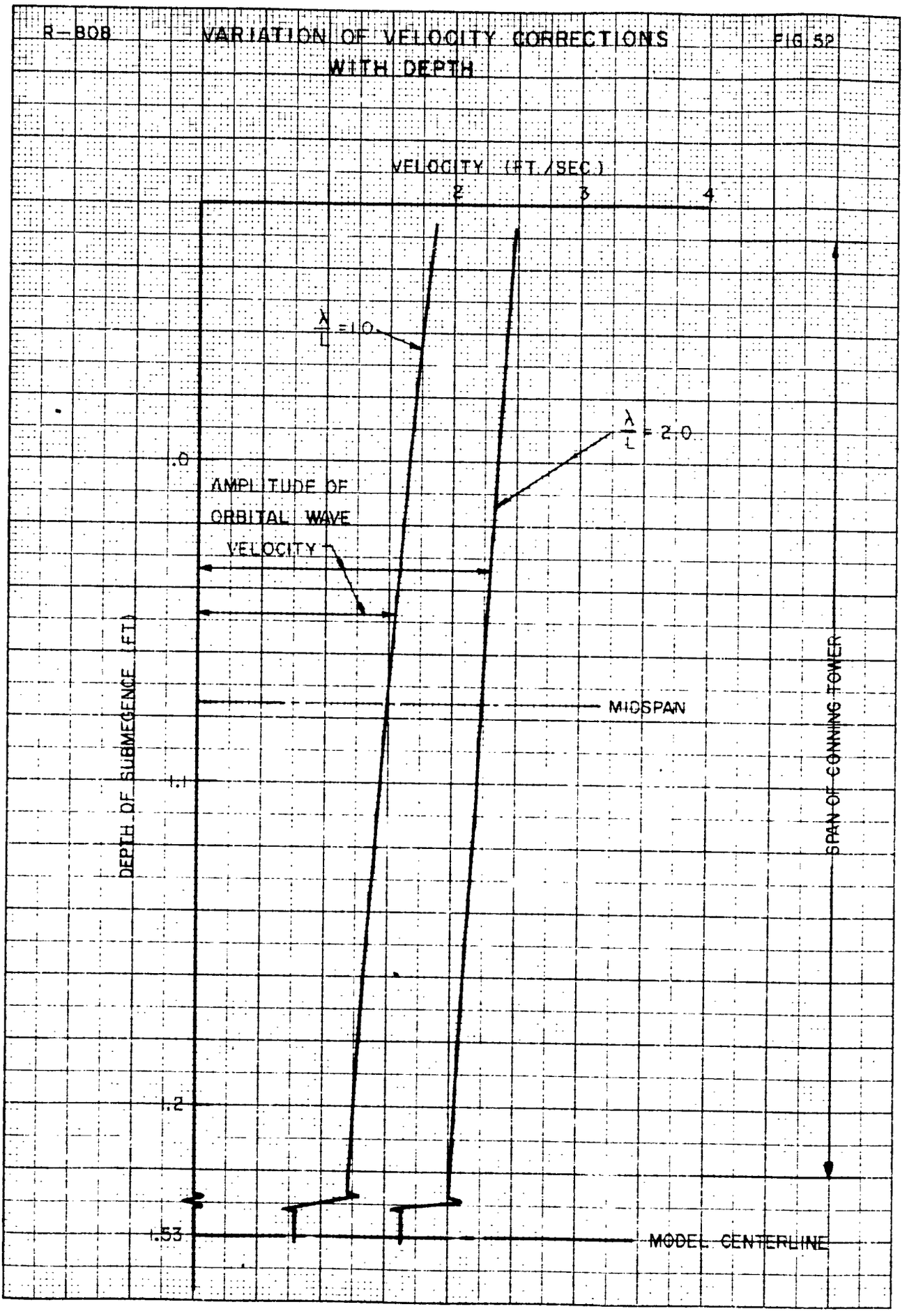
VARIATION OF VELOCITY CORRECTIONS WITH DEPTH
FIG. 52
VELOCITY (FT./SEC.)
2
3
4
λ/L = 1.0
λ/L = 2.0
.0
AMPLITUDE OF ORBITAL WAVE VELOCITY
MIDSPAN
1.1
1.2
1.53
MODEL CENTERLINE
DEPTH OF SUBMERGENCE (FT.)
SPAN OF CONNING TOWER

FIG. 53

SYSTEM OF COORDINATES

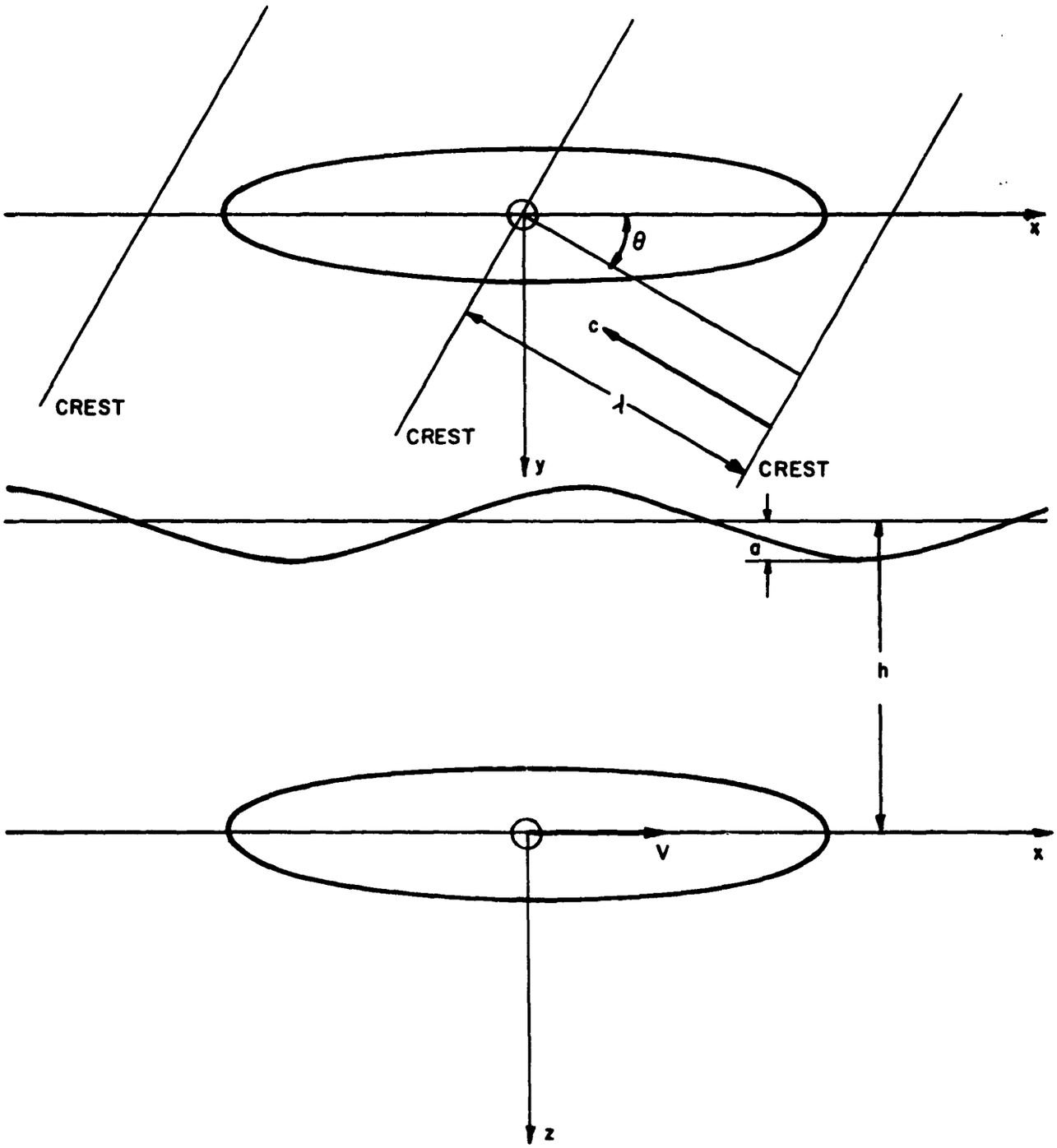

APPENDIX A:
THEORETICAL ANALYSIS

The results presented here summarize the analysis originally reported in reference 3. The problem is the prediction of the forces and moments acting on a submerged slender body moving under a regular wave system. The coordinate system and other nomenclature are illustrated in Figure 53. The body is constrained to move in a straight line at constant depth and with no angle-of-attack relative to calm water. The wave system is at an arbitrary heading-angle to the course of the body. The effect of the presence of a free surface is neglected in determining the forces and moments.

With these assumptions, the expressions for the forces and moments acting on the body are derived. The side and heave force are

$$Y = \int_{x_s}^{x_b} \left[\frac{D}{Dt} (A_{22}\, v_o) + m \frac{D\, v_o}{Dt} \right] dx \qquad \text{(A-1)}$$

$$Z = \int_{x_s}^{x_b} \left[\frac{D}{Dt} (A_{33}\, w_o) + m \frac{D\, w_o}{Dt} \right] dx \qquad \text{(A-2)}$$

where $D/Dt = \partial/\partial t - V\, \partial/\partial x$, w_o and v_o are the wave orbital velocities at the point (x, 0,0) of the body, and A_{22} and A_{33} are the two-dimensional stripwise added masses in the Y and Z directions due to translational motion in the Y and Z direction respectively, given by:

$A_{33} = \rho\pi R^2$ (at all sections)

$A_{22} = \rho\pi R^2$ (at sections where there is no conning tower)

$$A_{22} = \frac{\pi\rho}{4b^2}\left[(b + R)^4 - 12\ R^2\ b^2\right] \text{ (at fairwater sections)}$$

For the yaw and pitching moment the following equations were used:

$$N = \int_{x_s}^{x_b} x\frac{dY}{dx}dx \qquad \text{(A-3)}$$

$$M = -\int_{x_s}^{x_b} x\frac{dZ}{dx}dx \qquad \text{(A-4)}$$

For the roll moment

$$K = +\int_{x_s}^{x_b} \frac{D}{Dt}\left(A_{42}\ v_o\right)dx \qquad \text{(A-5)}$$

where A_{42}, the stripwise added mass moment about the x axis due to flow in the y direction is given by:

$$A_{42} = \rho\left[\frac{(b - R)^3}{4}\left(\frac{R}{b}\right)^{1/2}\left(\frac{14}{3}\frac{R}{b} + 1 + \frac{R^2}{b^2}\right) + \frac{(b - R)^2\ (b + R)^4}{8\ b^3}\left(\frac{\pi}{2} + \sin^{-1}\frac{b - R}{b + R}\right)\right] \qquad \text{(A-6)}$$

The wave orbital velocities at (x, 0, 0) are given by the following equations:

$$v_o = -kac\ \sin\theta e^{-kh}\ e^{ik\left[x\cos\theta + (V\cos\theta - c)t\right]} \qquad \text{(A-7)}$$

$$w_o = -ik\ ac\ e^{-kh}\ e^{ik\left[x\cos\theta + (V\cos\theta - c)t\right]} \qquad \text{(A-8)}$$

These results were applied to a series-58 hull with dimensions given in Table I of this report. The forces and

moments were evaluated for a submergence of 2.5 model diameters. The origin of the coordinate system was taken at the center-of-buoyancy and consequently the moments were calculated relative to the CB. These results were transferred vectorially to give the magnitude of the forces and moments acting at the center of the balance. The computed phase lags are relative to the wave height (η) at the CB given by

$$\eta = a \cos \omega t. \qquad \text{(A-9)}$$

APPENDIX B:
INERTIAL CORRECTIONS

The flexibility of the structure, used to support the strut, caused the records of the force and moment output to include inertial forces which were due to the motion of the model in response to the wave forces. The corrections, made necessary by these inertial forces, are discussed in this appendix.

The linear and angular displacement (δ and β) of the model in the x,y plane relative to the strut were measured and recorded. These displacements were proportional to the force and moment ($-k_\delta \delta$ and $-k_\beta \beta$) that were applied to the model by the balance, where k_δ and k_β were the calibrated spring constants of the balance. The wave force and moment relative to the center-of-buoyancy (Y and N) are the quantities which must be found. Using the usual nomenclature for the linearized hydrodynamic forces acting on a submerged body, the equations of motion of the model relative to the center-of-buoyancy are:

$$Y + Y_{\ddot{y}}\ddot{y} + Y_{\dot{y}}\dot{y} + Y_{\ddot{\beta}}\ddot{\beta} + Y_{\dot{\beta}}\dot{\beta} + Y_{\beta}\beta - k_\delta \delta = m\ddot{y} - m\xi\ddot{\beta} \qquad \text{(B-1)}$$

and

$$N + N_{\ddot{y}}\ddot{y} + N_{\dot{y}}\dot{y} + N_{\ddot{\beta}}\ddot{\beta} + N_{\dot{\beta}}\dot{\beta} + N_{\beta}\beta - k_\beta \beta + \ell k_\delta \delta = I_{zz}\ddot{\beta} - m\xi\ddot{y} \qquad \text{(B-2)}$$

where ℓ is the distance from the center of the balance to the center-of-buoyancy and ξ is the distance from the center-of-gravity to the center-of-buoyancy which are both positive when the center-of-buoyancy is forward. The hydrodynamic derivatives and the moment of inertia (I_{zz}) are all relative to the center-of-buoyancy. The total linear translation of the

model along the y-axis was found to be large in comparison with the total angular displacement. Therefore, the angular displacement β is assumed to be entirely due to the distortion of the balance, while the total linear translation is denoted as y, and the linear distortion of the balance in the y-direction is δ ($< y$). The hydrodynamic inertia coupling terms $Y_{\ddot{\beta}}$ and $N_{\ddot{y}}$ are taken to be zero in this analysis. Solving these equations for the force and moment due to the wave forces and transferring the moment axis to the center of the balance results in the following expressions:

$$Y = (m - Y_{\ddot{y}})\,\ddot{y} - Y_{\dot{y}}\dot{y} - m\xi\ddot{\beta} - Y_{\ddot{\beta}}\ddot{\beta} - Y_{\beta}\beta + k_{\delta}\delta \qquad \text{(B-3)}$$

and

$$N + \ell Y = [(m - Y_{\ddot{y}})\ell - m\xi]\,\ddot{y} - [\ell Y_{\dot{y}} + N_{\dot{y}}]\,\dot{y} +$$
$$\alpha\,[(I_{zz} - N_{\ddot{\beta}}) - m\xi\ell]\,\ddot{\beta} - [N_{\dot{\beta}} + Y_{\dot{\beta}}\ell]\,\dot{\beta} -$$
$$[N_{\beta} + Y_{\beta}\ell\,]\beta + k_{\beta}\beta \qquad \text{(B-4)}$$

Assuming simple harmonic motion with frequency (ω) equal to the frequency of wave encounter for the displacements of y, δ, and β and assuming that all of these motions are in phase with each other, equations B-3 and B-4 become:

$$Y_o = -\omega^2 y_o\,(m - Y_{\ddot{y}}) - i\omega y_o\,Y_{\dot{y}} + \omega^2\,\beta_o\,m\ell - i\omega\beta_o\,Y_{\dot{\beta}} - Y_{\beta}\beta_o + k_{\delta}\delta_o \qquad \text{(B-5)}$$

and

$$N_o + \ell Y_o = -\omega^2 y_o\,[(m - Y_{\ddot{y}})\,\ell - m\xi] - i\omega\,y_o\,[\ell Y_{\dot{y}} + N_{\dot{y}}) -$$
$$\omega^2\beta_o\,[I_{zz} - N_{\ddot{\beta}} - m\xi\ell] - i\omega\beta_o\,[N_{\dot{\beta}} + Y_{\dot{\beta}}\ell] -$$
$$[N_{\beta} + Y_{\beta}\ell]\,\beta_o + k_{\beta}\beta_o \qquad \text{(B-6)}$$

where an $e^{i\omega t}$ has been cancelled from each term; y_o, β_o, and δ_o denote the real amplitudes of the respective motions and N_o and Y_o are the complex amplitudes of the wave force and

moment. In these equations, the hydrodynamic terms involving β_o were small in comparison with y_o and the terms $i\omega y_o \ell Y_{\dot{y}}$, $\omega^2 y_o m\xi$ and $i\omega y_o \ell Y_{\dot{y}}$ were small in comparison with the remaining terms. Neglecting these terms, equations B-5 and B-6 reduce to:

$$Y_o = -\omega^2 y_o (m - Y_{\ddot{y}}) + k_\delta \delta_o \qquad \text{(B-7)}$$

and

$$N_o + \ell Y_o = -\omega^2 y_o (m - Y_{\ddot{y}})\ell - i\omega y_o N_{\dot{y}} + k_\beta \beta_o \qquad \text{(B-8)}$$

In equations B-7 and B-8, the terms $k_\delta \delta_o$ and $k_\beta \beta_o$ represent the recorded balance forces; the left-hand sides (Y_o and $N_o + \ell Y_o$), represent the complex amplitudes of the force and moment applied to the model by the wave forces relative to the center of the balance, and the remaining terms are corrections to the forces measured by the balance, which are necessary because of the model motion of amplitude y_o and frequency ω in response to the wave force excitation. From these equations, the phase and magnitude corrections to the measured force and moment may be found.

The corrections indicated by equations B-7 and B-8 were evaluated for several tests. The acceleration ($\omega^2 y_o$) and frequency (ω) were measured from the records and the velocity (ωy_o) was calculated. However, the recorded accelerations at frequency ω were indiscernable because of the hash in the accelerometer records so that an estimate of the worst possible value for the magnitude of the acceleration was the best information that could be obtained. Using this value, it was found that the phase correction was always less than 5-degrees and that the magnitude correction was less than 10 percent for 90 percent of the runs. As a result, including these corrections in the calculation of the experimental forces and moments was considered to be not worth the time involved. For those cases investigated, the inclusion of

these corrections did not lessen the scatter in the results for either the magnitude or phase of the measured forces and moments. In all cases, when the magnitude corrections are included, the magnitude is reduced. The side force data corrected on the basis of the previous analysis are shown as the flagged points in Figure 16 and in Figure 19 for the yaw moment.

DISTRIBUTION LIST

Copies	
50	Commanding Officer and Director David Taylor Model Basin Washington 7, D. C. Attn: Code 513
10	Commander Armed Services Technical Information Agency Arlington Hall Station Arlington 12, Virginia Attn: TIPDR
1	Commander Boston Naval Shipyard Boston, Massachusetts
1	California Institute of Technology Pasadena 4, California Attn: Dr. T. Y. Wu
1	Commander Charleston Naval Shipyard Charleston, South Carolina
1	Colorado State University Department of Civil Engineering Fort Collins, Colorado Attn: Mr. A. R. Chamberlain, Chief Engineering, Mathematics and Physics Research
1	University of Notre Dame Notre Dame Indiana Attn: Dr. A. G. Strandhagen Dept.of Engineering Science
1	Chief of Naval Research (Code 438) Department of the Navy Washington 25, D. C.
2	Chief, Bureau of Naval Weapons (R) Department of the Navy Washington 25, D. C.
1	Special Projects Office Department of the Navy Washington 25, D. C. Attn: Chief Scientist
9	Chief, Bureau of Ships Department of the Navy Washington 25, D. C. Attn: Code 320 (Lab N.G.T.) (1) 335 (Technical Information Branch) (3) 345 (Ship Silencing Branch) (1) 420 (Preliminary Design Branch) (1) 421 (Preliminary Design Branch) (1) 440 (Hull Design Branch) (1) 442 (Scientific and Research) (1)
1	Chief, Bureau of Yards and Docks Department of the Navy Washington 25, D. C. Attn: Code D-400 (Research Div.)
2	Iowa Institute of Hydraulic Research State University of Iowa Iowa City, Iowa Attn: Dr. H. Rouse, Director Dr. L. Landweber
2	Institute of Mathematical Sciences New York University 25 Waverly Place New York 3, New York Attn: Prof. J. Stoker (1) Prof. A. Peters (1)
1	Commander Long Beach Naval Shipyard Long Beach, California
1	Commander Mare Island Naval Shipyard Vallejo, California
1	Administrator U. S. Maritime Administration Department of Commerce Washington 25, D. C. Attn: Mr. Vito L. Russo, Deputy Chief, Office of Ship Construction

Copies

1 Maritime College
State University of New York
Fort Schulyer
New York 65, New York
Attn: Prof. J. J. Foody, Head
Engineering Department

1 Massachusetts Institute of
Technology
Cambridge 39, Massachusetts
Attn: Department of Naval
Architecture and
Marine Engineering

1 Commander
Military Sea Transportation Service
Department of the Navy
3800 Newark Street, N. W.
Washington 25, D. C.

1 Director
National Aeronautics and Space
Administration
1512 H Street, N. W.
Washington 25, D. C.

1 Director
National Bureau of Standards
Washington 25, D. C.
Attn: Dr. G. B. Schubauer
(Fluid Mechanics)

1 Mr. A. M. O. Smith
Douglas Aircraft Company, Inc.
El Segundo Division
El Segundo,
California

1 Oceanics, Inc.
114 East 40th Street
New York 16,
New York

1 Director
National Science Foundation
1951 Constitution Avenue, N. W.
Washington, D. C.

6 Director
U. S. Naval Research Laboratory
Code 2020
Washington 25, D. C.

Copies

1 Commander
New York Naval Shipyard
Brooklyn, New York

1 New York University
University Heights
New York 53, New York
Attn: Dr. W. J. Pierson, Jr.

1 Commander
Norfolk Naval Shipyard
Portsmouth, Virginia

25 Commanding Officer
Office of Naval Research
Navy 100, Fleet Post Office
New York, New York

1 Commanding Officer
Office of Naval Research Branch Office
1000 Geary Street
San Francisco 9, California

1 Commanding Officer
Office of Naval Research Branch Office
1030 East Green Street
Pasadena 1, California

1 Commanding Officer
Office of Naval Research Branch Office
346 Broadway
New York 13, New York

1 Commanding Officer
Office of Naval Research Branch Office
The John Crerar Library Building
85 East Randolph Street
Chicago 1, Illinois

1 Commander
Pearl Harbor Naval Shipyard
Navy 120, Fleet Post Office
San Francisco, California

1 Pennsylvania State University
University Park, Pennsylvania
Attn: Director
Ordnance Research Laboratory

1 Commander
Philadelphia Naval Shipyard
Philadelphia, Pennsylvania

Copies	
1	Commander Portsmouth Naval Shipyard Portsmouth, New Hampshire
1	Commander Puget Sound Naval Shipyard Bremerton, Washington
1	Commander San Francisco Naval Shipyard San Francisco, California
1	Society of Naval Architects and Marine Engineers 74 Trinity Place New York 6, New York
1	Dr. L. C. Straub, Director St. Anthony Falls Hydraulic Laboratory University of Minnesota Minneapolis 14, Minnesota
3	University of California Berkeley 5, California Attn: Department of Engineering Prof. H. A. Schade, Head Dept. of Naval Architecture (1) Prof. J. Johnson (1) Prof. J. V. Wehausen, Institute of Engineering Research (1)
1	University of Maryland College Park, Maryland Attn: Institute for Fluid Dynamics and Applied Mathematics
1	University of Michigan Ann Arbor, Michigan Attn: Prof. R. B. Couch, Chairman Department of Naval Architecture and Marine Engineering
1	Commanding Officer Headquarters U. S. Army Transportation Command Fort Eustis, Virginia Attn: Research Reference Center

Copies	
2	U. S. Coast Guard 1300 E Street, N. W. Washington 25, D. C. Attn: Secretary, Ship Structure Committee (1) Commandant (1)
1	Chief, Applied Naval Architecture Department of Nautical Science U. S. Merchant Marine Academy Kings Point, Long Island, New York
1	Superintendent U. S. Naval Academy Annapolis, Maryland Attn: Library
1	Superintendent U. S. Naval Postgraduate School Monterey, California
1	Commander U. S. Naval Proving Ground Dahlgren, Virginia
1	Commanding Officer U. S. Naval Repair Facility U. S. Naval Station San Diego, California
1	Administrator Webb Institute of Naval Architecture Crescent Beach Road Glen Cove, Long Island, New York Attn: Technical Library
1	Director Woods Hole Oceanographic Institute Woods Hole, Massachusetts Attn: Dr. C. Iselin, Senior Oceanographer
1	Editor Engineering Index, Inc. 29 West 39th Street New York, New York
1	Librarian Society of Naval Architects and Marine Engineers 74 Trinity Place New York 6, New York

Davidson Laboratory Report No. 808 UNCLASSIFIED

WAVE FORCES ON SUBMERGED BODIES

by Charles J. Henry, Milton Martin, and Paul Kaplan, June 1961

A series of experiments, in which the forces and moments acting on a slender, submerged body-of-revolution moving under regular waves were measured, provided data to verify theoretical predictions of these forces and moments. The measured and predicted results over a range of speeds, heading angles, and wave lengths agreed. The measured and predicted roll moments, acting on the same model but with a conning tower, did not agree; however, the measured and predicted heave and side forces and the pitch and yaw moments did agree.

Davidson Laboratory Report No. 808 UNCLASSIFIED

WAVE FORCES ON SUBMERGED BODIES

by Charles J. Henry, Milton Martin, and Paul Kaplan, June 1961

A series of experiments, in which the forces and moments acting on a slender, submerged body-of-revolution moving under regular waves were measured, provided data to verify theoretical predictions of these forces and moments. The measured and predicted results over a range of speeds, heading angles, and wave lengths agreed. The measured and predicted roll moments, acting on the same model but with a conning tower, did not agree; however, the measured and predicted heave and side forces and the pitch and yaw moments did agree.

Davidson Laboratory Report No. 808 UNCLASSIFIED

WAVE FORCES ON SUBMERGED BODIES

by Charles J. Henry, Milton Martin, and Paul Kaplan, June 1961

A series of experiments, in which the forces and moments acting on a slender, submerged body-of-revolution moving under regular waves were measured, provided atat to verify theoretical prediction of these forces and moments. The measured and predicted results over a range of speeds, heading angles, and wave lengths agreed. The measured and predicted roll moments, acting on the same model but with a conning tower, did not agree; however, the measured and predicted heave and side forces and the pitch and yaw moments did agree.

Davidson Laboratory Report No. 808 UNCLASSIFIED

WAVE FORCES ON SUBMERGED BODIES

by Charles J. Henry, Milton Martin, and Paul Kaplan, June 1961

A series of experiments, in which the forces and moments acting on a slender, submerged body-of-revolution moving under regular waves were measured, provided data to verify theoretical predictions of these forces and moments. The measured and predicted results over a range of speeds, heading angles, and wave lengths agreed. The measured and predicted roll moments, acting on the same model but with a conning tower, did not agree; however, the measured and predicted heave and side forces and the pitch and yaw moments did agree.